AQUIFER MANAGEMENT FOR CO2 SEQUESTRATION

A Thesis

by

ABHISHEK ANCHLIYA

Submitted to the Office of Graduate Studies of
Texas A &M University
in partial fulfillment of the requirements for the degree of

MASTER OF SCIENCE

December 2009

Major Subject: Petroleum Engineering

AQUIFER MANAGEMENT FOR CO2 SEQUESTRATION

A Thesis

by

ABHISHEK ANCHLIYA

Submitted to the Office of Graduate Studies of
Texas A&M University
in partial fulfillment of the requirements for the degree of

MASTER OF SCIENCE

Approved by:

Chair of Committee,	Christine Ehlig-Economides
Committee Members,	Akhil Datta-Gupta
	Hamn-Ching Chen
Head of Department,	Steve Holditch

December 2009

Major Subject: Petroleum Engineering

ABSTRACT

Aquifer Management for CO_2 Sequestration.

(December 2009)

Abhishek Anchliya, B.S., Indian School of Mines, Dhanbad, India

Chair of Advisory Committee: Dr. Christine Ehlig-Economides

Storage of carbon dioxide is being actively considered for the reduction of green house gases. To make an impact on the environment CO_2 should be put away on the scale of gigatonnes per annum. The storage capacity of deep saline aquifers is estimated to be as high as 1,000 gigatonnes of CO_2.(IPCC). Published reports on the potential for sequestration fail to address the necessity of storing CO_2 in a closed system. This work addresses issues related to sequestration of CO_2 in closed aquifers and the risk associated with aquifer pressurization. Through analytical modeling we show that the required volume for storage and the number of injection wells required are more than what has been envisioned, which renders geologic sequestration of CO_2 a profoundly nonfeasible option for the management of CO_2 emissions unless brine is produced to create voidage and pressure relief. The results from our analytical model match well with a numerical reservoir simulator including the multiphase physics of CO_2 sequestration.

Rising aquifer pressurization threatens the seal integrity and poses a risk of CO_2 leakage. Hence, monitoring the long-term integrity of CO_2 storage reservoirs will be a critical aspect for making geologic sequestration a safe, effective and acceptable method for greenhouse gas control. Verification of long-term CO_2 residence in

receptor formations and quantification of possible CO_2 leaks are required for developing a risk assessment framework. Important aspects of pressure falloff tests for CO_2 storage reservoirs are discussed with a focus on reservoir pressure monitoring and leakage detection. The importance of taking regular pressure falloffs for a commercial sequestration project and how this can help in diagnosing an aquifer leak will be discussed.

The primary driver for leakage in bulk phase injection is the buoyancy of CO_2 under typical deep reservoir conditions. Free-phase CO_2 below the top seal is prone to leak if a breach happens in the top seal. Consequently, another objective of this research is to propose a way to engineer the CO_2 injection system in order to accelerate CO_2 dissolution and trapping. The engineered system eliminates the buoyancy-driven accumulation of free gas and avoids aquifer pressurization by producing brine out of the system. Simulations for 30 years of CO_2 injection followed by 1,000 years of natural gradient show how CO_2 can be securely and safely stored in a relatively smaller closed aquifer volume and with a greater storage potential. The engineered system increases CO_2 dissolution and capillary trapping over what occurs under the bulk phase injection of CO_2.

This thesis revolves around identification, monitoring and mitigation of the risks associated with geological CO_2 sequestration.

DEDICATION

To my parents, family, teachers and friends

ACKNOWLEDGEMENTS

I would like to express my sincere gratitude to Dr. Christine Ehlig-Economides for her invaluable guidance and support. Working under her supervision has been a great experience and I cannot thank her more for the time she devoted discussing the outcomes of my research. I appreciate her passion for earth and energy industry. Her feedback and advice always helped me find direction when I was not sure where the research was headed. I learned a lot from her and she helped me directly and indirectly in my academic, professional and personal development.

I am grateful to The Crisman Institute for Petroleum Research at Texas A&M University for financially supporting this research and my studies at Texas A&M University. I would also like to thank Dr. Akhil Datta-Gupta and Dr. Hamn-Ching Chen for serving on my committee and for being a reader for this thesis. A special thanks goes out to Dr. Behnam Jafarpour for his interesting ideas and suggestions during this project. I would also like to thank my fellow graduate student Bo Song for his help during this research.

I would like to express my appreciation to the Computer Modeling Group (CMG) and Kappa Engineering for providing the uninterrupted license of the software packages. I am grateful to Mr. Bob Brugman from CMG for his help with the GEM-GHG (Green House Gas) module of CMG. I would like to extend my special thanks to Michael, David, Brandon and Jason from the IT support group at the Department of Petroleum Engineering, Texas A&M University.

Finally, thanks to my mother, father and family for their encouragement and unconditional love and support. Lastly, but in no sense the least, I am thankful to all

colleagues and friends who made my stay at the university a memorable and valuable experience.

TABLE OF CONTENTS

Page

ABSTRACT iii

DEDICATION v

ACKNOWLEDGEMENTS vi

TABLE OF CONTENTS viii

LIST OF FIGURES x

LIST OF TABLES xx

1. INTRODUCTION AND LITERATURE REVIEW 1

1.1 Introduction 1
1.2 Geologic CO_2 Storage 2
1.3 Research Objectives 4
1.4 Literature Survey 6
1.4 Review of Sections 19

2. BASE CASE SIMULATION FEATURES 21

2.1. Phase Behavior of CO_2 -Brine System 21
2.2. Modeling Solubility and H_20 Vaporization 22
2.3. Land's Model for Gas Trapping 25
2.4 Description of Base Case Model 26
2.5. Section Conclusions 30

3. AQUIFER PRESSURIZATION DUE TO CO_2 INJECTION 31

3.1. Flaws With Current Modeling Approaches 31
3.2. Local Injectivity Issues 34
3.3. Analytical Model for Injection in Closed Aquifers 40
3.4. Section Conclusions 55

4. PRESSURE FALLOFF TESTING FOR AQUIFER CHARACTERIZATION AND LEAKAGE DETECTION 56

4.1 Introduction 56
4.2 Why Monitoring Is Needed 56

Page

4.4 Saturation Profiles Around CO_2 Injection Well 60
4.5 Pressure Profiles Around CO_2 Injection Well 63
4.6 Pressure Derivative Plot 66
4.7 Determination of Average Aquifer Pressure 74
4.8 Detection of an Aquifer Leak 79
4.9 Section Conslusions 89

5. BRINE PRODUCTION FOR PRESSURE CONTROL 90

5.1 Introduction 90
5.2 Reduction of Aquifer Pressurization Risk 90
5.3 Section Conclusions 94

6. AQUIFER MANAGEMENT TO ACCELERATE CO_2 DISSOLUTION AND TRAPPING 95

6.1 Introduction 95
6.2. System Design: Adressing Risks 96
6.3 Gravity Number 101
6.4. System Design for 500-Mw Power Plant 104
6.5 Applications of Engineered Case 119
6.6 Section Conclusions 132

7. CONCLUSIONS AND RECOMMENDATIONS 135

7.1 Conclusions 135
7.2 Recommendations 137

REFERENCES 139

APPENDIX. EXAMPLE CMG SIMULATION INPUT FILE 151

VITA 161

LIST OF FIGURES

Page

Fig. 1.1—World CO_2 emissions from combustion and flaring of fossil fuels (EIA 2006). 2

Fig. 1.2—Overview of geological storage options (IPCC, 2007). 3

Fig. 1.3—Risks of underground CO2 sequestration. Black and gray arrows represent CO2 and CH4 flows (along abandoned wells, fractures, faults). White arrows represent brine displacement as a consequence of CO2 injection. (Figure from Damen et al. 2006.) 9

Fig. 1.4—Relative permeability hysterisis. The blue curve is for drainage and red for imbibition. Figure illustrates two imbibition cases with different starting points on the drainage curve, resulting in different residual saturation. (Figure from Kumar et al. 2008.) 14

Fig.1.5—The solubility in mole percent predicted by the Duan EOS (Hangx 2005) for a temperature and pressure gradient of 1°F/100 ft and 0.44 psi/ft. Surface temperature and pressure were assumed to be 61°F and 14.7 psia, respectively. Solubility increases with depth to ~2,000 ft, then remains fairly constant. Brine salinity has a significant effect on the plateau solubility. (Figure from Burton and Bryant 2007.) 16

Fig. 1.6—Timing of various mechanisms for storage security (IPCC, 2005). 18

Fig. 2.1—Land's residual gas trapping model (Nghiem et al. 2009) 25

Fig. 2.2—Schematic of the base case aquifer model. 27

Fig. 3.1—CMG simulations comparing annual pressure profiles for the bounded and open aquifer cases, both in a square drainage area with side 20 mile. CO2 was injected for 30 years at 52 million scf/D (~1 million T/yr). The initial hydrostatic pressure of the reservoir was 2,600 psi. The fracture pressure of the reservoir is 4,200 psi. 34

Page

Fig. 3.2—CMG simulations comparing annual pressure profiles for the bounded and open aquifer cases, both in a square drainage area with side 20 mile. The logarithmic distance scale facilitates observation of the expanding single and two-phase zone radii. CO2 was injected for 30 years at 52 million scf/D (~1 million T/yr). The initial hydrostatic pressure of the reservoir was 2,600 psi. The fracture pressure of the reservoir is 4,200 psi. 34

Fig. 3.3—Plot comparing well BHP obtained from simulation for different aquifer dimensions. CO2 was injected for 30 years at 52 million scf/D (~1 million T/yr). The initial hydrostatic pressure of the reservoir was 2,600 psi. The fracture pressure of the reservoir is 4,200 psi. 36

Fig. 3.4—Plot comparing injectivity obtained from simulation for different aquifer dimensions. CO2 was injected for 30 years at 52 million scf/D (~1 million T/yr). The initial hydrostatic pressure of the reservoir was 2,600 psi. The fracture pressure of the reservoir is 4,200 psi. The red curve shows the injectivity of a 5-mile aquifer with constant-pressure boundaries. 39

Fig. 3.5—Plot comparing steady-state injectivity obtained from simulation for different aquifer dimensions. CO2 was injected for 30 years at 52 million scf/D (~1 million T/yr). The initial hydrostatic pressure of the reservoir was 2,600 psi. The fracture pressure of the reservoir is 4,200 psi. The red curve shows the injectivity of a 5 miles aquifer with constant-pressure boundaries. 40

Fig. 3.6--Schematic showing different flow regions when anhydrous CO2 is injected in the system. 41

Fig. 3.7—Average reservoir pressure predicted by the simplified model for a closed system compares well with the CMG numerical simulator. CO2 was injected for 30 years at 52 million scf/D (~1 million T/yr). The initial hydrostatic pressure of the reservoir was , psi. The fracture pressure of the reservoir is 4,200 psi..... 48

Fig. 3.8—Average reservoir pressure predicted by the simplified model for a closed system compares well with the CMG numerical simulator. CO2 was injected for 30 years at 52 million scf/D (~1 million T/yr). The initial hydrostatic pressure of the reservoir was 2,650 psi. The fracture pressure of the reservoir is 4,200 psi..... 48

Page

Fig. 3.9—Relationship between well count, permeability-thickness, and the compression pressure as a fraction of Δpmax for given relative permeability, porosity, Δpmax, and aquifer depth. 50

Fig. 3.10—Relationship between well count, permeability-thickness, and the required minimum pore volume for given relative permeability, porosity, Δpmax, and aquifer depth. 51

Fig. 3.11—Plot showing the difference between the fracture and hydrostatic pressures, pf — phyd, for an aquifer with depth. 51

Fig. 3.12—Relationship between well count, permeability-thickness, and the storage potential for given relative permeability, porosity, Δpmax,, and aquifer depth. 53

Fig. 4.1—Diagram showing CO2 injection in deep saline aquifer. 59

Fig. 4.2—Radial saturation variation around the CO2 injection well. 60

Fig. 4.3—Graph showing simulated saturation profiles for CO2 injection well. 61

Fig. 4.4—Pressure profiles vs radial distance for CO2 injection well. CO2 is injected for 30 years at 52 million scf/D (~1 million T/yr). The initial hydrostatic pressure of the reservoir is 2,600 psi. The fracture pressure of the reservoir is 4,200 psi. 64

Fig. 4.5—Simulated injection falloff test after 20 days on injection. CO2 is injected for 30 years at 52 million scf/D (~1 million T/yr). The initial hydrostatic pressure of the reservoir is 2,600 psi. The fracture pressure of the reservoir is 4,200 psi. The falloff was taken over a period of 5 days. The analytical model for the simulated data is also shown with solid lines. 67

Fig. 4.6—Plot shows simulated injection falloff test after 30 years on injection. CO2 was injected for 30 years at 52 million scf/D (~1 million T/yr). The falloff was taken for a period of 1.5 years. The simulation boundary is about 25,000 ft from the injection well. The analytical model for the simulated data is also shown with solid lines. 69

Page

Fig. 4.7—Plot shows simulated injection falloff test after 30 years on injection. CO2 was injected for 30 years at 52 million scf/D (~1 million T/yr). The falloff was taken for a period of 1.5 years. The simulation boundary is at infinite distance from the injection well. The analytical model for the simulated data is also shown with solid lines. 69

Fig. 4.8—Succession of injection falloff tests showing advance of dry and two-phase zones. 70

Fig. 4.9—A comparison of the radius of dry zone obtained from CMG simulator and pressure falloff test at different injection time. CO2 was injected for 30 years at 52 million scf/D (~1 million T/yr). 71

Fig. 4.10—Comparison of the mobility of the dry zone obtained from the numerical reservoir simulator and pressure falloff test at different injection times. CO2 was injected for 30 years at 52 million scf/D (~1 million T/yr). 72

Fig. 4.11—Comparison of the mobility of two-phase zone obtained from numerical reservoir simulator and pressure falloff test at different injection time. CO2 was injected for 30 years at 52 million scf/D (~1 million T/yr). 73

Fig. 4.12—Comparison of the mobility of shock front obtained from numerical reservoir simulator and pressure falloff test at different injection time. CO2 was injected for 30 years at 52 million scf/D (~1 million T/yr). 73

Fig. 4.13—Horner analysis for estimation of average aquifer pressure, open aquifer case. CO2 was injected for 30 years at 10 million scf/D (~0.2 million T/yr). The initial hydrostatic pressure of the reservoir was 2,600 psi. The fracture pressure of the reservoir is 4,200 psi. 77

Fig. 4.14—Trend from extrapolated pressures values determined from Horner analysis compared to values determined from the CMG numerical, open aquifer case. CO2 was injected for 30 years at 10 million scf/D (~0.2 million T/yr). The initial hydrostatic pressure of the reservoir was 2,600 psi. The fracture pressure of the reservoir is 4,200 psi. 77

Fig. 4.15—Horner analysis for estimation of average aquifer pressure-bounded aquifer case. CO2 was injected for 30 years at 10 million scf/D (~0.2 million T/yr). The initial hydrostatic pressure of the reservoir was 2,600 psi. The fracture pressure of the reservoir is 4,200 psi. 78

Page

Fig. 4.16—Trend from extrapolated pressure values determined from Horner analysis compared to values determined from the CMG numerical simulation, bounder aquifer case. CO2 was injected for 30 years at 10 million scf/D (~0.2 million T/yr). The initial hydrostatic pressure of the reservoir was 2,600 psi. The fracture pressure of the reservoir is 4,200 psi. 78

Fig. 4.17—Simulated leak positions. 80

Fig. 4.18—Horner analysis for estimation of average aquifer pressure, bounded aquifer with leak in the dry zone. CO2 was injected for 30 years at 25 million scf/D (~0.5 million T/yr). The initial hydrostatic pressure of the reservoir was 2,600 psi. The fracture pressure of the reservoir is 4,200 psi. The leak is is located at a distance of 1,000 ft from the wellbore. 81

Fig. 4.19—Trend from extrapolated pressure values determined from Horner analysis compared to values determined from the simulation, bounded aquifer with leak in the dry zone. CO2 was injected for 30 years at 25 million scf/D (~0.5 million T/yr). The initial hydrostatic pressure of the reservoir was 2,600 psi. The fracture pressure of the reservoir is 4,200 psi. The leak is located at a distance of 1,000 ft from the wellbore. 81

Fig. 4.20— Simulated fluids leaking from the dry zone. CO2 was injected for 30 years at 25 million scf/D (~0.5 million T/yr). The initial hydrostatic pressure of the reservoir was 2,600 psi. The fracture pressure of the reservoir is 4,200 psi. The leak is located at a distance of 1,000 ft from the wellbore. 82

Fig. 4.21—Horner analysis for estimation of average aquifer pressure — bounded aquifer with leak in the two-phase zone. CO2 was injected for 30 years at 25 million scf/D (~0.5 million T/yr). The initial hydrostatic pressure of the reservoir was 2,600 psi. The fracture pressure of the reservoir is 4,200 psi. The leak is located at a distance of 7,000 ft from the wellbore. 83

Page

Fig. 4.22—Trend from extrapolated pressure values determined from Horner analysis compared to values determined from the simulation, bounded aquifer with leak in the two-phase zone. CO2 was injected for 30 years at 25 million scf/D (~0.5 million T/yr). The initial hydrostatic pressure of the reservoir was 2,600 psi. The fracture pressure of the reservoir is 4,200 psi. The leak is located at a distance of 7,000 ft from the wellbore. 83

Fig. 4.23—Simulated fluids leaking from the two-phase zone. CO2 was injected for 30 years at 25 million scf/D (~0.5 million T/yr). The initial hydrostatic pressure of the reservoir was 2,600 psi. The fracture pressure of the reservoir is 4,200 psi. The leak is located at a distance of 7,000 ft from the wellbore. 84

Fig. 4.24—Horner analysis for estimation of average aquifer pressure, bounded aquifer with leak in the brine zone. CO2 was injected for 30 years at 25 million scf/D (~0.5 million T/yr). The initial hydrostatic pressure of the reservoir was 2,600 psi. The fracture pressure of the reservoir is 4,200 psi. The leak is located at a distance of 15,000 ft from the wellbore. 85

Fig. 4.25—Trend from extrapolated pressure values determined from Horner analysis compared to values determined from the simulation, bounded aquifer with leak in the brine zone. CO2 was injected for 30 years at 25 million scf/D (~0.5 million T/yr). The initial hydrostatic pressure of the reservoir was 2,600 psi. The fracture pressure of the reservoir is 4,200 psi. The leak is located at a distance of 15,000 ft from the wellbore. 86

Fig. 4.26—Simulated fluids leaking from the brine zone. CO2 was injected for 30 years at 25 million scf/D (~0.5 million T/yr). The initial hydrostatic pressure of the reservoir was 2,600 psi. The fracture pressure of the reservoir is 4,200 psi. The leak is located at a distance of 7,000 ft from the wellbore. 86

Fig. 4.27—Simulated fluids leaking from the brine zone. CO2 was injected for 30 years at 25 million scf/D (~0.5 million T/yr). The initial hydrostatic pressure of the reservoir was 2,600 psi. The fracture pressure of the reservoir is 4,200 psi. The leak is located at a distance of 7,000 ft from the wellbore. 87

Page

Fig. 4.28—Comparison of simulated fluids leaking from the brine zone and prediction from simple material balance. CO2 was injected for 30 years at 25 million scf/D (~0.5 million T/yr). The initial hydrostatic pressure of the reservoir was 2,600 psi. The fracture pressure of the reservoir is 4,200 psi. The leak is located at a distance of 7,000 ft from the wellbore. 88

Fig. 5.1—The + 50 psi overpressure contour for the bulk injection case with no brine production. The contour extends for a radial distance of 23 miles from the injection well. The boundaries of the reservoir are at 100 miles from the center of the well. CO2 is injected for 30 years at 52 million scf/D (~1 million T/yr). The initial hydrostatic pressure of the reservoir is 2,600 psi. The fracture pressure of the reservoir is 4,200 psi. 91

Fig. 5.2—The + 50 psi overpressure contour for the bulk injection case with two brine producers (P1 and P2). The contour extends for a radial distance of 0.5 miles from the injection well. The boundaries of the reservoir are at 100 miles from the center of the well. CO2 is injected for 30 years at 52 million scf/D (~1 million T/yr). The initial hydrostatic pressure of the reservoir is 2,600 psi. The fracture pressure of the reservoir is 4,200 psi. 93

Fig. 6.1— (a) Base case with one horizontal CO2 injector (b) Engineered case with a horizontal CO2 and a brine injector and two horizontal brine producers 98

Fig. 6.2— (a) Top view of the streamlines originating from the brine injector (source) to brine producer (sink) (b) 3D view of the streamlines originating from brine injector (source) to brine producer (green) and CO2 injector (source) to brine producer (red) 98

Fig. 6.3— Schematic of three engineered patterns place side by side 100

Page

Fig. 6.4— a) Shape of the plume for the high gravity number (0.19) after 30 years of injection. Strong buoyant movement drives the gas towards the top seal as soon as the gas is injected b) Shape of he plume for the low gravity number (0.01) after 30 years of injection. CO2 seems to travel more horizontal distance due to high viscous forces. 103

Fig. 6.5— Size of the required pattern for case 1. 3MMT/yr of gas was injected for a 1,000 ft thick interval for 30 years (The plot is not to scale. It has been enlarged in the Z direction for better visibility)..... 105

Fig. 6.6—Vertical gas velocity from horizontal well (a) Base case (b) Engineered case . Approximately 3 MMT/yr (~156 MMscf/D) of gas is injected over a period 30 years. Brine injection rate from the top injector is approximately 340 bbl/D and brine production from each producer is 200 bbl/D. An extra 60 bbl/Day of brine is produced to control aquifer pressurization. The length of the CO2 injector is 4000 ft. 106

Fig. 6.7— Horizontal gas velocity away from horizontal well (a) Base case (b) Engineered case. Approximately 3 MMT/yr (~156 MMscf/D) of gas is injected over a period 30 years. Brine injection rate from the top injector is approximately 340 bbl/D and brine production from each producer is 200 bbl/D. An extra 60 bbl/Day of brine is produced to control aquifer pressurization. The length of the CO2 injector is 4000 ft. 106

Fig. 6.8— (a) Top view of free gas saturation for the base case after 1,000 years. (b) Top view of free gas saturation for the engineered case after 1,000 years. 3MMT/yr of gas was injected along with brine recirculation for the 30 years. 108

Fig. 6.9— A comparison of trapped gas saturation for the base case and engineered case after 1,000 years. 3MMT/yr of gas was injected for the 30 years. (a1) 3D view of trapped gas saturation for the base case. (a2) 3D view of trapped gas saturation for the engineered case (b1) X-Z view of trapped gas saturation for the base case (Ngv=1.25) (b2) X-Z view of trapped gas saturation for the engineered case (Ngv=0.5)..... 109

Fig. 6.10— (a) Plot comparing dissolved CO2 with time for the base case (blue) and the engineered case (red). (b) Plot comparing trapped CO2 with time for the base case and the engineered case. 3MMT/yr of gas was injected for the 30 years in a 1,000 ft thick interval. 111

Page

Fig. 6.11—Plot comparing mobile CO2 with time for the base case (blue) and the engineered case (red). The brown curve shows the total gas injected for 30 years at the rate of 3MMT/yr. 112

Fig. 6.12—Cumulative gas production rate (gmoles) from the brine producers (red curve). The brown curve shows the cumulative gas injection (gmoles) through the CO2 injector. 114

Fig. 6.13—CO2 injection rate (MMT/yr) for the base case engineered pattern for different vertical permeability values (red curve). The brown curve shows the water injection rate for a specific vertical permeability. The thickness of the base case aquifer is 1,000 ft. 115

Fig. 6.14—CO2 injection rate (MMT/yr) for the base case engineered pattern for different horizontal permeability values (red curve). The brown curve shows the distance between the CO2 injector and brine producer in ft. The thickness of the base case aquifer is 1,000 ft. 116

Fig. 6.15—CO2 injection rate (MMT/yr) for varying aquifer thickness (red curve). The brown curve shows the number of patterns required to sequester 3 MMT/yr of CO2 in an aquifer for a particular aquifer thickness. 117

Fig. 6.16—Horizontal permeability in md for heterogeneous case 120

Fig. 6.17—Relative permeability and capillary pressure curves for Rock Type 1 (Kumar et al. 2002) 121

Fig. 6.18—Relative permeability and capillary pressure curves for Rock Type 2 (Kumar et al. 2002) 122

Fig.6.19—Relative permeability and capillary pressure curves for Rock Type 3 (Kumar et al. 2002) 122

Fig.6.20—Relative permeability and capillary pressure curves for Rock Type 4 (Kumar et al. 2002). 123

Fig. 6.21—Free gas saturation for the heterogeneous case just below the top seal after 1,000 years. 124

Fig. 6.22— 3D view of trapped gas saturation for the heterogeneous engineered case after 1,000 years. 3MMT/yr of gas was injected for the 30 years. Brine recirculation was stopped along with CO2 injection. 125

Page

Fig. 6.23— X-Z view of trapped gas saturation for the heterogeneous engineered case after 1,000 years. 3MMT/yr of gas was injected for the 30 years. Brine recirculation was stopped along with CO2 injection. 125

Fig. 6.24—Plot showing the Z velocity profile along the horizontal well direction in ft/D. The top plot shows the water velocity flowing downwards from the top brine injector and the bottom plots shows the Z velocity of the gas rising upwards. 127

Fig.6.25—Plot showing mobile CO2 with time for the heterogeneous engineered case (red) The brown curve shows the total gas injected for 30 years at the rate of 3MMT/yr. 127

Fig. 6.26—Horizontal permeability in md for the heterogeneous dipping aquifer 128

Fig. 6.27—Plot showing X-Z view of the streamlines originating from the top brine injector to the bottom brine producers. 129

Fig. 6.28—Free gas saturation for the heterogeneous dipping aquifer just below the top seal after 1,000 years. 130

Fig. 6.29—3D view of trapped gas saturation for the heterogeneous dipping aquifer after 1,000 years. 3MMT/yr of gas was injected for the 30 years 131

Fig. 6.30—X-Z view of trapped gas saturation for the heterogeneous dipping aquifer after 1,000 years. 3MMT/yr of gas was injected for the 30 years 131

Fig. 6.31—Plot showing mobile CO2 with time for the heterogeneous dipped aquifer engineered case (red) The brown curve shows the total gas injected for 30 years at the rate of 3MMT/yr. 132

LIST OF TABLES

Page

Table 1.1—Monitoring approaches and options for measuring emissions from geological storage formations. Methods in bold type are best developed. (Table from Benson et al. 2002.) 13

Table 2. 1—Aquifer properties and injection details 27

Table 2. 2—Relative permeability parameters for base case aquifer model 29

Table 2.3—Water/gas relative permeability curve for the base case. 29

Table 6. 1—Parameter values for obtaining zero gas saturation below the top seal .. 107

Table 6.2—Values used in different relative permeability tables (Kumar et al. 2002) 121

1. INTRODUCTION AND LITERATURE REVIEW

1.1 Introduction

The United Nations Intergovernmental Panel for Climate Change (IPCC 2007) insists that anthropogenic greenhouse gas emissions are harmful to the planet and are causing global climate change evident as global temperatures rise and local weather reaches extremes. Total emissions (Fig. 1.1) from fossil fuel consumption and flaring of natural gas were approximately 30 Gt CO_2 in 2006 (EIA 2006). In order to stabilize the concentration of greenhouse gases in the atmosphere, many countries have committed themselves to reduce their greenhouse gas emissions. The IPCC estimates that global emissions will reach ~77 Gt CO_2 /yr by 2100, and the average atmospheric CO_2 concentration will reach ~750 ppm (Albritton and Meira-Filho 2001). To stabilize atmospheric CO_2 concentrations at 550 ppm, global emissions must be continuously reduced so that by 2050, global emissions are 15 Gt CO_2 /yr less than the usual projections, and by 2100, emissions are 50 Gt CO_2 /yr less (Albritton and Meira-Filho 2001, Wigley et al. 1996). This task is enormous and will be exacerbated further by recent legislation that proposes even more stringent goals. To achieve these substantial emission reductions, projects from a diverse portfolio of options should be employed. Projects improving energy conversion and efficiency of fossil fuels, shifting energy production to low-carbon or non-carbon fuel sources, switching to renewable sources of energy, enhancement of natural biological sinks of CO_2 and decreasing the carbon intensity of fossil fuels should be considered. Out of all the potential mitigation options for stabilizing atmospheric GHG concentrations, including injection into deep oceans, depleted oil reservoirs, and unminable coal seams, storage in deep saline aquifers appears to be the most viable option, considering their storage capacity. Efforts across the globe have already begun on

---

This thesis follows the style and format of *SPE Reservoir Engineering and Evaluation.*

storing CO_2 in deep saline aquifers. Industrial scale projects like (> 1 $MtCO_2$/ yr or more) the Sleipner project in the North Sea, the Weyburn project in Canada and the In Salah project in Algeria are often cited as examples of successful CO_2 sequestration. Through these projects, about 3—4 $MtCO_2$ that would otherwise be released to the atmosphere is being captured and stored annually in geological formations.

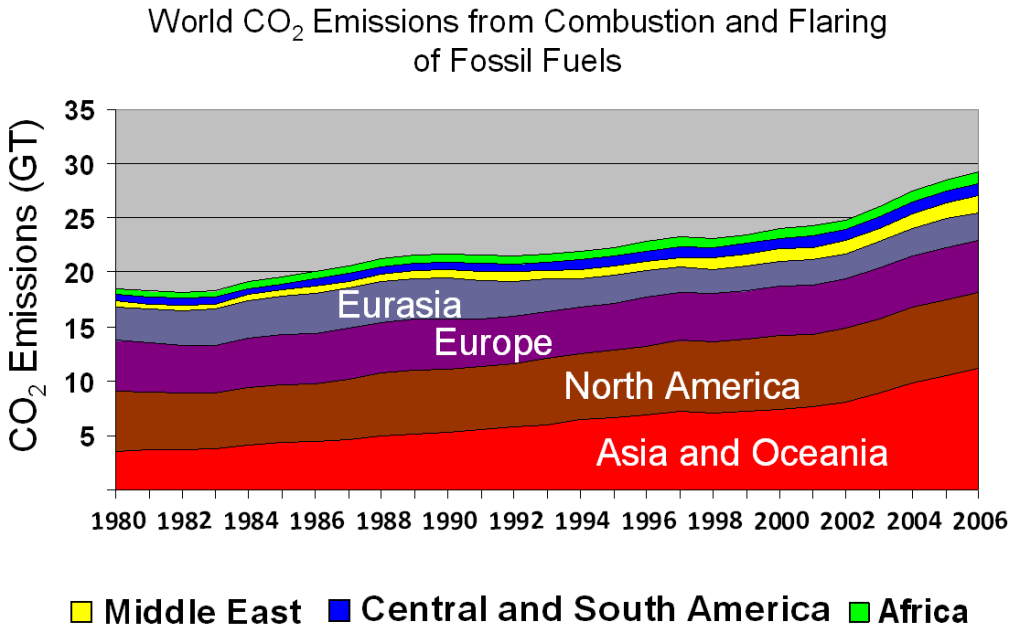

Fig. 1.1—World CO_2 emissions from combustion and flaring of fossil fuels (EIA 2006).

1.2 Geologic CO_2 Storage

Fig. 1.2 is a schematic of various options available for geologic CO_2 storage. While there are uncertainties, given the large amount of anthropogenic CO_2 to be stored, geologic storage is regarded as a likely mechanism to substantially reduce global CO_2 emissions. Capacity of unminable coal formations is uncertain, with estimates ranging from as little as 3 $GtCO_2$ up to 200 $GtCO_2$. Depleted oil and gas reservoirs are estimated to have a storage capacity of 675 to 900 $GtCO_2$. Deep saline formations are presumed to have a storage capacity varying from 100 to 10,000 $GtCO_2$ and some

studies (Davidson et al. 2001; Omerod 1994; Beect et al. 2001) suggest it may be an order of magnitude greater than this. Filling this capacity would account for hundreds to thousands of years of CO_2 emissions. It is difficult to quantify the upper range until additional studies are undertaken (IPCC 2005).

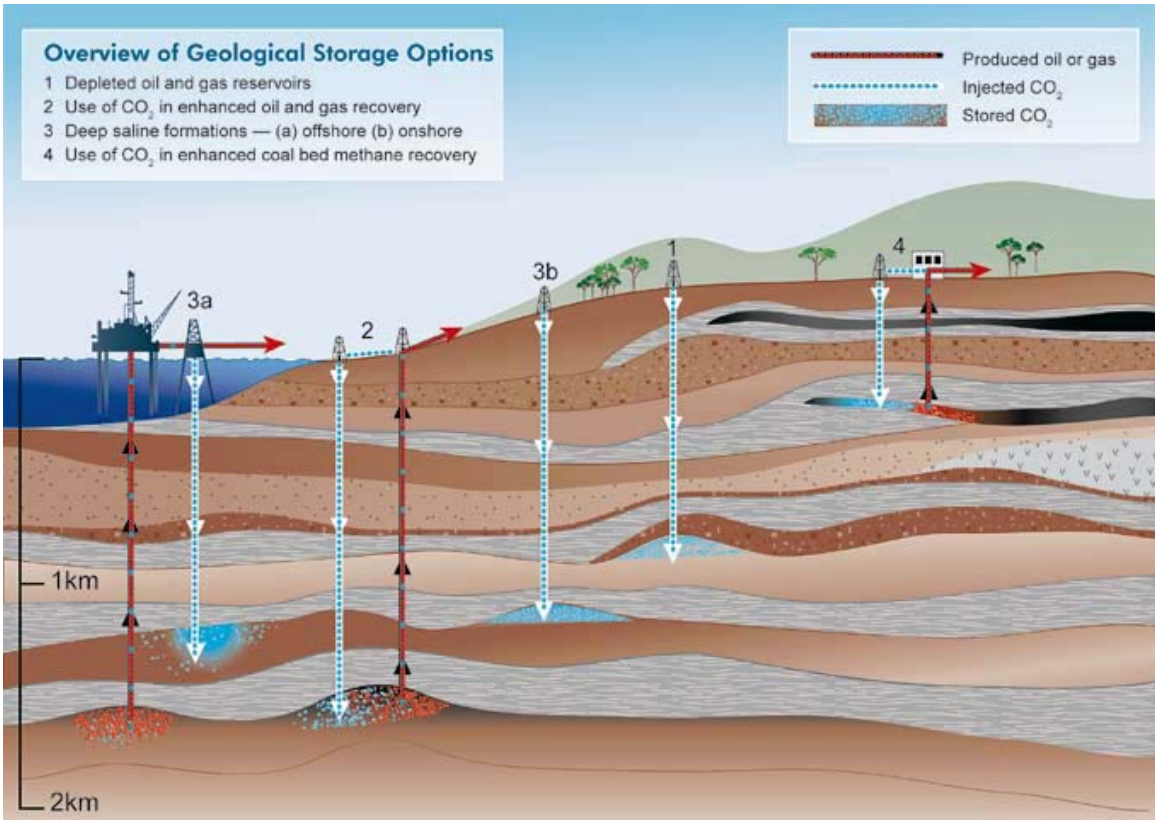

Fig. 1.2— Overview of geological storage options (IPCC, 2007).

Even with this large potential capacity, a major obstacle to public acceptance of sequestration is the lack of insights into the risks associated with it. It is very important to demonstrate that safety and environmental protection of subsurface CO_2 storage can be assured.

One of the critical criteria for evaluating the economics of a geologic sequestration project is the storage potential. It is defined as the amount of CO_2 stored per unit pore volume of aquifer pore volume.

$$s_{CO_2} = \frac{V_{CO_2}}{V_p} \quad \text{.....(1.1)}$$

where V_{CO_2} = Total volume of injected CO_2

V_p = Total available pore volume of aquifer

1.3 Research Objectives

Among various possible solutions to mitigate the increasing concentration of "greenhouse gases" in the atmosphere, geological sequestration seems to be the most attractive and promising one. This research explores various issues related to carbon dioxide sequestration in deep saline aquifers. Issues related to aquifer pressurization, monitoring, and risk mitigation have been studied using a numerical reservoir simulator that models the multiphase flow physics of CO_2 process using the Peng-Robinson equation of state (EOS).

1.3.1 Identifying Risk

Published reports on the potential for sequestration fail to address the necessity of storing CO_2 in a closed system. Injecting such large quantities of CO_2 obviously has a risk associated with it. Several authors have employed a constant-pressure boundary to the reservoir models for calculation of storage potential in the aquifer, an approach that is highly misleading. A closed boundary is not same as an effectively infinite boundary, and an effectively infinitely infinite boundary is not the same as a constant-pressure boundary. Aquifer pressurization can severely limit the storage capacity of an aquifer. The injection pressure should not go above a geomechanically determined fracture pressure. An elevated fluid pressure in the aquifer is risky since the free CO_2 can easily escape from the cap rock due to any breach in the seal integrity over time. Through analytical modeling we show that the pressure buildup in the aquifer over time is substantial and that the required aquifer volume for storage is astronomically

more than what has been envisioned. This renders geologic sequestration of CO_2 a profoundly non-feasible option for the management of CO_2 emissions, unless brine is produced to create voidage and pressure relief.

1.3.2 Monitoring Risk

Aquifer pressurization introduces a risk of CO_2 leakage and a threat to seal integrity. Verification of long-term CO_2 residence in receptor formations and quantification of possible CO_2 leaks are required for developing a risk assessment framework. Important aspects of pressure falloff tests for CO_2 storage reservoirs must focus on reservoir pressure monitoring and leakage detection. Monitoring the long-term integrity of CO_2 storage reservoirs will be a critical aspect for making geologic sequestration a safe, effective, and acceptable method for greenhouse gas control. Although measurement technology applicable for monitoring geologic storage is available from a variety of applications including, natural gas storage, disposal of liquid and hazardous waste, groundwater monitoring, etc., under envisioned carbon emissions constraints, both the volume to be stored and the length of time required for monitoring to mitigate emissions from electric power generation and other applications is imposing.

Pressure behavior in CO_2 storage aquifers has been neglected thus far in the literature because current models assume constant-pressure or infinite-acting aquifer behavior. In reality, a closed aquifer will have significant pressure response during injection, and this research spells out why pressure monitoring makes sense.

1.3.3 Mitigating Risk

The CO_2 injected in bulk form into a deep aquifer is less dense than the resident brine. In this situation buoyancy forces will drive the injected CO_2 upwards in the aquifer until a geological seal is reached. Free-phase CO_2 below the top seal is prone to leak if a breach happens in the top seal. Convective displacement due to small density gradients is a very slow process and the time scales for this process with natural

aquifer flow is thousands of years (Ennis-King and Paterson 2002; Riaz et al. 2006; Hesse et al. 2006). It is important to explore techniques to eliminate buoyancy-driven accumulation of a mobile free-phase CO_2 below the top seal. The main motivation behind this research is addressing two kinds of risks that exist in sequestering CO_2 in deep saline aquifer: the free gas saturation below the top seal and the increase in average reservoir pressure due to CO_2 injection. This research will propose a way to engineer the CO_2 injection system to accelerate dissolution and trapping and control aquifer pressurization. Engineering will eliminate buoyancy-driven accumulation of free gas and avoid aquifer pressurization in the reservoir by producing brine out of the system (equal to the volume of injected CO_2). With this model, risk assessment may ignore the leakage pathways owing to very slow movement of CO_2-saturated brines. This research will show how CO_2 can be securely and safely stored in a relatively smaller and closed aquifer volume and with a greater storage potential.

At this point, it is important to note that this research does not deal with the in-situ mineralization of CO_2 in aquifers. CO_2 mineralization is one of the safest forms of geological storage (Gunter et al. 1993, Noh et al. 2004). However, mineralization takes hundreds to thousands of years and there are many uncertainties in the prediction of the process (Kumar et al. 2004; Pruess et al. 2003). The time scale considered for this study is much smaller than that.

1.4 Literature Survey

Risks to the planet and its societal implications of climate change have been clearly identified by several national and international agencies (DEFRA 2003; IPCC 2007; Stern 2006; EIA 2006). CO_2 capture from stationary point sources and long-term storage in underground geological formations offers a viable means of contributing to an overall global warming mitigation strategy (IPCC 2007; Holloway 2001).

A number of projects involving the underground storage of CO_2 are currently in progress worldwide. These range from small pilot projects like the Nagakoa pilot

project in Japan (Kikuta *et al.* 2005) and the Frio brine project in Texas (Hovorka et al.2006) to industrial scale projects (> 1Mt of CO_2 per year) like Sleipner in the North Sea (Baklid et al. 1996), In Salah in Algeria (Riddiford et al. 2003), and the enhanced oil recovery project at Weyburn in Canada (Wilson and Monea 2004).

The small-scale projects are aimed at developing a better understanding of the multiphase physics of CO_2 injection, whereas the industrial-scale projects have demonstrated the feasibility of injecting CO_2 into subsurface geological reservoirs and are providing platforms for scaling ongoing research efforts (time-lapse geophysical monitoring, reservoir history matching, reaction-transport modeling). Based on the acquired data, reservoir simulation models are being calibrated to replicate the behavior of CO_2 in the ground. The ability to inject a large amount of CO_2 equivalent to the output from a 500 MW (3MMT/yr CO_2) or greater plant is untested as yet.

1.4.1 Aquifer Pressurization Risk

The storage capacity of deep saline aquifers has usually been estimated under the assumption that brine displacement is not a limiting factor and that the in-situ brine will be pushed away to create space for the injected CO_2. The studies for CO_2 disposal purposes assume that the reservoir has infinite extent, a condition that is unlikely to met by the real-world aquifers close to the stationary CO_2 sources. Several authors (Kumar et al. 2005; Baklid and Korbo 1996; Pruess 2004; Nghiem et al. 2004; Sengul 2006; and Izpec et al. 2006) employ a constant-pressure outer boundary when modeling CO_2 injection, which is convenient but misleading. Actually, flow behavior in a reservoir with a constant-pressure boundary does not mimic that of an effectively infinite aquifer, and authors who employ this condition are significantly misrepresenting this case. It is to be understood that sequestration is not a displacement process but permanent storage in a secure, closed system.

Authors like Orr (2004) and Noh et al. (2004), who emphasize the analogies with EOR, are on the wrong track. The consequence of these misrepresentations is that the

volume required for CO_2 storage has been severely underestimated. Schembre-McCabe et al. (2007) demonstrated that mechanisms present during sequestration are very different from traditional EOR operations.

The hydraulic connectivity between deep saline formations and overlying freshwater aquifers updip could be a risk. The displaced brine can migrate to shallower aquifers and can decrease the pH of fresh drinking water and change the level of the water table. According to Holloway (1996), even small CO_2 leaks can severely deteriorate the potable water quality.

Rigg et al. (2001) reports that in continents like Australia most of the desirable basins ("open" aquifers) lie far from the required stationary CO_2 sources. Sometimes the lack of a large aquifer near a high CO_2 emission site requires consideration of a relatively smaller and closed aquifer for CO_2 storage. Through analytical modeling, Economides and Ehlig-Economides (2009) showed that instead of the 1 to 4% of pore volume storage potential indicated prominently in the literature, which is based on an erroneous steady-state modeling approach, CO_2 can occupy no more than 1% of the pore volume, and the pore volume requirement is going to be considerably higher than quoted in the sequestration literature.

Van der Meet et al. (2006) explored various aspects of storage pressure limiting storage potential in finite saline aquifers. Storage capacity is limited by space within a certain geological structure; moreover, the injection pressure at the well will gradually increase as the volume of CO_2 buildup. Thus the maximum amount of CO_2 that can be injected depends on the maximum acceptable pressure increase without fracturing the formation and moving the existing faults. Thus, in a storage operation, a geomechanically determined pressure threshold can be established, above which pressure should not rise (Law 1996; Obdam et al. 2003).

Zhou et al. (2007) studied compartmentalized formations, from which the displaced brine can not easily escape laterally to make room for the injected CO_2 (closed systems). Becker et al. (2009) discussed application of the pressure decline and initial bottomhole pressure vs depth curves to define some of the limiting factors for CO_2 sequestration in Frio brine pilot project. They showed that the fluid flow in the Frio formation is strongly compartmentalized. In some cases even though the aquifer is open, the pressure gradient necessary to displace the native brine out of the system may exceed the fracture pressure gradient.

1.4.2 Leakage Risk

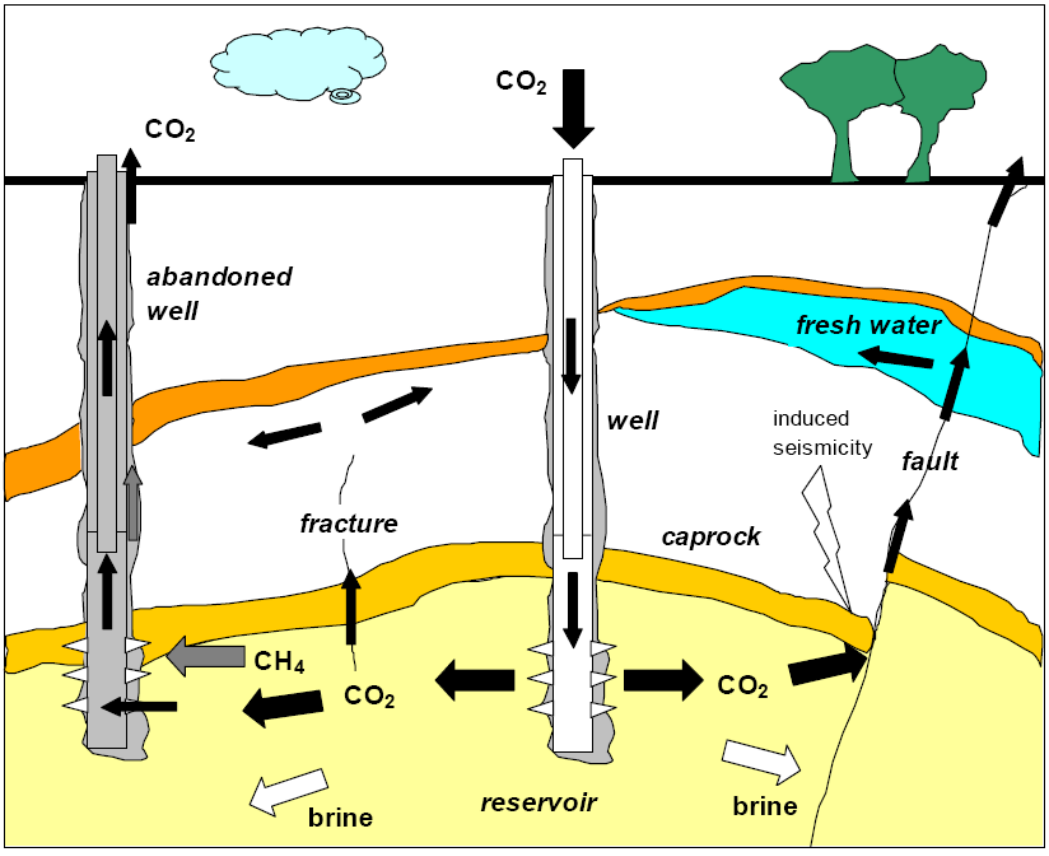

Fig. 1.3—Risks of underground CO_2 sequestration. Black and gray arrows represent CO_2 and CH_4 flows (along abandoned wells, fractures, faults). White arrows represent brine displacement as a consequence of CO_2 injection. (Figure from Damen et al. 2006.)

The injected CO_2 is less dense than the brine; once injected, it has a tendency to move upwards. It might potentially migrate out of the system if it finds a leak, to the subsurface first and then finally to surface. Fig. 1.3 is a schematic of potential leakage pathways for the injected CO_2.

The resident time of CO_2 in the aquifer is considered to be ranging from 1,000 years to 100,000 years (Gunter et al. 1993). Diffusion of CO_2 through the cement is a very slow process, traveling 20 cm in 100 years (Gunter et al. 1993). However, such a long timescale for the resident CO_2 can cause deterioration of the casing and cement plugs. These wells may serve as short-circuit pathways for leakage, with possible contamination of shallow subsurface zones, and ultimately leaking back into the atmosphere (Celia and Bachu 2003).

Another important mechanism for leakage is cap rock failure. Deep saline aquifers have not been characterized and researched as well as hydrocarbon reservoirs due to the limited penetration of their wells. Confirming the integrity of the aquifer seal over its extension is a tedious task. Sometimes the data may not be accurate enough to predict the seal integrity with confidence.

Leakage through fractures and faults that extends through the cap rock and connect to a shallow aquifer updip is a possibility for deep saline aquifers (Zhou et al. 2009). Pasla et al. (2003) varied the range of permeability values to study the impact of fault permeability/porosity structures on the migration of CO_2. Their simulation results show that the fault zone properties, especially permeability in the reservoir, can influence the flow of CO_2 in the reservoir as a consequence of bypassing through conduits or flow compartmentalization because of permeability barriers or low-permeability layers.

It is also very important to keep the injection pressure below the formation fracturing pressure or below the pressure at which the caprock may shear (Law 1996 ; Obdam et

al. 2003). The CO_2 may react with the cap rock, causing it to dissolve and form high-permeability zones (Damen et al. 2006). Seismic disturbance can also cause cap rock failure (Saripalli et al. 2003).

Of all these mechanisms, CO_2 leakage through the wellbore is more controllable than leakage through a cap rock. The leakage through the cap rock depends more on the geological characteristics and extends for a longer distance as compared to well failures. Modern well completion techniques from the oil industry can help identify leaks along the wellbore and squeeze them off using squeeze cementing and zonal isolation techniques.

1.4.3 Pressure Monitoring

Pressure monitoring is one of the critical factors of the overall risk management strategy for geological sequestration projects. Monitoring is likely to be required as of part of the permitting process and public acceptance of CO_2 sequestration. It will be used for various processes like tracking the location and understanding the behavior of the plume, validating the physics of the disposal process, and ensuring the security of storage by leak detection in abandoned wells or through aquifer seals. Additionally, monitoring is necessary for satisfying regulatory requirements. It is important to ensure that the CO_2 is not leaking in the shallow natural resources such as ground water and endangering local populations.

Monitoring also provides feedback to reservoir simulation studies. Commonly obtained pressure and temperature data can be integrated into the reservoir models to improve accuracy and to estimate unknown parameters by history matching.

Each of the three existing CO_2 storage projects uses a different kind of monitoring technique, depending upon the specific need of the project (Benson 2006). For example, at Weyburn, a combination of geochemical sampling and soil gas surveys along with 3D time-lapse seismic is used to demonstrate the containment of injected

gas (Wilson et al. 2004). Sleipner uses a combination of 2D and 3D time lapse seismic monitoring to track the movement of the plume in the Utsira formation in the North Sea (Arts et al. 2002). The In Salah project in Algeria plans to install permanent 3D seismic monitoring array and introduce tracers for tracking CO_2 breakthrough into the gas reservoir (Ebrom et al. 2006). In addition to these major commercial scale projects, monitoring methods have been implemented on smaller projects like the Nagakoa pilot project in Japan (Kikuta et al. 2005), the Otway basin in Australia (Watson et al. 2004), and the Frio brine pilot in Texas (Hovorka 2006). Surface-to-borehole seismic imaging, cross-well seismic, cross-well electronic monitoring, well logs, pressure transients, natural and introduced tracers, brine and gas composition sampling and analysis, flux accumulation chambers, soil gas sampling, and ground water sampling have been used to monitor the fate and migration of injected CO_2 (Benson et al. 2002).

Newer techniques such as gravity and electrical measurements may also be useful (Hoversten et al. 2002). Geochemical methods are useful for directly monitoring the movement of CO_2 in the subsurface and for understanding the mineralization trapping mechanisms (Gunter et al. 1998; Gunter and Perkins 2001). Miles et al. (2005) assessed the eddy covariance method for assessing surface fluxes. Well logs are one of the common methods for evaluating geological formations. For the purpose of CO_2 storage, routine well logs will be most useful for ensuring that the well is not providing a leakage pathway to the injected CO_2, but the resolution of well logs may not be enough to detect very small seepage rates through micro-cracks (Benson et al. 2002).

Table 1.1 summarizes a large of number of approaches for monitoring geological storage. The reliability, resolution and sensitivity of these techniques need to be tested since all of these monitoring techniques have been adapted from other applications (Benson 2006). The most practical and effective monitoring approach will depend on a combination of various monitoring techniques. Different monitoring techniques will

be applicable to different sequestration projects. For upcoming sequestration projects, there should be enough flexibility to deploy some of these methods and tailor them based on the new requirements and outputs from research and development.

Several innovative and relatively new monitoring methods are available today that can be used to detect, locate, and quantify emissions. However, it is expected that some parameters such as injection rate and injection well pressure will be measured routinely.

Table 1.1—Monitoring approaches and options for measuring emissions from geological storage formations. Methods in bold type are best developed. (Table from Benson et al. 2002.)

System Component	Monitoring Methods	Benefits	Drawbacks
Storage reservoir	**Seismic** Gravity Well logs Fluid sampling	History match to calibrate and validate models Early warning of migration from the storage reservoir	Mass balance difficult to monitor Dissolved and mineralized CO_2 difficult to detect
Shallower saline formations below secondary seals	**Seismic** **Pressure** Gravity Well logs Fluid sampling	Good sensitivity to small secondary accumulations (~10^3 tonnes) and leakage rates Early warning of leakage	Detection difficult if secondary accumulations do not occur Dissolved and mineralized CO_2 difficult to detect
On-shore			
Groundwater aquifers	**Seismic** **Pressure** **EM** Gravity SP Well logs Fluid sampling	Sensitivity to small secondary accumulations (~10^2-10^3 tonnes) and leakage rates More monitoring methods available Detection of dissolved CO_2 less costly with shallow wells	Detection after significant migration has occurred Detection after potential groundwater impacts have occurred
Vadose zone	**Soil gas and vadose zone sampling**	CO_2 accumulates in vadose zone making detection easier compared to atmospheric detection Early detection in vadose zone could trigger remediation before large emissions occur	Significant effort for null result (e.g. no CO_2 from storage detected) Detection only after some emissions are imminent Does not provide quantitative information on emission rate
Terrestrial ecosystems	**Vegetative stress**	Vegetative stress can be readily observed using routine observation Satellite and plane-based methods available for quick reconnaissance	Detection only after emissions have occurred Vegetative stress can be caused by other factors Land use change could alter the baseline Does not provide quantitative information on emission rates May not be useful in some ecosystems (e.g. deserts)
Atmosphere	**Eddy covariance** **Flux accumulation chamber** Optical methods	Good for quantification of emissions	Distinguishing storage emissions from natural ecosystem and industrial sources necessitates comprehensive monitoring May not be best suited for detecting anomalous emissions due to relatively small footprint compared to the size of the plume Significant effort for null result
Offshore			
Water Column	Ship based fluid sampling and analysis Autonomous vehicles with CO_2, pH and carbon cycle sensors	Direct measurement of water column and fluxes (using inverse models)	Distinguishing storage related fluxes from natural variability comprehensive monitoring Quantifying separate phase CO_2 flux Significant effort for null result
Atmosphere	Optical methods Eddy covariance	Direct measurement of emission rate	Technology not well developed for this application Quantification of emissions may be impractical Changing emission footprint from ocean currents Likely to be costly to maintain Significant effort for null result

1.4.4 Residual Trapping

Immobilization of CO_2 injected into a saline aquifer can occur in variety of ways: by capillary trapping, solubility trapping, structural trapping, and mineralization trapping. When CO_2 is injected, it displaces the in-situ brine, in a process called drainage. After the cessation of injection, the CO_2 rises to the top of the aquifer since it is less dense than the resident brine. Due to this countercurrent flow, the brine interacts with the tail of the rising CO_2 plume. Thus, wetting phase (brine) enters the pores occupied by the non-wetting phase (CO_2), leading to a significant trapping of the nonwetting phase inside the pores. This process is called imbibition. Due to the difference in the saturation history during imbibition and drainage, the system experiences a relative permeability hysterisis. Consequently, the drainage relative permeability curve follows a different path than the imbibition relative permeability curve (Fig. 1.4).

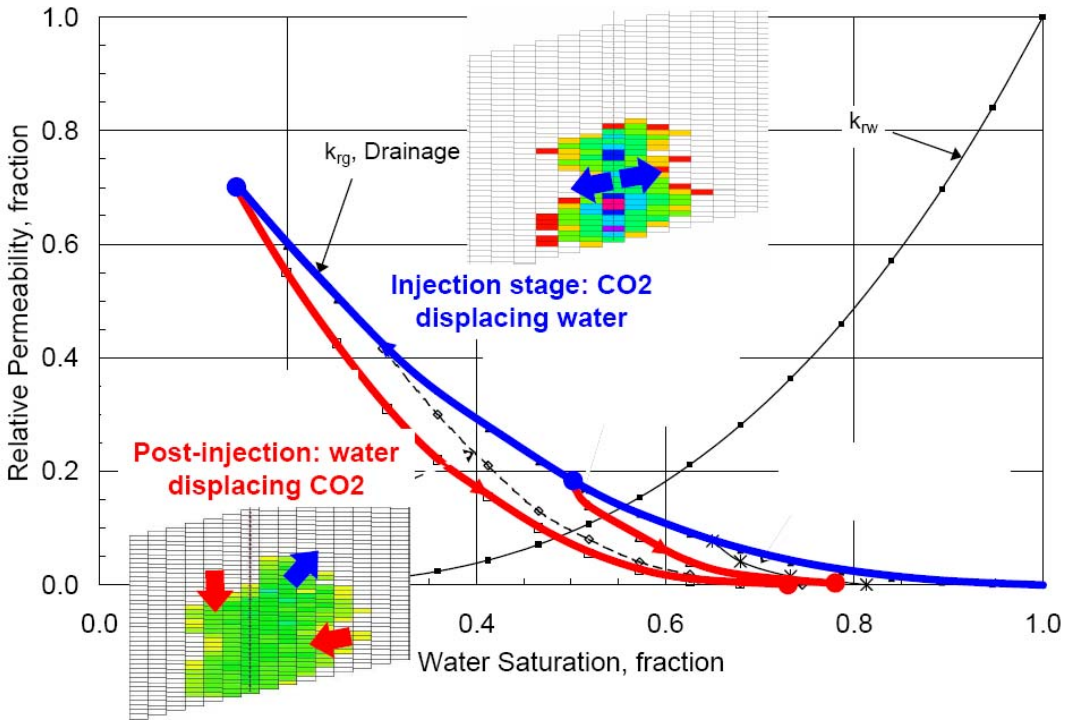

Fig. 1.4—Relative permeability hysterisis. The blue curve is for drainage and red for imbibition. Figure illustrates two imbibition cases with different starting points on the drainage curve, resulting in different residual saturation. (Figure from Kumar et al. 2008.)

Kumar et al. (2005) studied these mechanisms for a heterogeneous aquifer and concluded that well completion is a very important factor in deciding the fate of injected CO_2. A substantial amount of CO_2 can be trapped if injected at the bottom of the aquifer to rise under the effect of buoyancy. Spiteri et al. (2005) and Juanes et al. (2006) investigated the effects of hysteresis in the relative permeability of the hydrocarbon phase in a two-phase system. They proposed a new model of trapping and showed that capillary trapping can significantly limit the movement of CO_2 inside the aquifer. Their proposed formulation overcomes some of the limitations of existing trapping and relative permeability models.

Mo et al. (2005) suggested that increase in viscous to gravity forces will increase the sweep efficiency resulting in more CO_2 trapping as residual gas. Ide et al. (2007) studied the interplay between the viscous and gravity forces and capillary trapping of CO_2. They correlated the amount of trapping after the cessation of injection to the ratio of gravity to viscous forces, also called as gravity number.

1.4.5 Solubility Trapping

Injection of CO_2 into aquifers is carried out at supercritical conditions. The concentration of aqueous CO_2 in solution is important for estimating the amount of carbon-dioxide that can be stored. Hangx (2005) summarized the experimental studies done on understanding the solubility behavior of CO_2. Along with the experimental studies, theoretical efforts have been made to model the solubility of carbon dioxide in aqueous solutions (Nighswander et al. 1989; Carroll et al. 1991; Duan and Sun 2003; Duan et al. 2005).

Fig. 1.5 shows the solubility of CO_2 in mole fraction vs depths at different salinities when the temperature and pressure gradients are assumed to be 1°F/100 ft and 0.44 psi/ft respectively. Clearly, the solubility of CO_2 is constant after a depth of 2,000 ft for a specific salinity. In general, the solubility of CO_2 in brine increases with

pressure, decreases with temperature, and decreases with increasing salinity (Hangx 2005).

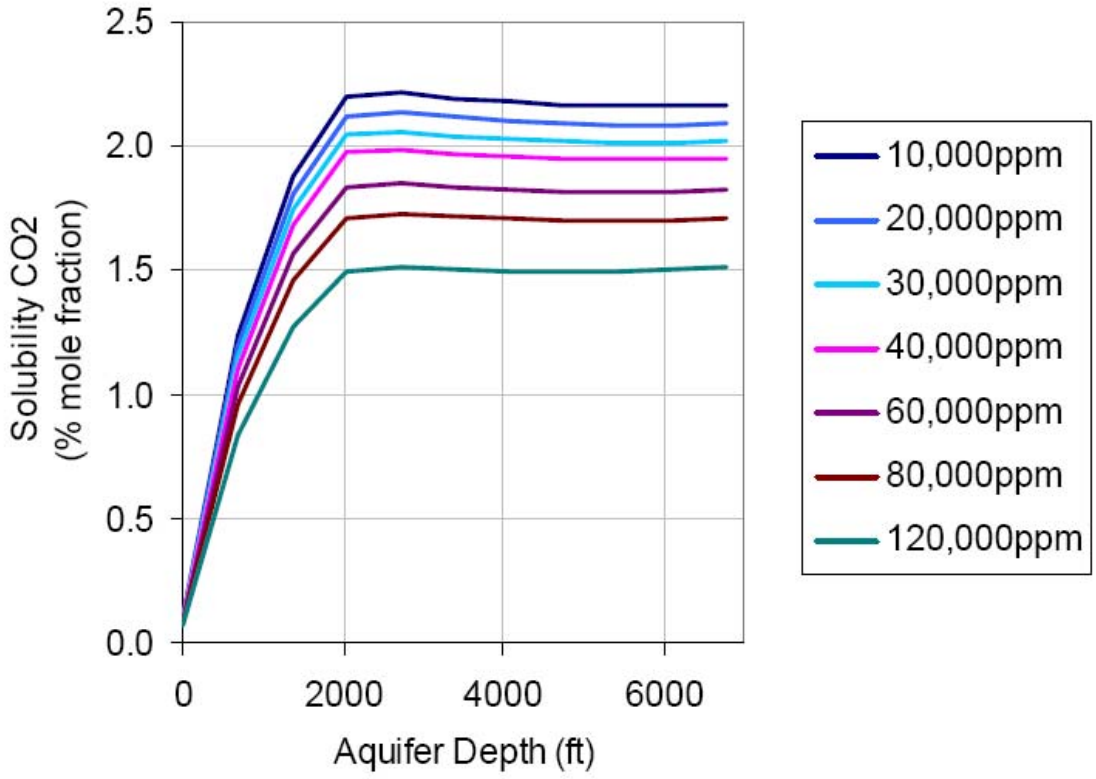

Fig.1.5—The solubility in mole percent predicted by the Duan EOS (Hangx 2005) for a temperature and pressure gradient of 1°F/100 ft and 0.44 psi/ft. Surface temperature and pressure were assumed to be 61°F and 14.7 psia, respectively. Solubility increases with depth to ~2,000 ft, then remains fairly constant. Brine salinity has a significant effect on the plateau solubility. (Figure from Burton and Bryant 2007.)

Duan and Sun (2003, 2005) is the most complete model that exists to date for modeling solubility of CO_2 in pure water and aqueous solutions from 0 to 260°C and from 0 to 2,000 bar total pressure. The model is extended to not only predict the solubility of CO_2 in pure water and NaCl solutions but also in more complex systems, which may include Ca^{2+}, K^{+}, Mg^{2+}, and SO_4^{2-} ions.

1.4.6 Accelerating Residual and Dissolution Trapping

After the end of injection, free-phase CO_2 slowly dissolves in the contacted brine, slightly increasing the brine density. With time, CO_2-laden brine sinks to the bottom of the aquifer, and instability due to density inversion kicks off a natural convection mechanism, inducing additional contact with undersaturated brine and further dissolution. However, convective displacement due to small density gradients is a very slow process and the time scale for the dissolution process under natural aquifer flow is thousands of years (Ennis-King and Paterson 2002; Riaz et al.2006; Hesse et al. 2007). The dissolution mechanism (under diffusion) does not significantly increase the storage potential of the aquifer, and the CO_2 stays for a long time as a free phase below the top seal.

Fig. 1.6 from IPCC (2008) shows the quantitative timings of storage security for various trapping mechanisms. Stratigraphic trapping is one of the fastest trapping mechanisms. However, it is highly risk prone since the free CO_2 can easily escape from the cap rock due to any breach in the seal integrity over time. The solubility of CO_2 in brine is extremely low (3 to 5% by mass) at reservoir conditions (Burton and Bryant 2007). Model calculations of simulations in the Upper Plover formation (Australia) indicate that complete dissolution is expected to take place on a time scale ranging from 10,000 to 100,000 years (Ennis-King and Paterson 2003). Simulation studies on the Utsira formation at Sliepner suggest that CO_2 will take 5,000 years to dissolve (Lindeberg and Wessel-Berg 1997). As CO_2 is dissolved, it will form ionic species (H^+ and HCO_3^-), accompanied by a rise in the pH. These ions in turn react with the minerals of the formation; depending upon the mineralogy of the formation, some fraction may be converted to stable carbonate minerals (mineral trapping). CO_2 mineralization is one of the safest forms of geological storage (Gunter et al. 1993).

However, it takes hundreds to thousands of years and there are many uncertainties in the prediction of the process.

Kumar et al.2005 proposed a strategy to inject low and let rise, where CO_2 is injected in the bottom part of the aquifer, and after the injection is finished, the CO_2 will continue to migrate under the effect of buoyancy. As the CO_2 rises, it will leave a trail of residually trapped gas behind it. With this approach, vertical movement toward the seal is retarded and the storage is permanent. In principal, CO_2 can be prevented from reaching the aquifer seal by choosing the right amount of CO_2 to be injected through each well (Bryant et al. 2006). However, this strategy is extremely sensitive to aquifer dip and thickness, and it is often difficult to achieve very low gas saturation below the top seal at practical injection rates for a commercial sequestration project. A typical 500 MW power plant will produce 3 million tones (~ 156 million scf/D) of CO_2 every year. Several injection wells will be needed to optimize the sequestration operation with the inject-low-and-let-rise strategy.

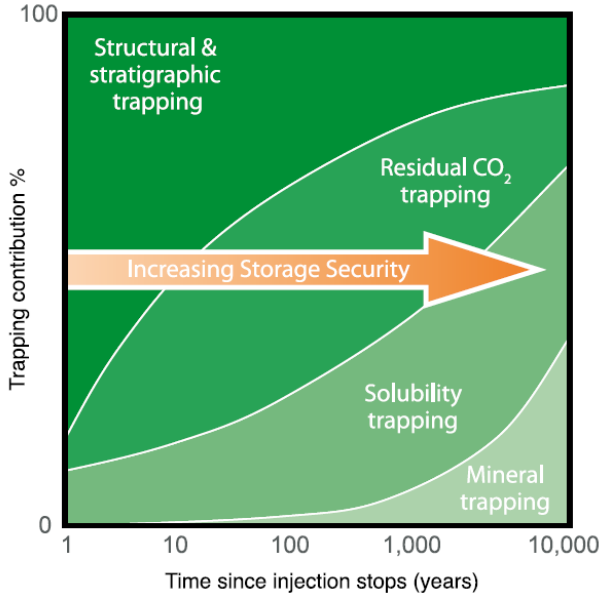

Fig. 1.6—Timing of various mechanisms for storage security (IPCC, 2008).

Another approach suggests brine injection to accelerate dissolution by pumping brines from regions where it is undersaturated to regions occupied by CO_2 (Leonenko et al. 2006). Even though that technique has advantages in securing the storage, it will severely limit the storage potential of the aquifer. Since the brine injection is uncontrolled, there are chances that the injected CO_2 may move to thief zones such as fractures, faults, and abandoned wells. The timeframe of brine injection considered by Leonenko et al. is 200 years, which is much larger than observed in the oil industry. The cost to operate a brine injection/extraction system for a couple of centuries could be prohibitive. The rate at which the injected CO_2 comes into contact with undersaturated brine limits the rate of dissolution, and considering practical injection rates for a 500-MW to 1-GW power plant, it is highly probable that the injected CO_2 would be more buoyant than the brine, so it would migrate upward and accumulate below the top seal more quickly than its competing dissolution trapping mechanism.

1.4 Review of Sections

Section 2 summarizes some key features of CMG's compositional simulator for generalized EOS for greenhouse gas (GEM-GHG). It describes how solubility and relative permeability hysterisis is modeled in the simulator. To correctly set up a compositional simulation, it is important to understand various physical and chemical processes involved.

Section 3 discusses issues related to aquifer pressurization due to CO_2 injection. An analytical model is developed for injection into a closed system. The results from the analytical model match well with a numerical reservoir simulator.

Section 4 discusses the importance of taking regular pressure falloff tests for CO_2 injection. It also discusses how average pressure of the reservoir can be monitored and leakage can be detected using pressure falloff tests.

Section 5 discusses the importance of producing brine from the aquifer for pressure relief and increased storage potential.

Section 6 discusses engineering techniques to accelerate CO_2 dissolution and trapping in aquifers and further increases the storage potential. It addresses various risks associated with bulk-phase CO_2 injection.

Section 7 summarizes and concludes the overall findings from this thesis.

2. BASE CASE SIMULATION FEATURES

In this section, some of the important features of CMG's generalized EOS model simulator for green house gases (GEM GHG) are applied to set up the base case simulation parameters used throughout this study. GHG, the new additional module from CMG, is an adaptive tool for carrying out compositional simulation for sequestration of CO_2 and other greenhouse gases in saline aquifers. The modeling of CO_2 storage in saline aquifers involves the solution of the component transport equations, the equations for thermodynamic equilibrium between the gas and aqueous phases, and the equations for geochemistry. The latter involve reactions between the aqueous species and mineral precipitation and dissolution. They are based on an adaptive implicit formulation, which helps in deciding for each grid and each time step whether to use fully implicit or explicit solution methods. During subsequent simulation runs, blocks may be switched to explicit if an adaptive/implicit formulation and a stability-switching criterion is used. Consisting of the usual capability of other simulators, CMG's GHG simulator brings advance options for modeling mass transfer of components into different phases (solubility) and aqueous phase density and viscosity correlations. In this section, Section 2.1 discusses the modeling of phase behavior of a CO_2-brine system, followed by Section 2.2 that discusses the specifics of solubility modeling in CMG. Section 2.3 discusses the model used to model residual trapping and hysteresis, and Section 2.4 describes the properties of the base case simulation model considered for this research.

2.1. Phase Behavior of Co_2 -Brine System

The Peng-Robinson (1976) EOS (PR-EOS) is used for modeling CO_2 —H_2O-C1 mixture behavior. CO_2, H_2O, and C1 are used as pure components. Standard properties are given for the PR-EOS for these components. Typically C1, is used as a "trace gas" (CMG keyword "TRACE-COMP"). The idea is to have a tiny trace of C1 present as residual gas in the aquifer to add some compressibility to the system; this helps

converge the equations as reservoir simulation techniques were not really designed to handle nearly incompressible systems. This "limitation' could be removed by using keyword "AQFILL ON," but this adds complexity to the model and numerical solutions. The solubility of CO_2 in brine is modeled using dynamic phase partitioning by Henry's law. Enhanced solubility models are used in GEM-GHG for specific components, making the Henry's constant a function of temperature, pressure and salinity. The gas density is calculated with the PR-EOS. The gas viscosity is estimated from the Jossi, Stiel, and Thodos correlation (Reid et al. 1977). The aqueous phase density and viscosity are calculated respectively from the Rowe and Chou (1970) correlation and the Kestin et al. (1981) correlation.

2.2. Modeling Solubility and H_20 Vaporization

CO_2 solubility in brine is calculated by solving the equality of fugacities of CO_2 in the gas and aqueous phase (Nghiem et al., 2004). Upon injection, CO_2 dissolves in the aqueous phase, and it can be represented by the following chemical reaction:

$$f_{CO_2,g} = f_{CO_2,aq} . \quad \text{..... (2.1)}$$

The = sign represents a reaction that is reversible. The gas fugacity $f_{CO_2,g}$ is calculated with a cubic equation of state (Peng and Robinson 1976) and the aqueous phase fugacity $f_{CO_2,aq}$ is calculated from Henry's law.

$$f_{CO_2,aq} = H_{CO_2,aq} . y_{CO_2,aq} . \quad \text{..... (2.2)}$$

In Eq. 2-2 , $H_{CO_2,aq}$ is Henry's constant for CO_2 solubility in brine and $y_{CO_2,aq}$ is the mole fraction of CO_2 in brine. Since Henry's law constant is a function of pressure, temperature, and salinity, in GEM-GHG it is calculated using several correlations. Harvey (1996) published correlations for Henry's constant of many gaseous components including CO_2. Gas solubility depends on the salinity of the aqueous phase. The solubility of light gases normally decreases with increasing salinity; this

phenomenon is referred to as the salting-out process. Models for salting-out coefficients have also been implemented in GEM-GHG.

$$\ln(H^s{}_i) = \ln(p^s{}_{H_2O}) + A(T_{r,H_2O})^{-1} + B(1-T_{r,H_2O})^{0.355}(T_{r,H_2O})^{-1} + C[\exp(1-T_{r,H_2O})](T_{r,H_2O})^{-0.41}$$

..... (2.2)

where

$H^s{}_i$ = Henry's constant for component i at the saturation pressure of H_2O $p^s{}_{H_2O}$ = Saturation pressure of H_2O in MPa at T(K)

T_{c,H_2O} = Critical temperature of H_2O (K)

T_{r,H_2O} = Reduced temperature of H_2O

A = -9.4234

B = 4.0087

C = 10.3199

The saturation pressure of H_2O at T is calculated from the Saul and Wagner (1987) correlation. The Henry's law constant at p and T is then given by:

$$\ln(H_i) = \ln(H^s{}_i) + \frac{1}{RT}\int_{p^s{}_{H_2O}}^{p} \bar{V}_i dP \text{ , ...} \quad (2.3)$$

where $\bar{V}_i$ is the partial molar volume of component i in the aqueous phase. For CO_2, the correlation due to Garcia (2001) is used:

$$\bar{V}_{CO_2}(cm^3/mol) = 37.51 - 9.585 \text{ X } 10^{-2}T + 8.740 \text{ X } 10^{-4}T^2 - 5.044 \text{ X } 10^{-7}T^3 \text{ , (2.4)}$$

where T is the temperature in °C.

The salting-out coefficient is defined by the following relation between Henry's constant in pure water and in brine:

$$\ln\left(\frac{H_{salt,i}}{H_i}\right) = k_{salt,i}.m_{salt}\ , \quad \text{..... (2.5)}$$

where

$H_{salt,i}$ = Henry's constant of component *i* in brine (salt solution)

H_i = Henry's constant of component *i* at zero salinity

$k_{salt,i}$ = salting-out coefficient for component i

m_{salt} = molality of the dissolved salt (mol/kg H_2O)

Bakker (2003) gives the following correlations for the salting-out coefficients for CO_2 and CH_4:

$$K_{salt,CO_2} = 0.11572 - 6.0293 \text{ X } 10^{-4}T + 3.5817 \text{ X } 10^{-6}T^2 - 3.7772 \text{ X } 10^{-9}T^3, \text{ . (2.6)}$$

where T is the temperature in °C.

The related GEM-GHG keyword is "SOLUBILITY HENRY," "HENRY-CORR-CO_2." These keywords activate the use of Harvey's correlation for CO_2 Henry's constant. Use of this option makes the Henry's constant a function of pressure, temperature, and salinity.

Another important aspect is the vaporization of H_2O. It has been reported that complete vaporization of H_2O can occur during gas injection around the wellbore, which would in turn affect the gas injectivity. The associated GEM keyword to model water vaporization is "H2O_INCLUDED."

2.3. Land's Model for Gas Trapping

Residual trapping is caused by wettability and capillary effects in porous media. Spiteri et al. (2005) provide a comprehensive summary of several residual gas trapping models. The dependence of the relative permeability on the saturation path or history causes residual trapping. It is also is referred to as *capillary hysteresis*. In this thesis, Land's model (Land 1968) is used to calculate the trapped gas saturation. The input parameter for this model is maximum residual gas saturation for a particular rock type.

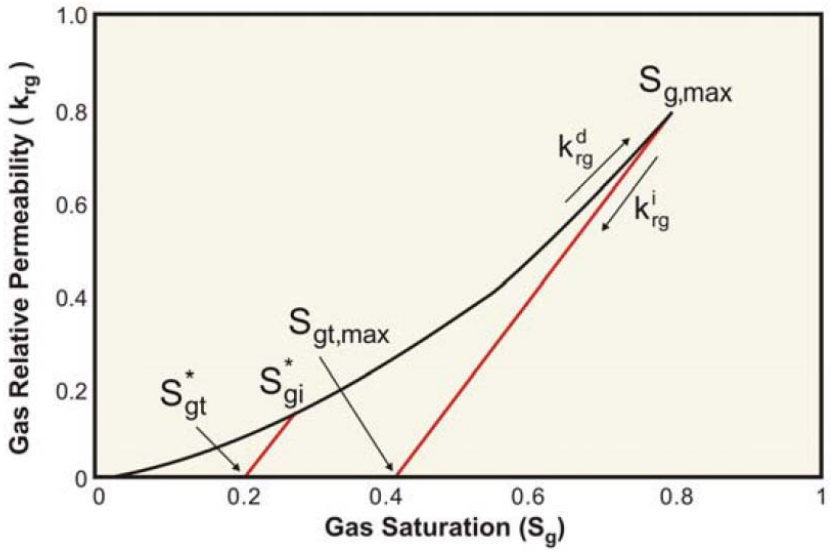

Fig. 2.1—Land's residual gas trapping model (Nghiem et al. 2009).

Fig. 2.1 shows a sample relative permeability curve exhibiting hysteresis. As the gas saturation increases during the injection, the gas relative permeability follows the drainage curve k^d_{rg} (black curve). At a saturation S^*_{gi}, the saturation history reverses and the gas saturation decreases. The gas relative permeability then follows the imbibition curve ki_{rg} (red curve). The Land's coefficient C is expressed as:

$$C = \frac{1}{S_{gt,\max} - S_{g,\max}}, \quad \text{..... (2.7)}$$

where, $S_{g,\max}$ is the maximum gas saturation that could be attained and $S_{gt,\max}$ is the maximum trapped gas saturation. The residual gas saturation for a given S^*_{gi} can be calculated as

$$S^*_{gt}(S^*_{gi}) = \frac{S^*_{gi}}{1 + CS^*_{gi}} \quad \text{.....(2.8)}$$

The amount of trapped gas is sensitive to relative permeability curves and maximum trapped gas saturation. The related GEM keyword is "HYSKRG."

2.4 Description of Base Case Model

A 3D homogeneous aquifer with a constant-rate injector was simulated for the base case. The GEM simulator was used with the GHG option. Simulations for 30 years of CO_2 injection followed by 1,000 years of natural gradient flow were made.

The model dimensions are 25,000 ft X 25,000 ft X 1,000 ft, as shown in Fig. 2.2. The boundary conditions are no flow, which a default for CMG-GEM. However, for simulating an aquifer with an open boundary with a large part of the aquifer outside the simulation domain, volume modifiers are used. Large pore volume multipliers of the order of 10^6 (keyword VOLMOD in GEM) are used on the boundary blocks to provide a constant-pressure boundary effect.

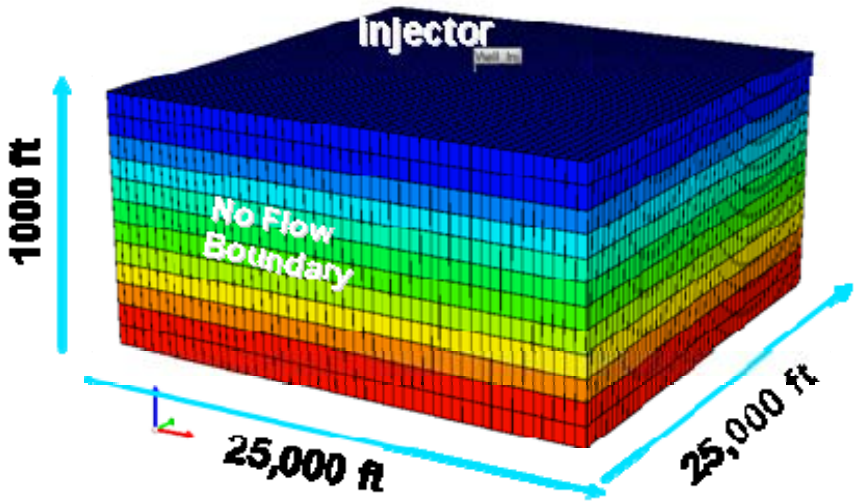

Fig. 2.2—Schematic of the base case aquifer model.

Table 2. 1—Aquifer properties and injection details

Reservoir Description	
Length (ft)	25,000 (~ 5 Miles)
Width(ft)	25,000 (~ 5 Miles)
Height (ft)	1,000
Depth of Top Seal of the Aquifer (ft)	6000
Pressure at the Top Seal (Psi)	2,600
Temperature (^{o}F)	150
Salinity (ppm)	100,000
Porosity	0.25
Permeability (md)	100 (Homogeneous)
Kz/Kx	0.1
Dip , degree	0
Injection Details	
Maximum Injection BHP (psi)	4,200
Maximum Injection Rate (million scf/D)	10 (30 Years)
Injection Well Skin	0
Injection Gas Composition	100% ,CO_2
Simulation Period	1,000 years

The relative permeability curve (Tables 2.2 and 2.3) was calculated using the following equations and parameters (Kumar 2004) :

For $S_g \leq S_{gr}$:

$k_{rg} = 0.$ .....(2.9)

For $S_g > 1\text{-}S_{:}$

$k_{rw} = 0.$ .....(2.10)

For $S_g \geq S_{gr}$:

$$k_{rg} = k_{rg}^{o}\left(\frac{S_g - S_{gcr}}{1 - S_{wrg} - S_{wirg}}\right)^{N_g} . \quad \text{.....(2.11)}$$

For $S_g \leq 1 \leq S_{wrg}$:

$$k_{rwg} = k_{rw}^{o}\left(1 - \frac{S_g - S_{gcon}}{1 - S_{wrg} - S_{gcon}}\right)^{Nw} , \quad \text{.....(2.12)}$$

where k_{rg} = gas end point relative permeability

k_{rw} = water end point relative permeability

S_g = gas saturation

S_{gcr} = critical gas saturation

S_{wirg} = irreducible water saturation

S_{wrg} = residual water saturation during a gas flood

S_{gcon} = connate gas saturation

N_g = gas relative permeability exponent

N_w = water relative permeability exponent in gas water curves

Table 2. 2—Relative permeability parameters for base case aquifer model

Gas end point relative permeability , k_{rg}	1.0
Water end point relative permeability, k_{rw}	0.334
Connate gas saturation, S_{gcon}	0.25
Critical gas saturation, S_{gcr}	0.25
Irreducible water saturation, S_{wirg}	0.25
Residual water saturation , S_{wrg}	0.25
Water relative permeability exponent, N_w	2
Gas relative permeability exponent, N_g	2.5

Table 2.3—Water/gas relative permeability curve for the base case.

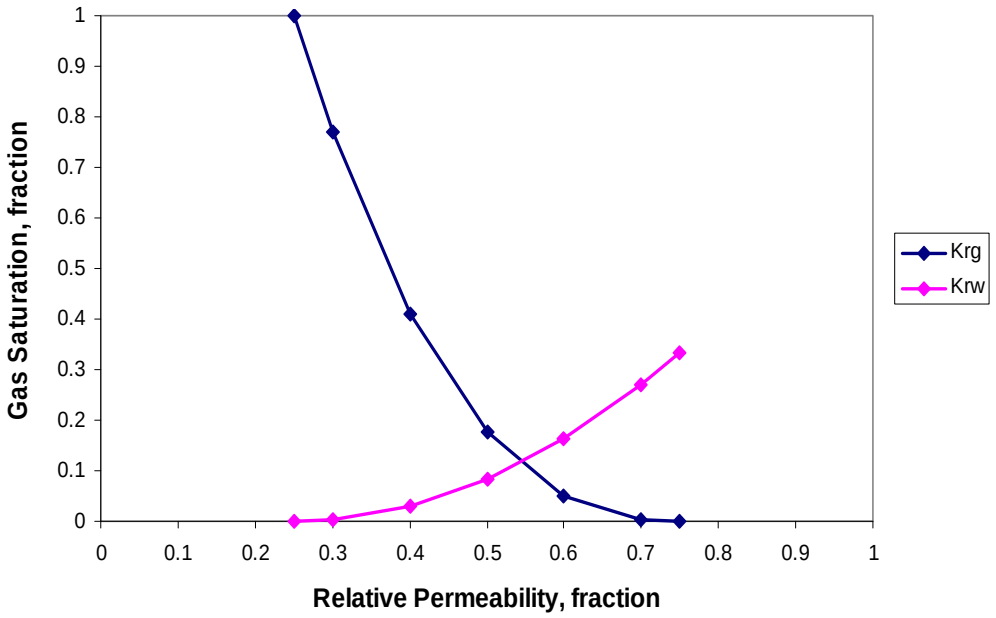

Land's model is used for modeling residual trapping. The Holtz (2002) correlations were used to calculate the maximum residual gas saturation since they are applicable for typical sandstones found deep in the earth and are a possible target for geological sequestration. The proposed model is a function of porosity, permeability, capillary pressure, and initial water saturation.

$$\phi = \left(\frac{k}{7X10^{7}} \right)^{\frac{1}{9.606}} , \quad \text{.....(2.13)}$$

$$S_{gr}^{\max} = 0.5473 - 0.9696\phi , \quad \text{.....(2.14)}$$

$$S_{wirr} = 5.6709 \bullet \left(\frac{\log(k)}{\phi} \right)^{-1.6439} , \quad \text{..... (2.15)}$$

where

ϕ is porosity

k is permeability in md

$S^{\max}_{gr}$ is the maximum residual gas saturation

S_{wirr} is the irreducible water saturation

For a porosity value of 0.25 for the base case, the maximum residual gas saturation is approximately 0.3.

2.5. Section Conclusions

The GEM-GHG simulator reproduced results very similar to those shown by other investigators (Kumar et al. 2004, Kumar 2008, Burton and Bryant 2007). This tool is used for other studies done in the thesis.

3. AQUIFER PRESSURIZATION DUE TO CO_2 INJECTION

IPCC estimates the storage capacity of deep saline aquifers to be at least 1,000 gigatonnes. Injecting such large quantities of CO_2 in a limited volume will result in elevated fluid pressures in the formation. Injecting at a pressure above the formation fracture pressure causes a fracture to form in the formation. This fracture may extend to the aquifer seal, providing a pathway for CO_2 and saline brine to flow towards overlying freshwater aquifers used for drinking and irrigational purposes (Braunt et al. 2002; Nicot 2008). The most important question to answer here is the aquifer volume required to sequester such large quantities of CO_2 given how much the aquifer will be pressurized above the initial aquifer pressure. If the pore volume of the aquifer is too small, then the pressure increase can be too high too soon.

This section will try to explore answers to some of the questions raised above and dispel myths associated with bulk phase CO_2 injection. Section 3.1 of this section compares various modeling approaches for CO_2 injection. Section 3.2 compares the injectivity behavior of aquifers with drainage area of different sizes and boundary conditions. Section 3.3 show the analytical model as an alternative to simulation that enables accurate measure of storage potential and the sheer number of wells needed for bulk CO_2 injection, and Section 3.4 concludes the section.

3.1. Flaws With Current Modeling Approaches

Most of the prior modeling work has assumed infinite capacity of the target aquifer and that injected CO_2 will displace the water in the pore space. Various authors (Balkid and Korbo 1996; Xu et al. 2004; Kumar et al. 2004; Nghiem et al. 2004; Sengul 2006; Izpec et al.2006; Burton et al. 2008; Oruganti and Bryant 2008) have simulated the multiphase physics and thermodynamics of CO_2 injection using a constant-pressure outer boundary on their models. In reality, a constant-pressure

boundary exists only if the aquifer outcrops to the atmosphere, or at the bottom of a surface water body (ocean, river, lake).
Such systems are frequently referred to as "Open" systems. Other authors like Pruess et al. (2003) tried to model the aquifer as effectively infinite, probably because aquifers are known to extend from several acres to thousands of miles wide and from a few feet to hundreds of feet thick. Orr (2004) and Noh et al. (2004) emphasize the analogies of sequestration operation with EOR, thus treating CO_2 injection as a steady-state displacement process.

However, these modeling approaches neglect to consider the fact that commercial-scale sequestration projects (>1 million T/yr), will have multiple injectors sequestering CO_2 at constant injection rates. Even in the case of an effectively infinite or an open aquifer, the drainage area will be limited by feedback from the nearest injectors and water will not move out of the limited drainage area. Hence, the drainage area available to each well will be limited and the claim that the pore water will be pushed away to create space for the injected CO_2 may not be applicable in that case. Therefore, the conclusions drawn from constant-pressure boundary modeling approaches may not be very practical and applicable to field-scale sequestration projects.

Injection in a limited drainage area must cause the aquifer pore pressure to rise; only the compression of formation and brine will yield space for the injected fluids as no fluid is moving out of the system. A limited drainage area can also be referred to as a closed system and should be modeled using no-flow outer boundaries. Consequently, any pressurization of closed aquifer extends farther in the aquifer, leading to greater risk (Oruganti et al. 2008).

Authors like van Engelenburg and Blok (1993), Schembre-McCabe et al. (2007), van der Meer and van Wees (2006), and Ennis-Ling and Patterson (2002) have already

tried to alert investigators to the issue of pressurization in a limited aquifer, and Zakrisson et al. (2008) discussed the implication of multiple injectors in one aquifer.

Figs. 3.1 and 3.2 illustrate a fundamental difference between a model with limited aquifer volume (using a no-flow boundary) and a model for an open aquifer (using a constant-pressure boundary) using CMG numerical simulations. With a constant-pressure boundary, it is possible to continue injecting as long as the injection pressure does not exceed the fracture pressure. In this case, the injected CO_2 displaces the reservoir water, leading to a minimal pressure increase above hydrostatic pressure so that the injection can continue much longer, eventually filling more of the pore space with CO_2. For the closed reservoir, injection rate must decrease after some time to avoid exceeding the fracture pressure constraint. If the pressure of the reservoir rises above a certain minimum value in order to maintain a constant injection rate (with fixed number of wells), additional infill drilling may be required in that case to maintain the target injection rate. Fig. 3.1 compares the bounded and open aquifer cases both in a square drainage area with 20-mile sides. The characteristics of the pressure profile are similar for the bounded aquifer, but pressure increases with time throughout the aquifer as indicated by the material balance. Fig. 3.2 shows the same comparison but with distance in the logarithmic scale. This comparison shows that injection in an open aquifer is largely a steady-state process as compared to the classic pseudosteady-state behavior shown by the closed aquifer. To sum, the constant-pressure modeling approach is simple and convenient but highly misleading.

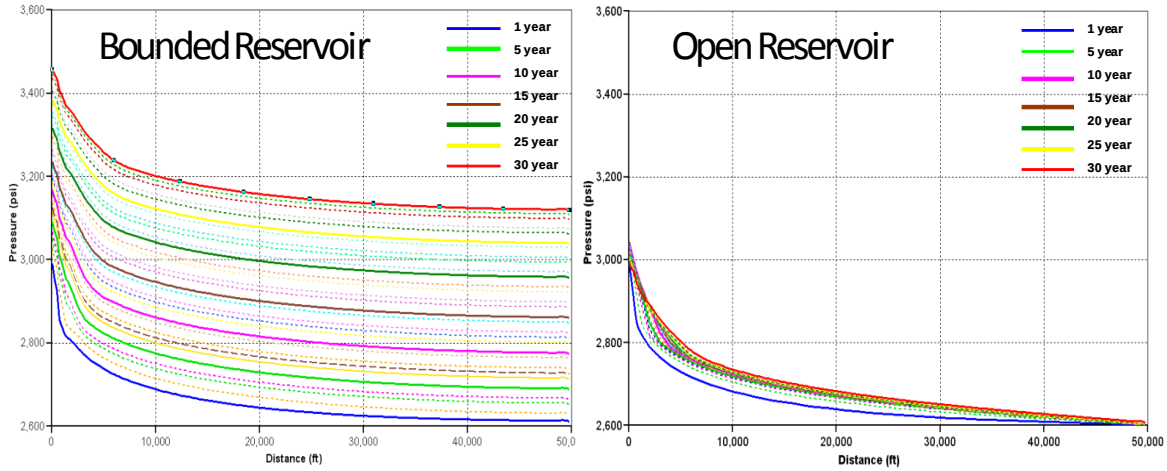

Fig. 3.1—CMG simulations comparing annual pressure profiles for the bounded and open aquifer cases, both in a square drainage area with side 20 mile. CO_2 was injected for 30 years at 52 million scf/D (~1 million T/yr). The initial hydrostatic pressure of the reservoir was 2,600 psi. The fracture pressure of the reservoir is 4,200 psi.

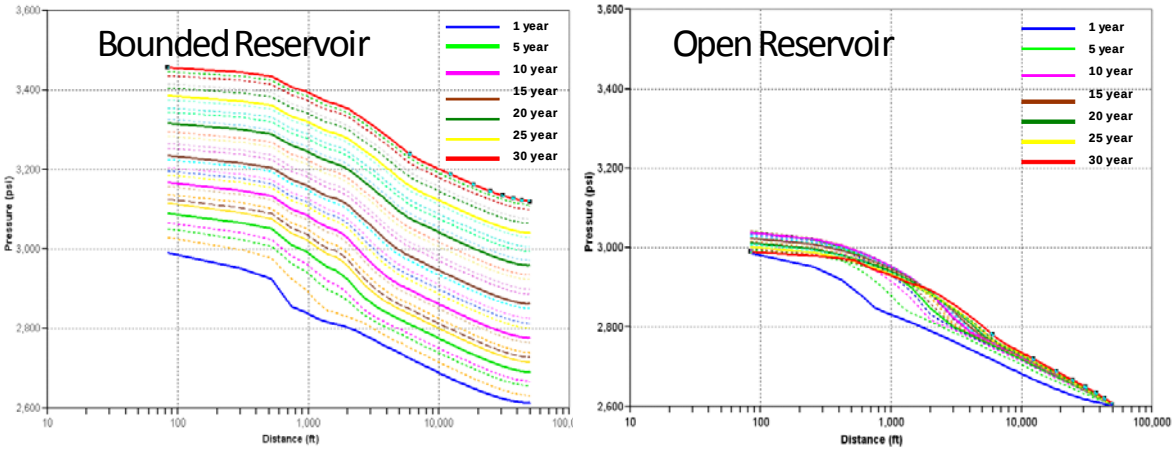

Fig. 3.2—CMG simulations comparing annual pressure profiles for the bounded and open aquifer cases, both in a square drainage area with side 20 mile. The logarithmic distance scale facilitates observation of the expanding single and two-phase zone radii. CO_2 was injected for 30 years at 52 million scf/D (~1 million T/yr). The initial hydrostatic pressure of the reservoir was 2,600 psi. The fracture pressure of the reservoir is 4,200 psi.

3.2. Local Injectivity Issues

The bottomhole pressure (BHP) behavior of an injection well in a limited drainage area is significantly different from the behavior in a drainage area modeled using

constant- pressure boundaries. The next part of this section discusses the BHP and injectivity behavior of CO_2 injection wells.

3.2.1 Well BHP Behavior

Fig. 3.3 shows the plot of well BHP behavior as a function of time for different aquifer sizes with square drainage area. CO_2 is injected for 30 years at 52 million scf/D (1 million T/yr). The initial hydrostatic pressure of the reservoir is 2,600 psi. At first, the BHP during CO_2 injection at a constant rate is governed by transient flow of single phase brine given by the following equation:

$$P_{wi} = P_i - \frac{70.6(-q_{CO_2})\mu}{kh} \ln\left(\frac{kt}{1688\phi\mu c_{ti} r_w}\right), \quad \text{..... (3.1)}$$

where the injection rate is shown as $-q_{CO2}$ in BPD, wellbore injection and initial reservoir pressures are p_{wi} and p_i both in psi, t in hours, k and φ the aquifer absolute permeability in md and porosity, r_w the well radius in ft, and c_{ti} the initial total compressibility in psi^{-1} accounting for brine and rock compressibility at initial injection conditions.

During the first few hours of injection, very high pressures are developed near the wellbore. This is because the full rate of injection, 1 million T/yr, was imposed instantaneously from t=0, requiring a large amount of water to be displaced around a small expanding bubble of CO_2 at high fluid displacement velocities. This effect can also be seen in the BHP curves: in early time the BHP is at the maximum value of 4,200 psi, and with time eventually this pressure goes down. During this early injection period, the injection rate may be ramped up gradually to avoid injecting at a pressure above the formation fracture pressure.

After a relatively shorter period of injection, the injected CO_2 vaporizes the brine around the wellbore and this results in a 100% gas saturation zone, also defined as the

drying zone. As the drying zone expands, the total mobility of the system increases with time, leading to a constant increase in the injectivity of the system. Fig. 3.3 shows clearly that the BHP behavior of a well in a closed drainage area is vastly different from a well in a drainage area with constant-pressure boundaries.

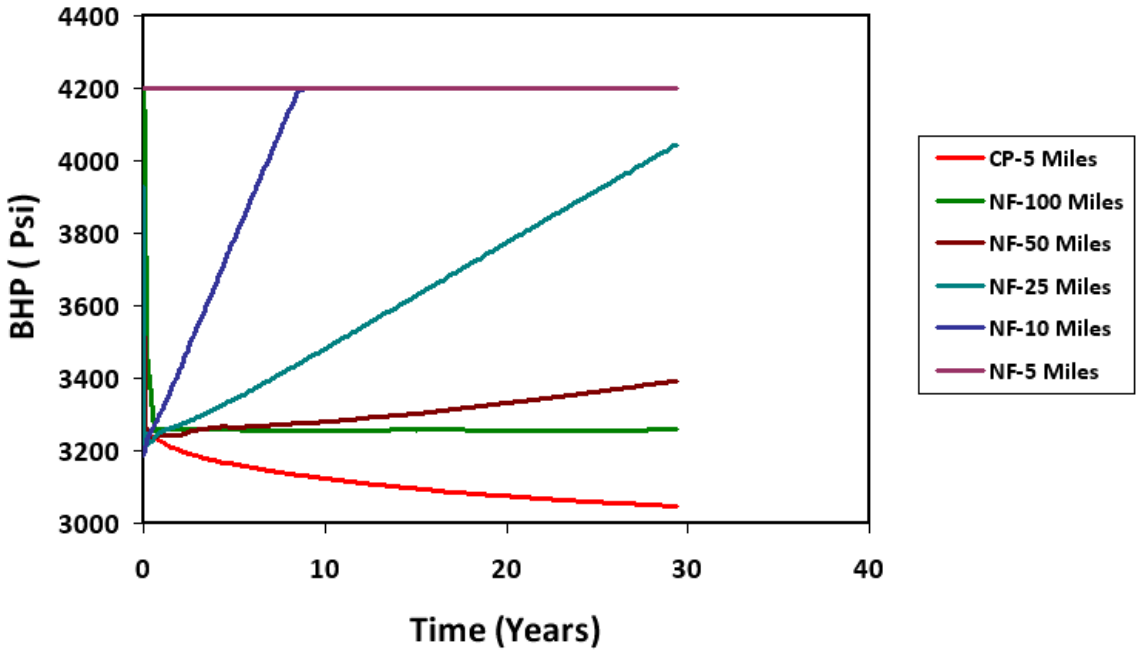

Fig. 3.3—Plot comparing well BHP obtained from simulation for different aquifer dimensions. CO_2 was injected for 30 years at 52 million scf/D (~1 million T/yr). The initial hydrostatic pressure of the reservoir was 2,600 psi. The fracture pressure of the reservoir is 4,200 psi.

The injected BHP of a well in a constant-pressure drainage area (red in Fig. 3.3) decreases with time because of the increasing injectivity behavior during CO_2 injection. Despite increasing injectivity, the BHP increases with time for a well in a closed drainage area. While the injection BHP decreases very early in time as the dry zone expands, once the pressure disturbance reaches the boundary of the drainage area, the BHP starts to rise. The reservoir pressure during injection may reach the fracture pressure before a target amount of gas is injected, forcing a need to cut back the injection rate. From Fig. 3.3, as the size of the drainage area increases, the rise in the BHP is less severe, enabling injection at a constant rate for a longer period of time.

In Fig 3.3, one very interesting thing to note is that the BHP behavior for a well with a drainage area as large as 100 mile X 100 mile (10,000 mile^2) cannot be matched with the behavior shown by the constant-pressure boundary at 5 miles from the injection well. It can be clearly seen that the drainage area modeled using a constant-pressure boundary misinterprets the expected BHP behavior. Moreover, for commercial scale sequestration projects (>1 million T/yr), multiple injectors will be required to sequester the target amount of CO_2. It will be practically infeasible for one well to inject into an area as large as 10,000 mile^2. For the purpose of illustration, the area of the state of Massachusetts in United States is 10,555 mile^2, slightly larger than the drainage area of a square well with 100-mile sides. Further, 8 out of 50 states in United States have an area less than or equal to 10,000 mile^2. Legitimate questions that arise at this point are "Are we overestimating the storage capacity for CO_2 injection?" or "Are we underestimating the aquifer volume required to sequester the required amount of CO_2 ?" The answer to these questions will be explored in subsequent sections of this thesis.

3.2.2 Well Injectivity Behavior

Authors like Burton et al. (2008), Kumar (2008) and Oruganti et al. (2009) who insist on using constant-pressure boundaries for modeling purposes are missing the classic definition of injectivity. In the petroleum engineering literature, injectivity is defined as the ratio of well volumetric flow rate, q, to a characteristic pressure drop or flow potential. Injectivity is the ability of placing the fluid in a geological formation. It is one key parameter for economic evaluation of a CO_2 sequestration project.

The pressure drop is defined by

$$\Delta P = P_{wf} - \overline{P} \quad \text{..... (3.2)}$$

P_{wf} = well flowing BHP

$\overline{P}$ = average reservoir pressure

Injectivity, *I,* can be defined as

$$I = \frac{q}{\Delta P} = \frac{q}{P_{wf} - \overline{P}} \quad \text{..... (3.3)}$$

$\overline{P}$ is the average aquifer pressure that rises with time as the gas is injected. Some authors (Oruganti et al.2009) chose to define $\overline{P}$ as the initial aquifer pressure (often defined as boundary pressure for open aquifers). Oruganti et al. (2009) also concluded that the injectivity of the system decreases as the system confinement increases; thus, the injectivity of an aquifer with no fault is highest, and as the number of sealing faults increases, the injectivity decreases. This claim is misleading and is in stark contrast with the classic definition of injectivity discussed above.

Fig. 3.4 shows the injectivity vs time for square drainage areas with different sizes and the value of $\overline{P}$ is taken as average aquifer pressure. The red curve shows the injectivity behavior for a 5-mile aquifer with a constant-pressure boundary condition. As expected, the injectivity is the same for all the drainage areas (constant pressure and no flow). For constant-rate injection, under pseudosteady state, the difference between the flowing BHP and the average reservoir pressure is constant, and the pressure rise is a linear function of time. Well BHP reaches the fracture pressure with continued pseudosteady-state injection, and injection rate starts to decrease. However, the ratio of rate vs change in average pressure for different drainage areas remains constant; that is, the injectivity trend does not change with the change in aquifer dimension. Clearly, the authors cited above are on the wrong track and are confusing increase/decrease in the injection rate with an injectivity increase/decrease.

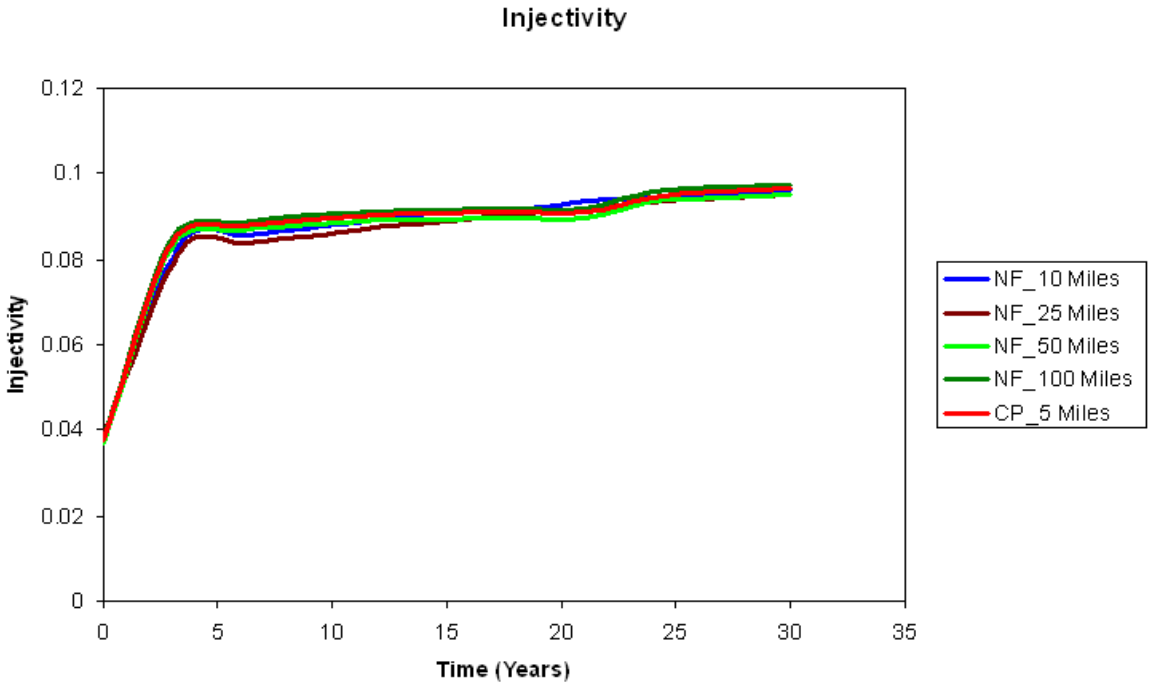

Fig. 3.4—Plot comparing injectivity obtained from simulation for different aquifer dimensions. CO_2 was injected for 30 years at 52 million scf/D (~1 million T/yr). The initial hydrostatic pressure of the reservoir was 2,600 psi. The fracture pressure of the reservoir is 4,200 psi. The red curve shows the injectivity of a 5-mile aquifer with constant-pressure boundaries.

Fig. 3.5 shows the behavior of $\frac{q}{P_{wf} - P_i}$ with the initial aquifer pressure as an illustration. CO_2 is injected for 30 years at 52 million scf/D (~1 million T/yr). The initial hydrostatic pressure of the reservoir is 2,600 psi and the fracture pressure is 4,200 psi. It is quite obvious from the curves that the aquifer with a constant-pressure boundary shows the highest values for this ratio, followed by the closed aquifer with the largest dimension. It can be clearly seen that this ratio for a 10-mile X 10-mile aquifer is decreasing with time, and this means that the system is overpressurized and no longer able to sustain the applied injection rate. Hence, the BHP is increasing and the rate is decreasing. The reservoir pressure during injection may exceed the fracture pressure very fast and injection should be stopped before the target amount is injected. A 25-mile X 25-mile aquifer is sufficient to inject the gas without exceeding the fracture pressure. A comparison of the behavior from Figs. 3.4 and 3.5 highlights the

classic pseudosteady-state behavior shown by bounded aquifers and illustrates why it is essential to stick to the classic meaning of injectivity.

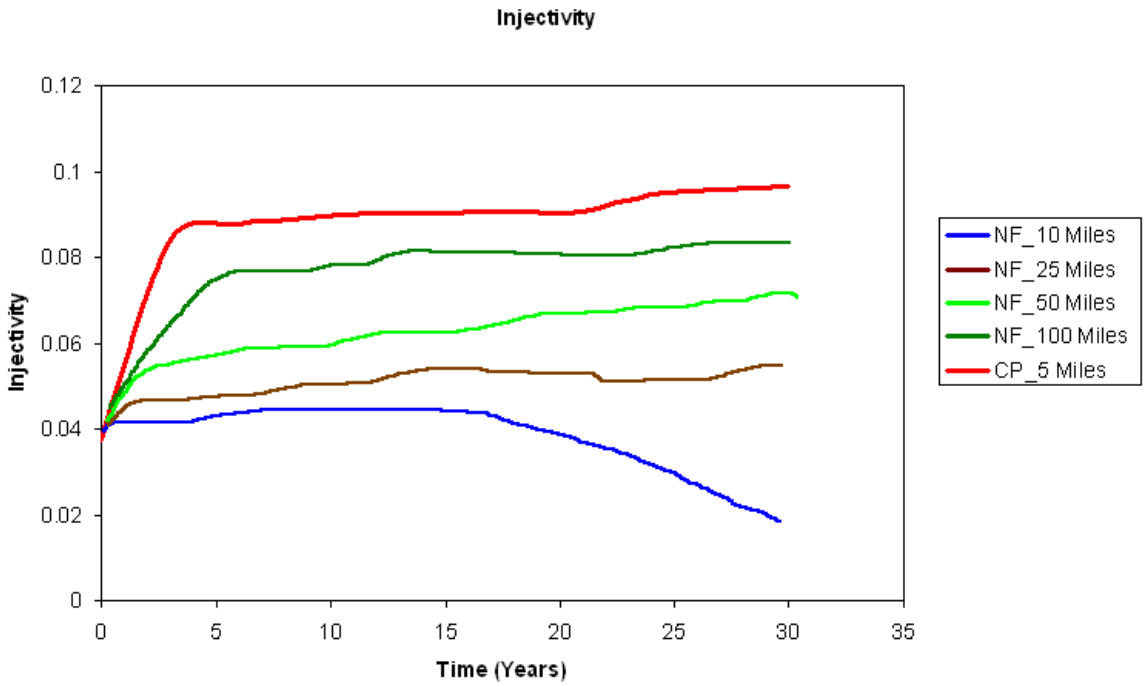

Fig. 3.5—Plot comparing steady-state injectivity obtained from simulation for different aquifer dimensions. CO_2 was injected for 30 years at 52 million scf/D (~1 million T/yr). The initial hydrostatic pressure of the reservoir was 2,600 psi. The fracture pressure of the reservoir is 4,200 psi. The red curve shows the injectivity of a 5 miles aquifer with constant-pressure boundaries.

3.3. Analytical Model for Injection in Closed Aquifers

Noh et al. (2004) and Burton et al.(2008) explained that the CO_2 injected into a deep saline aquifer can be divided into three dominant regions (Fig. 3.6).

a) Single-phase CO_2 zone
b) Two-phase zone (brine-dominated aqueous phase and CO_2-dominated gas phase)
c) Single-phase brine zone

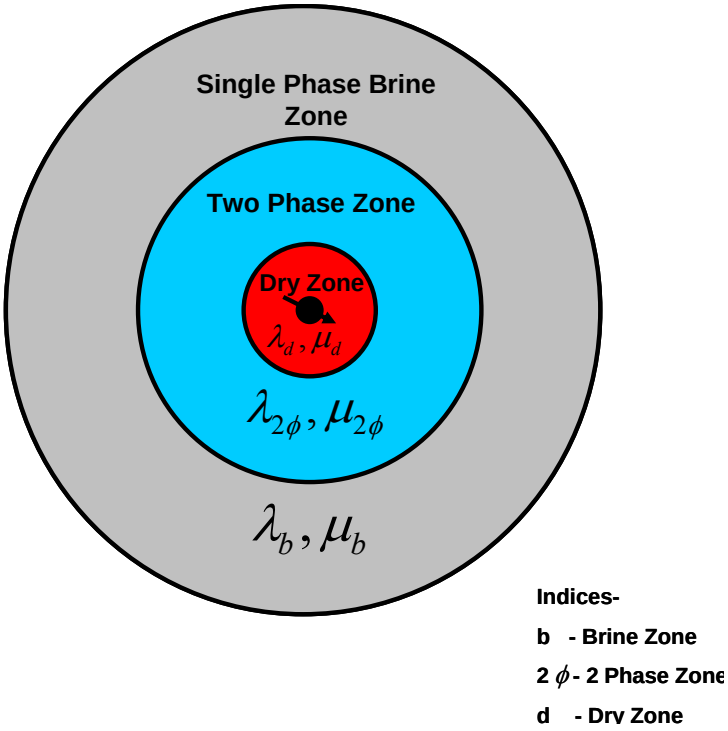

Fig. 3.6--Schematic showing different flow regions when anhydrous CO_2 is injected in the system.

Farthest upstream, closest to the injection well, is the drying zone. When anhydrous CO_2 is injected into the reservoir, it vaporizes the brine around the wellbore and gets saturated. After continuous injection vaporizes all the brine around the wellbore, it results in a 100% gas saturation zone, also defined as a drying zone. Consideration of this zone is very important for accurate prediction of CO_2 injectivity. The two-phase zone contains a brine-dominated aqueous phase and a CO_2-dominated gas phase. The phase saturation in this zone varies continuously with position and time. This region separates the drying zone from the single-phase brine zone.

In the next part of this section we extend Burton et al.'s (2008) steady-state injectivity model for application to a closed aquifer. The objective is to find the aquifer volume required to sequester CO_2 from a typical coal power plant. Given aquifer depth, porosity, thickness, permeability, rock compressibility, and relative permeability data

along with the brine salinity, the analytical model offers a quick estimate for the required aquifer size for a target total mass of CO_2 to be sequestered. The results from the analytical model compare closely with simulation results.

3.3.1 Mathematical Modeling

Burton et al. (2008) provide equations for the radii of the single phase and two-phase zones and the pressure drop across each of these zones as well as the pressure drop in the single-phase brine.. They assumed that the pressure gradient across the drying, two-phase brine zone can be computed by considering the flow as steady state. They further assumed that the fractional flow theory can be applied to this situation and that viscosity of each phase is constant and independent of composition. Temperature was assumed to be constant and no geochemical reactions were considered.

Basic Model

The pressure drop across the three regions can be written in terms of Darcy's law as follows.

Dry CO_2 Region

$$\Delta p_{dry} = \int_{p_w}^{p_{dry}} dp = \frac{q\mu_g}{2\pi kh}\int_{r_w}^{r_{dry}} \frac{1}{r} dr = \frac{q\mu_g}{2\pi hkk_{r,S_g=1}} \ln\left(\frac{r_{dry}}{r_w}\right), \quad \text{..... (3.4)}$$

where $k_{r,Sg=1}$ is permeability reduction due to salt precipitation.

Burton et al. (2008) also proposed a simple calculation method for estimation of $k_{r,Sg=1}$. They assumed that the salt will be distributed evenly in the pore space. The salinity expressed in parts per million can be converted to volume fraction ($V_{f,\ \text{salt}}$) with the knowledge of density of salt (ρ_{salt}) and density of solution (ρ_{sol}).

$$V_{f,salt} = \frac{S\ X\ \rho_{sol}}{10^6\ X\ \rho_{salt}} \quad \text{..... (3.5)}$$

The reduced porosity can be found by subtracting the volume of water from the original volume.

$$\phi = \phi_o - \phi_o(1 - S_{g,dry})V_{f,salt} \quad \text{..... (3.6)}$$

The permeability reduction can then be described by the Kozeney-Carman relationship:

$$k_{r,S_{g=1}} = \frac{k}{k_o}\left(\frac{\phi}{\phi_o}\right)\left(\frac{1-\phi_o}{1-\phi}\right) \quad \text{..... (3.7)}$$

Two-Phase Region

The pressure drop across the two-phase region can be estimated as

$$\Delta p_{2\phi} = \int_{p_{dry}}^{p_{2\phi}} dp = \frac{q}{2\pi kh}\int_{r_{dry}}^{r_{2\phi}}\left(\frac{k_{rg}}{\mu_g}+\frac{k_{rw}}{\mu_w}\right)^{-1}\frac{1}{r}dr \approx^{-1} \frac{q}{2\pi hk}\ln\left(\frac{r_{2\phi}}{r_{dry}}\right)\left(\frac{k_{rg}}{\mu_g}+\frac{k_{rw}}{\mu_w}\right)^{-1}\Bigg|_{S_{g,avg}}$$

(3.8)

Burton et al. (2008) simplified right-hand side of the expression by approximately replacing the radial-position weighted mobility with the mobility at some average saturation within the two-phase region. This is reasonable if the range of saturations in the two-phase region is narrow. The average gas saturation was calculated as the average of CO_2 phase saturation

$$\frac{S_{g,dry} + S_{g,2\phi}}{2}, \quad \text{..... (3.9)}$$

where $S_{g,\mathrm{dry}}$ is the CO_2 gas saturation upstream of the two-phase region and $S_{g,2\varphi}$ is the gas saturation downstream of the two-phase region, and each can be determined from CO_2-water fractional flow theory (Lake 1989; Noh et al. 2004).

Brine Region

The pressure drop across the brine region can be estimated as

$$\Delta p_{brine} = \int_{p_{2\varphi}}^{p_e} dp = \frac{q\mu_w}{2\pi kh}\int_{r_{2\varphi}}^{r_e}\frac{1}{r}dr = \frac{q\mu_w}{2\pi kh}\ln\left(\frac{r_e}{r_{2\varphi}}\right). \quad \text{(3.10)}$$

Total Pressure Drop

The total pressure drop in the system for a steady state case can be written as :

$$\Delta p_{total} = \Delta p_{brine} + \Delta p_{2\phi} + \Delta p_{dry}$$

$$= \frac{q}{2\pi kh}\left[\frac{1}{\lambda_{dry}}\ln\left(\frac{r_{dry}}{r_w}\right) + \frac{1}{\lambda_{2\phi}}\ln\left(\frac{r_{2\phi}}{r_{dry}}\right) + \frac{1}{\lambda_{brine}}\ln\left(\frac{r_e}{r_{2\phi}}\right)\right], \quad \text{(3.11)}$$

where

$$\lambda_{\mathrm{brine}} = \frac{1}{\mu_w} \quad \text{(3.12)}$$

is the mobility of the brine zone,

$$\lambda_{2\phi} = \left(\frac{k_{rg}}{\mu_g} + \frac{k_{rw}}{\mu_w}\right)\Bigg|_{s_{g,avg}} \quad \text{(3.13)}$$

is the total mobility of the two-phase region.

$$\lambda_{dry} = \frac{k_{r,S_{g=1}}}{\mu_w} \quad \text{.....(3.14)}$$

is the mobility of the single phase CO_2 zone.

In all of these equations, CO_2 and water viscosities are μ_g and μ_w in cp; relative permeabilities are k_{rg} and k_{rw}; and outer radii of the single phase CO_2, two-phase Buckley-Leverett, and single phase brine are r_{dry}, $r_{2\varphi}$, and r_e. The relative permeability of the CO_2 in the single-phase region is $k_{r,Sg=1}$, and relative permeability values in the two-phase region are evaluated at the average CO_2 saturation according to Buckley-Leverett displacement theory (1942).

For this study the pressure increase over the average reservoir pressure is given by

$$\Delta p_{total} = \frac{q_{CO_2}}{2\pi kh}\left[\frac{1}{\lambda_{dry}}\ln\left(\frac{r_{dry}}{r_w}\right)+\frac{1}{\lambda_{2\phi}}\ln\left(\frac{r_{2\phi}}{r_{dry}}\right)+\frac{1}{\lambda_{brine}}\ln\left(\frac{0.472r_e}{r_{2\phi}}\right)\right] \text{. ..... (3.15)}$$

Well BHP can be written in oilfield units as

$$p_{wi} = \overline{p} - \frac{141.2(-q_{CO_2})}{kh}\left[\frac{1}{\lambda_{dry}}\ln\left(\frac{r_{dry}}{r_w}\right)+\frac{1}{\lambda_{2\phi}}\ln\left(\frac{r_{2\phi}}{r_{dry}}\right)+\frac{1}{\lambda_{brine}}\ln\left(\frac{0.472r_e}{r_{2\phi}}\right)\right] \quad (3.16)$$

The factor 0.472 in the last natural logarithm term in Eq. 3.16 accounts for average reservoir pressure, $\overline{p}$, as the average pressure in the brine region and is a departure from the Burton et al. (2008) approach, which claimed, incorrectly, that treating the aquifer as open, with a constant-pressure outer boundary, was equivalent to modeling an effectively infinite aquifer. Eq. 3.16 assumes the aquifer volume is limited and that pseudosteady-state flow behavior is established.

The consequence of assuming the aquifer has a limited area is that the average aquifer pressure will increase over time. Thus, accounting for material balance,

$$V_{CO_2} = c_t\left(\overline{p}p_i\right)V_p\,, \quad \text{..... (3.17)}$$

where V_{CO_2} is the total volume of CO_2 to be injected over the life of the sequestration project, V_p is pore volume available for CO_2 storage, and c_t is the total compressibility accounting for CO_2, brine and rock compressibility using a bulk-volume weighted average. The expression for compressibility can be written as-

$$c_t = c_f + \frac{[(r_{dry}{}^2 - r_w{}^2)c_{CO_2} + (r_{2\phi}{}^2 - r_{dry}{}^2)(s_{g,avg}c_{CO_2} + (1-s_{g,avg})c_w) + (r_e{}^2 - r_{2\phi}{}^2)c_w]}{(r_e{}^2 - r_w{}^2)}$$

..... (3.18)

C_f is the formation compressibility in psi^{-1}.

Finally, the difference between the wellbore injection pressure and the initial reservoir pressure will be

$$p_{wi} - p_i = p_{wi} - \overline{p} + \overline{p} - p_i = -\frac{141.2(-q_{CO_2})}{kh}\left[\frac{1}{\lambda_{dry}}\ln\left(\frac{r_{dry}}{r_w}\right) + \frac{1}{\lambda_{2\phi}}\ln\left(\frac{r_{2\phi}}{r_{dry}}\right) + \frac{1}{\lambda_{brine}}\ln\left(\frac{0.472r_e}{r_{2\phi}}\right)\right] + \frac{V_{CO_2}}{V_pC_t}$$

..... (3.19)

Eq. 3.19 can be generalized as follows:

$$p_{wi} - p_i = \Delta p_{\max} = -\frac{141.2(-q_{CO_2})}{kh}\left[\frac{1}{\lambda_{dry}}\ln\left(\frac{r_{dry}}{r_w}\right)+\frac{1}{\lambda_{2\phi}}\ln\left(\frac{r_{2\phi}}{r_{dry}}\right)+\frac{1}{\lambda_{brine}}\ln\left(\frac{0.472r_e}{r_{2\phi}}\right)\right]+\frac{V_{CO_2}}{V_p\,C_t}$$

..... (3.20)

where $\Delta p_{\max}$ is the increase in well BHP due to injection and is limited to no more than the difference between fracture and hydrostatic pressures, p_f — p_{hyd}, for an aquifer. The pressure of a depleted oil or gas field may be less than hydrostatic. Denoting the term in brackets as $1/M_r$, this can be further generalized as the following equation:

$$\frac{\Delta p_{\max}}{V_{CO_2}} = \frac{0.069}{\mathrm{M_r} N_i kht_{\text{plant}}} + \frac{1}{V_r \mathrm{C}_t}, \quad \text{..... (3.21)}$$

where $\mathrm{M_r}$ can be written as

$$M_r = \left[\frac{1}{\lambda_{dry}}\ln\left(\frac{r_{dry}}{r_w}\right)+\frac{1}{\lambda_{2\phi}}\ln\left(\frac{r_{2\phi}}{r_{dry}}\right)+\frac{1}{\lambda_{brine}}\ln\left(\frac{0.472r_e}{r_{2\phi}}\right)\right], \quad \text{..... (3.22)}$$

N_i is the required number of wells, and t_{plant} is the life of the power plant or duration of CO_2 injection. Noh et al. (2004) provided expressions for calculation of the speed of the fronts and phase saturations on either side of the front using a modified Buckley-Leverett theory. Using the expressions for the dimensionless velocity of the fronts, the radial positions of the drying zone and the two-phase zone can be calculated.

3.3.2. Comparison With Numerical Reservoir Simulator

Using the derived Eq. 3.21 and reservoir properties from Table 2.1, we tried to compare the results of the analytical model to CMG numerical simulations for a square drainage area with 20-mile sides. Fig. 3.7 and 3.8 compare the average reservoir pressure and well BHP respectively. The analytical solution is sufficiently

close to the numerical solution, and major trends of the well BHP and average reservoir pressure are captured from the simplified theory for a closed system.

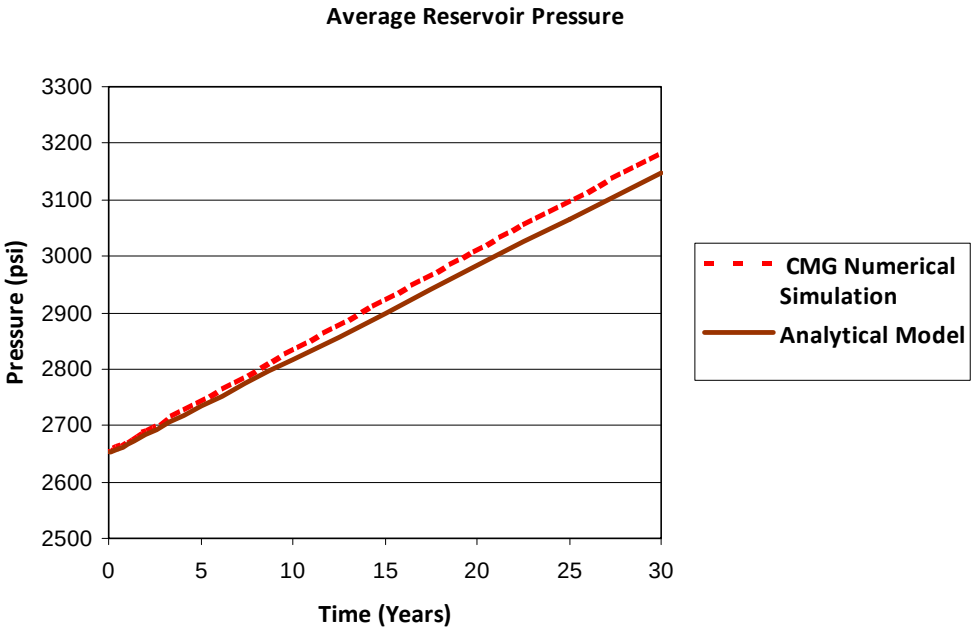

Fig. 3.7—Average reservoir pressure predicted by the simplified model for a closed system compares well with the CMG numerical simulator. CO_2 was injected for 30 years at 52 million scf/D (~1 million T/yr). The initial hydrostatic pressure of the reservoir was , psi. The fracture pressure of the reservoir is 4,200 psi.

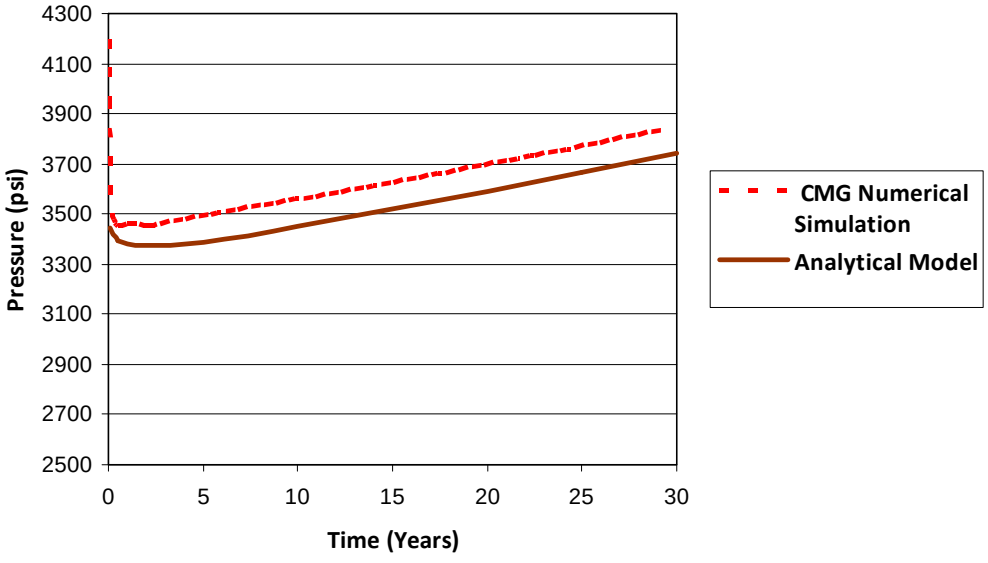

Fig. 3.8—Average reservoir pressure predicted by the simplified model for a closed system compares well with the CMG numerical simulator. CO_2 was injected for 30 years at 52 million scf/D (~1 million

T/yr). The initial hydrostatic pressure of the reservoir was 2,650 psi. The fracture pressure of the reservoir is 4,200 psi.

The discrepancy between the solutions is likely because of the difference in the CO_2 properties used for the analytical solutions and inside the numerical simulator. The CO_2 properties for the simulator are calculated from the Peng-Robinson EOS, whereas the properties for the analytical solution come from tabulated values (Jarrel et al. 2002).

3.3.3. Sensitivity Study

Several sensitivity plots can be generated from the generalized Eq. 3.21. Simple relationships were generated for the specific depths of 3,000, 6,000 and 10,000 ft and for injection of 3 million tonnes of CO_2 per year. Fig. 3.9 shows normalized compression pressure plotted vs a product of well count and permeability-thickness. Normalized compression pressure is defined as

$$P_{norm} = \frac{\overline{P}_t - P_i}{P_{frac} - P_i} \quad \text{..... (3.23)}$$

where P_{frac} is the fracture pressure, P_i is the initial reservoir pressure and $\overline{P}_t$ is the average reservoir pressure at a particular time *t* after starting injection.

It is clear that pressurization of the reservoir to its maximum value may lead to an exponential increase in well counts. However, at lower normalized compression pressure, the pore volume requirement is more than the requirement at the higher compression pressure (Fig. 3.10). There is obviously a trade-off between the pore volume and aquifer pressurization. If the former is more, the latter is less, and vice versa. For the same *kh* value, it is clear that the number of wells required is more for a shallower aquifer and less at lower normalized compression pressure. Fig. 3.11 shows that the shallower formation depth has a smaller window between formation and

fracture pressures, leading to a larger volume requirement. These results are clearly seen in Fig. 3.10. The pressure interference between the wells in same aquifer causes significant injection losses, and this can severely affect the well counts required to sequester a target amount of CO_2. The loss of injection rate and rise in average aquifer pressure depends on a number of parameters such as well spacing, permeability, thickness, differential pressures, and injection rates. At shallower depths, since the difference between the fracture pressure and initial aquifer pressure is less, an even greater number of wells is needed for the same well spacing and *kh*.

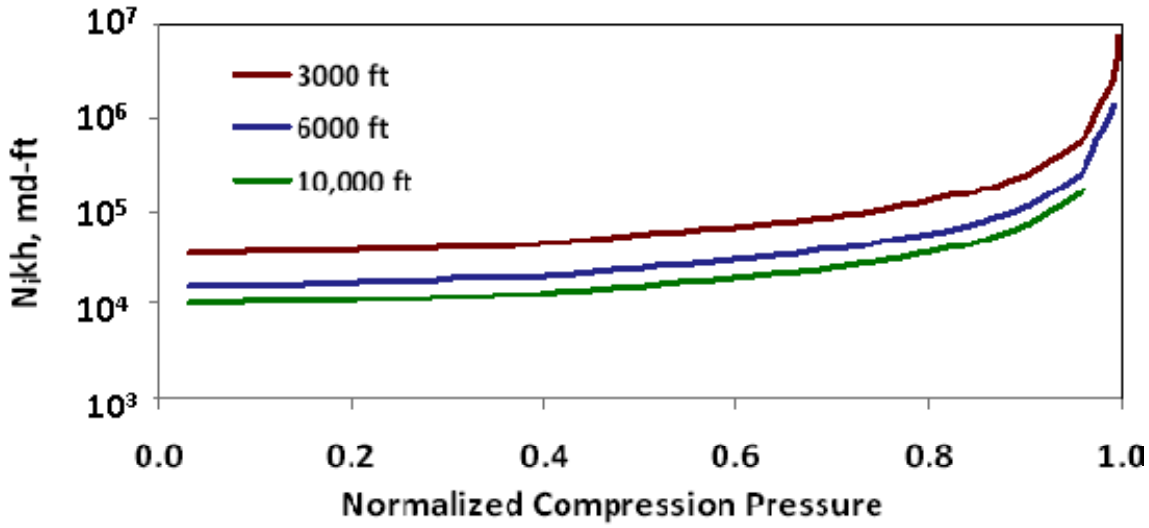

Fig. 3.9—Relationship between well count, permeability-thickness, and the compression pressure as a fraction of Δp_{max} for given relative permeability, porosity, Δp_{max}, and aquifer depth.

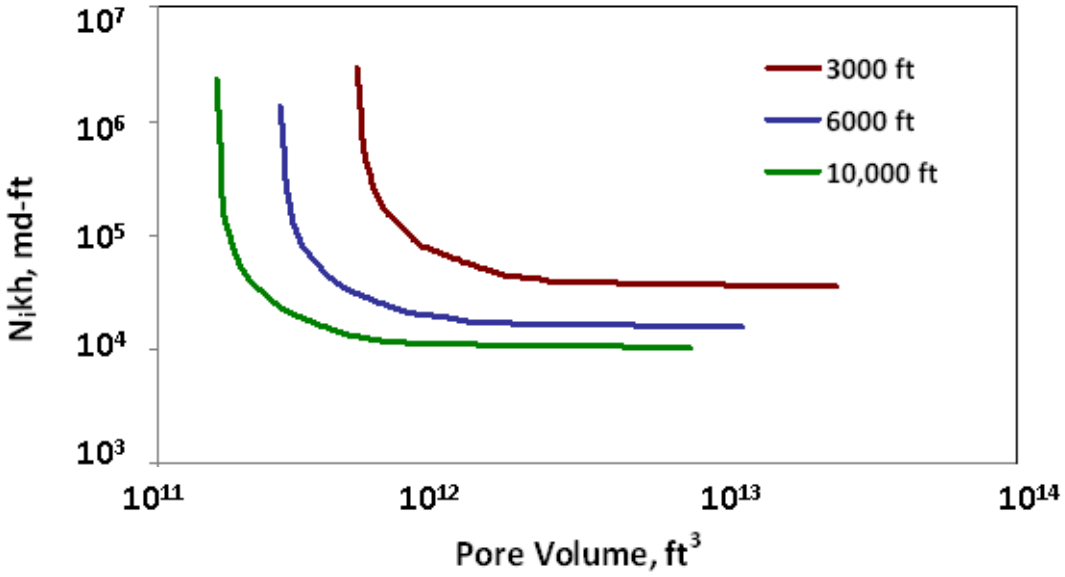

Fig. 3.10—Relationship between well count, permeability-thickness, and the required minimum pore volume for given relative permeability, porosity, Δp_{max}, and aquifer depth.

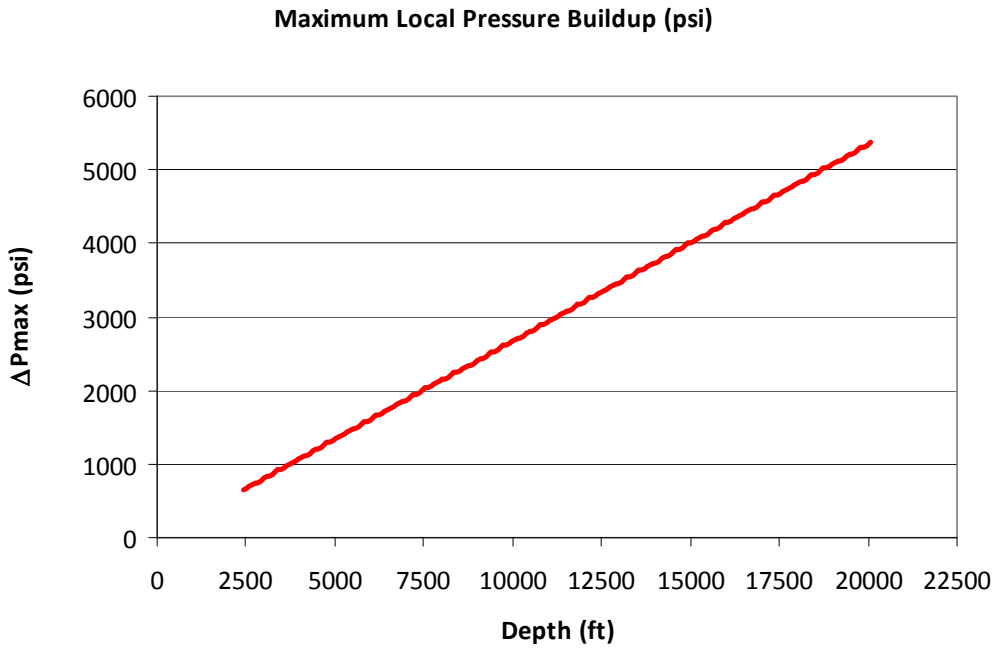

Fig. 3.11—Plot showing the difference between the fracture and hydrostatic pressures, $p_f - p_{hyd}$, for an aquifer with depth.

3.3.4 Storage Potential

A critically important message conveyed by the generalized Eq. 3.21 is storage potential. The following discussion explains how much pressure matters to the storage potential in a closed, liquid-saturated reservoir. The principal behind using the isothermal compressibility expression to estimate the storage potential is that for an incremental increase in pore volume due to the injected CO_2, the water volume will decrease and effective pore volume of rock will increase. This can be evaluated by starting with the expression for isothermal compressibility.

The isothermal compressibility is defined as

$$c = -\frac{1}{V}\left(\frac{\partial V}{\partial p}\right)_T , \quad \text{..... (3.24)}$$

where V is the volume of the fluid. By separation of variables,

$$\int_{p_i}^{\bar{p}} c\,dp = -\int_{V_p}^{V_f} \frac{dV}{V} . \quad \text{..... (3.25)}$$

Assuming that c is constant over the pressure range,

$$c(\bar{p} - p_i) = -\ln \frac{V_f}{V_p} . \quad \text{..... (3.26)}$$

Rearrangement of Eq 3-26 results in

$$\frac{V_f}{V_p} = e^{-c(\bar{p}-p_i)} . \quad \text{..... (3.27)}$$

The volume V_{CO_2} is equal to V_p — V_f; that is, the original pore volume minus that stored at the higher pressure. Finally, the storage potential, s_{CO_2}, is given by

$$s_{CO_2} = \frac{V_{CO_2}}{V_p} = 1 - e^{-c(\bar{p} - p_i)} < 1 - e^{-c(p_f - p_{hyd})}. \quad \text{..... (3.28)}$$

Fig. 3.12 shows the well count *kh* product as a function of the storage potential. It indicates that the best storage potential is about 2.5% of the pore volume for a depth of 10,000 ft.

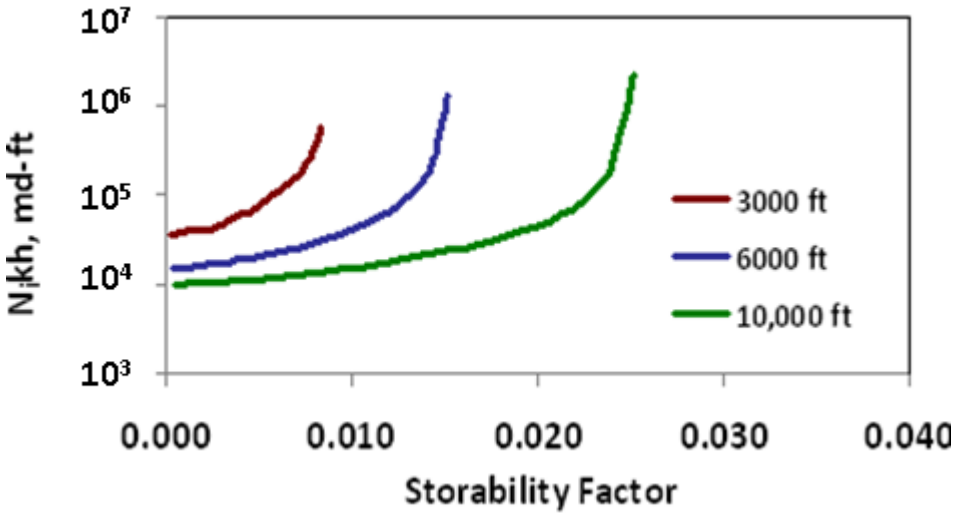

Fig. 3.12—Relationship between well count, permeability-thickness, and the storage potential for given relative permeability, porosity, Δp_{max}, and aquifer depth.

3.3.5 Application for a Single Power Plant

A modern commercial 500-MW coal power plant generates about 3 million metric tons of CO_2 per year. Assuming it is captured as a pure CO_2 stream, what will be the aquifer pore volume required to store the CO_2, and how many wells will be needed if the plant life is assumed to be 30 years?

Suppose an aquifer exists in the vicinity of the plant with porosity 20%, permeability 100 md, and thickness 100 ft. For an aquifer depth of 6,000 ft at a temperature of

150°F (assuming geothermal gradient of 1°F/100 ft) and hydrostatic pressure of about 2,598 psi, the supercritical fluid density at reservoir conditions will be about 41 lbm/ft^3 (Jarrell et al. 2002). At this density the total volume of CO_2 to inject in a 30-year period is 4.86 billion cu ft, or 865 million bbl. The volumetric injection rate is 71,300 BPD. To determine the aquifer area required to inject this volume of CO_2, it is necessary to decide how much the aquifer will be pressurized above the initial aquifer pressure. Certainly it should not be pressurized above the formation fracture pressure. Assuming the fracture gradient is 0.7 psi/ft, the average reservoir pressure should not exceed 4,200 psi. However, in order to inject at a constant rate for 30 years at the end of this time period, the wellbore injection pressure must exceed the average reservoir pressure as in Eq. 3.20, and this pressure must not exceed 4,200 psi.

Experience with natural gas storage indicates that it is not possible to recover all of the stored gas if the reservoir is pressurized well above the initial reservoir pressure. This has been interpreted as an indication that some of the stored gas has leaked out of the reservoir. Exactly the same result may occur for CO_2 storage in an aquifer. Therefore, as a first case, assume the aquifer average pressure will not be elevated by more than 100 psi over the initial aquifer pressure. With this assumption Eq. 3.21 implies that the required aquifer pore volume is 7.7 Tcf. For the given aquifer thickness and porosity, the resulting area is 13,800 sq mi. If the injection pressure is allowed to approach the formation fracture pressure, the difference between injection and average pressures is 4,200 -2598-100=1502 psi, and Eq. 3.17 indicates that ½ the required rate can be produced in ½ of this area without exceeding this pressure constraint. Therefore, two wells can inject all of the CO_2 produced by the plant for 30 years.

However, as points of reference, the Prudhoe Bay reservoir area is 337 sq mi, and 9 US states and the District of Columbia all have areas less than 13,800 sq mi. It is possible to reduce the required area by increasing the amount to pressurize the

reservoir. Assuming instead that the aquifer average pressure will be elevated by 1,000 psi, the required aquifer area is 1,371 sq mi, somewhat less than the area of the state of Rhode Island, which has an area of 1,545 sq mi. In this case, four wells will be sufficient. The minimum aquifer area, assuming pressurization of 1,600 psi is approximately 853 sq mi, and 1,155 wells are required.

Of course, greater aquifer thickness reduces the required aquifer area by increasing both injectivity and storage potential per unit area. If an otherwise similar aquifer is 200 ft thick instead of 100 ft, the area required with 1,000 psi pressurization is reduced to 686 sq mi and two wells, each requiring a square area approximately 17.5 mi on a side, are sufficient.

3.4 Section Conclusions

The ability to properly assess the "storage potential" of an aquifer is of critical importance for estimating the well count needed for storage. It is very important to understand that interference from the neighboring injectors limits the pore volume available for injection from the very beginning of a project even when the aquifer is estimated to have an unlimited storage capacity. Hence, the practical relevance of constant-pressure and infinite-acting reservoir models is questionable. Our simulations indicate that pressurization even in relatively large aquifers will not be small. The average reservoir pressure of an aquifer should and will rise under constant injection rate with multiple wells. Our analytical model compares wells with the numerical reservoir simulator. Sensitivity studies show that insufficient storage potential can lead to an impractically large operation area or too many injection wells. Authors using a constant-pressure boundary approach have overestimated the storage potential of aquifers. A realistic no-flow boundary model indicates that there is every possibility that volumes envisioned for CO_2 sequestration are underestimated at least by at least a factor of 5 and underscores the reason why aquifer pressure should be continuously monitored. This will be the outline of the next section.

4. PRESSURE FALLOFF TESTING FOR AQUIFER CHARACTERIZATION AND LEAKAGE DETECTION

4.1 Introduction

Section 3 showed why in most cases we should expect the aquifer pressure to rise during CO_2 injection. This section shows that a three-region composite reservoir model with sealing and constant pressure linear boundaries can be used to interpret simulated pressure falloffs. Section 4.2 through 4.4 builds the background needed to understand the behavior of a pressure falloff test. Section 4.5 explains how the pressure profile varies with radial distance from a CO_2 injection well relates it to the behavior of the pressure derivative of a falloff test discussed in Section 4.6. Section 4.7 discusses the application of Horner analysis for average pressure monitoring and relates it to Section 4.8, which explains how Horner analysis it can be used to detect an aquifer leak. Section 4.9 concludes the major findings from this section.

4.2 Why Monitoring Is Needed

The potential risks of storing a gas in a geological storage unit (coal seams, saline aquifers, and depleted oil and gas reservoirs) includes leakage of CO_2 along the abandoned wells, faults and fractures, and high-permeability zones and by a caprock failure. Leakage of faults and fractures is generally considered to be the most important natural leakage pathway because it extends for larger distances inside the subsurface. Typically, risk of leakage depends on the characteristics of the storage site. Hydrocarbon fields, which have been well studied, are often safe for storing CO_2, since they have held oil and gas for millions of years. On the other hand, storage candidates like deep saline aquifers have not been studied extensively. The risk of leakage is pertinent because of their extensive size and less confidence about the seal integrity.

Upwards migration of CO_2 after leakage may also affect the quality of ground and surface water, soil, energy, and mineral resources. This in turn may affect subsurface marine and aquatic ecosystems. Even small CO_2 leaks can severely deteriorate the potable water quality. A decrease in pH to a level of 4 to 5 may cause calcium dissolution, change in hardness of water and change in concentration of trace elements. (Holloway 1996). Elevation of CO_2 concentration in the soil due to leakage is likely to lower the soil pH and adversely impact the chemistry of nutrients, redox sensitive elements, and plant growth (Saripalli et al. 2003).

A detected leak in time can sometimes be remediated. Benson et al. (2002) suggested seven situations for which remediation may be required: 1) leakage out of the storage formation, 2) leakage from active or abandoned wells, 3) shallow groundwater remediation, 4) vadose zones and soil remediation, 5) surface fluxes, 6) carbon dioxide in indoor air, and 7) surface water.

While geophysical methods have proven successful in tracking migration of a CO_2 plume, it may be more cost-effective and fit-for-purpose to use permanent pressure gauges and monitor pressure dynamics. Pressure transient testing is a proven technique in oil and gas industry for reservoir characterization. Monitoring pressure during injection and regular falloff pressure measurements are very fundamental and relatively inexpensive techniques for monitoring the storage performance. Once equipped with downhole pressure gauges, reservoir pressure can be continuously monitored for any unexpected changes and for taking regular pressure falloffs. Pressure monitoring can be used for various purposes, such as tracking the location of the CO_2 plume, understanding the subsurface saturation behavior, monitoring average reservoir pressure, ensuring that injection and abandoned wells are not leaking, and for verification of the quantity of carbon dioxide that has been injected underground.

Several authors in the past (Hoversten et al. 2000; Arts et al. 2002; Newmark et al. 2002; Benson et al. 2002; Chalaturnyk and Gunter 2004; Pearce et al. 2005; Meckel et al. 2008) have focused on many aspects and pressure monitoring and measurements methods, including identification of potential technologies and the rationale. Although the application of pressure transient testing for monitoring is anecdotally mentioned throughout the sequestration literature, there is a little to be found in terms of its practical application for monitoring pressures in the active injection well. Pressure behavior in CO_2 storage aquifers has been neglected thus far in the literature. In reality, pressure transient analysis easily distinguishes whether a well drains a limited volume exhibiting quasisteady state behavior, an open aquifer with constant pressure support, or an effectively infinite aquifer, and this section spells out why pressure monitoring makes sense.

Thus, monitoring is important to demonstrate to regulatory oversight bodies that the practice of geological storage is safe and it does not create adverse local environmental problems.

4.3 Pressure Monitoring: Approach

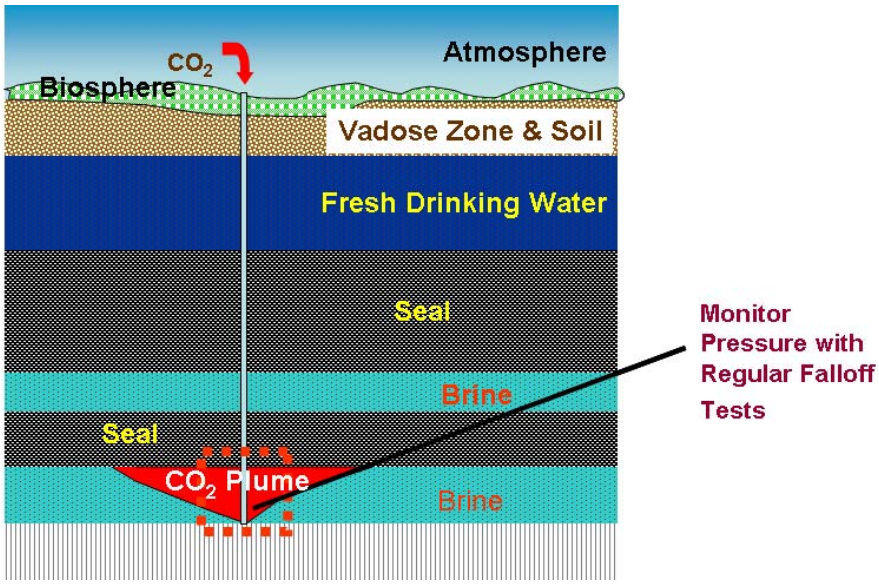

Fig. 4.1—Diagram showing CO_2 injection in deep saline aquifer**.**

Fig. 4.1 illustrates the concept of CO_2 sequestration. The dashed box around the well is the location for this study. As discussed earlier, periodic pressure falloff tests can be used to monitor the progress of CO_2 injection operations. Pressure falloff test design focuses on real-time pressure evolution in the active injection well or a dedicated observation well. The derivative of the pressure curve (rate of pressure change with elapsed time) reveals finer details of the pressure evolution in the aquifer. It can readily show the presence of leaking CO_2 or brine from the aquifer and is particularly very powerful for understanding the flow physics of CO_2 injection. Combining the observations with the pressure measurement data in the overlying permeable zone with other monitoring techniques can highlight unanticipated fluid migration out of the aquifer via leakage pathways. Chabora et al. (2009) provides a model for pressure monitoring above the zone. However, the focus of this thesis is on pressure monitoring in the active injection well. The information obtained can be integrated to

constrain and refine numerical simulation models. Pressure history matching can provide real-time assessment of CO_2 migration during geologic storage (Matilla et al. 2008).

The GEM-GHG simulator was used to generate models for pressure and saturation behavior during bulk CO_2 injection. No-flow and constant-pressure boundary conditions were simulated using the base case model discussed in Section 2. Periodic injection falloff tests were simulated to show what behavior can be expected over 30 years of continued injection.

4.4 Saturation Profiles Around Co_2 Injection Well

Fig. 4.2 diagrams a map view of the CO_2 injection well surrounded radially by the dry zone, which is in turn surrounded radially by a zone of two-phase flow where CO_2 and brine flow together. Outside the two-phase zone is the original single-phase brine. The details of the flow regions are discussed in Section 3.3.

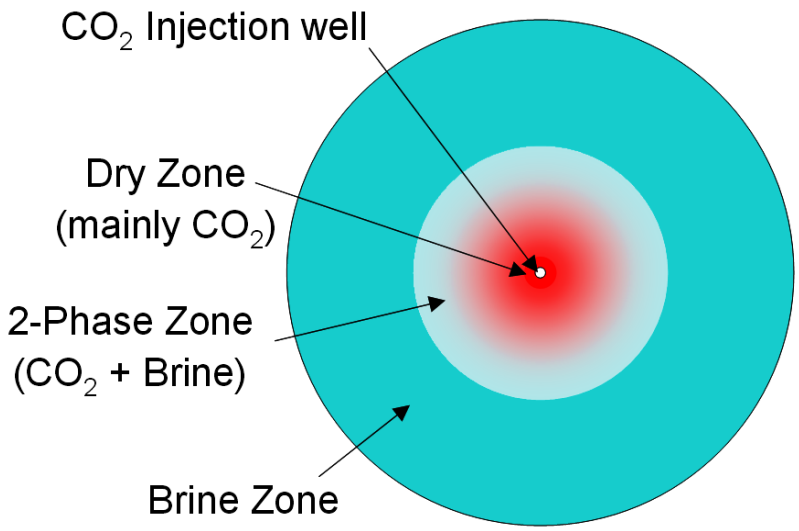

Fig. 4.2—Radial saturation variation around the CO_2 injection well.

Fig. 4.3 shows simulated saturation profiles for simulation times ranging from 1 to 30 years on injection. The dashed lines and arrows highlight the approximate radii of the dry, two-phase, shock, and brine zones for simulation after 30 years. This graph illustrates the reason for the shock front, which relates to Buckley-Leverett (1942) theory for immiscible displacements. It is also known as the mixing zone, as described by Lake (1989).

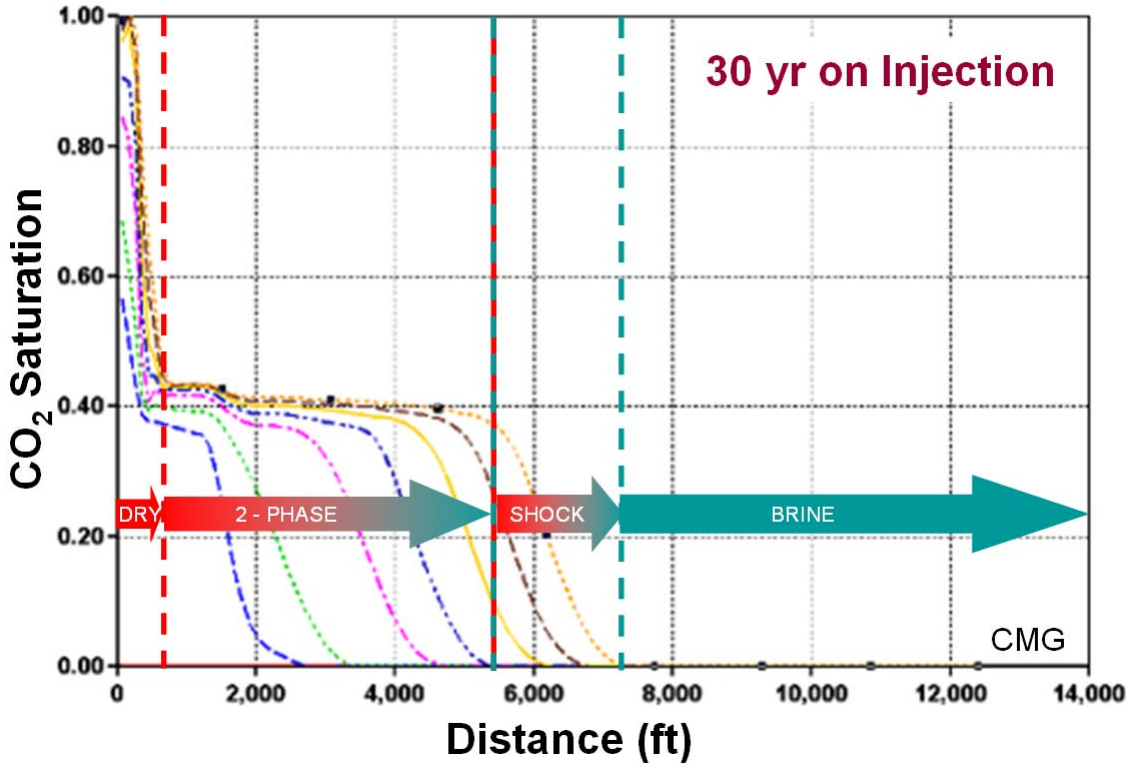

Fig. 4.3— Graph showing simulated saturation profiles for CO_2 injection well.

Lake (1989) describes the shock front in miscible displacements as a result of dispersion. It is described as in-situ mixing or dilution of chemical components as they are transported through a porous medium. It is a result of combined effects of molecular diffusion and fluid velocity gradients.

Following Lake (1989), the one-dimensional transport equation for isothermal miscible displacement of a tracer in homogeneous permeable media is

$$\frac{\partial C_D}{\partial t_D} + \frac{\partial C_D}{\partial x_D} - \frac{1}{N_{p_e}} \frac{\partial^2 C_D}{\partial x^2{}_D} = 0, \quad \text{..... (4.1)}$$

where C_D is the mass concentration (between 0 and1) at any point normalized to injection concentrations. The dimensionless time (pore volume injected) is

$$t_D = \frac{qt}{AL\phi} = \frac{Vt}{L} \ . \quad \text{..... (4.2)}$$

The dimensionless distance is

$$x_D = \frac{x}{L}, \quad \text{..... (4.3)}$$

where L is the length of the medium. The Peclet number, which is the ratio of convective to dispersive transport, is defined as

$$N_{P_e} = \frac{VL}{D_l} . \quad \text{..... (4.4)}$$

D_l is the longitudinal dispersion coefficient.

For continuous tracer injection, the analytical solution is (Lake 1989)

$$C_D = \frac{1}{2}\left[1 - erf\left(\frac{x_D - t_D}{2\sqrt{\frac{t_D}{N_{P_e}}}}\right)\right] + \frac{e^{x_D N_{P_e}}}{2}\left[1 - erf\left(\frac{x_D + t_D}{2\sqrt{\frac{t_D}{N_{P_e}}}}\right)\right], \quad \text{..... (4.5)}$$

where *erf* is the error function. From Eq. 5.4, as the value of Peclet number decreases, longitudinal dispersion coefficient increases. This means a large Peclet number yields a sharp shock front and a small peclet number yields a more spread-out front.

The dimensionless mixing zone length or length of the shock front is defined as

$$\Delta x_D = \frac{(x_{C_D=0.9} - x_{C_D=0.1})}{L} \quad \text{..... (4.6)}$$

The second term in Eq. 5.5 is neglected because its contribution becomes small for Peclet number greater than 50. Eq. 5.6 can now be simplified as

$$\Delta x_D = 3.625\sqrt{\frac{t_D}{N_{P_e}}} \quad \text{..... (4.7)}$$

Eq. 5.7 shows that the dispersive mixing zone grows in proportion to square root of time. Hold onto to this conclusion for now. We will use this in Section 4.6.

4.5 Pressure Profiles Around Co_2 Injection Well

Fig. 4.4 shows pressure profiles during CO_2 injection determined using the GEM-GHG numerical simulator for times ranging from 10 days to 30 years. CO_2 was injected for 30 years at 52 million scf/D (~1 million T/yr). The initial hydrostatic pressure of the reservoir is 2,600 psi. The fracture pressure of the reservoir is 4,200 psi. First, it is important to note that the pressure builds up around the well. Excessive aquifer pressurization could cause the seal above the aquifer to leak. An upper bound for the aquifer pressurization is given by the fracture pressure, which can be determined by specialized injection falloff tests (Nolte, 1979) that are routine in the petroleum industry. Dashed curves in Fig. 4.4 show different behavior for early times on injection from the later profile. As the pressure builds up around the injection well,

the pressure rise also propagates radially away from the well. The circle shows that in early time the pressure disturbance has not yet reached the simulation boundary at about 25,000 ft from the well. The total aquifer radius for this simulation is 5 miles, and the outer boundary of the aquifer is held at a constant pressure. Once the pressure disturbance reaches the outer boundary, the pressure profile follows an established trend that is highlighted by the slope lines shown for the profile after 5 years of injection.

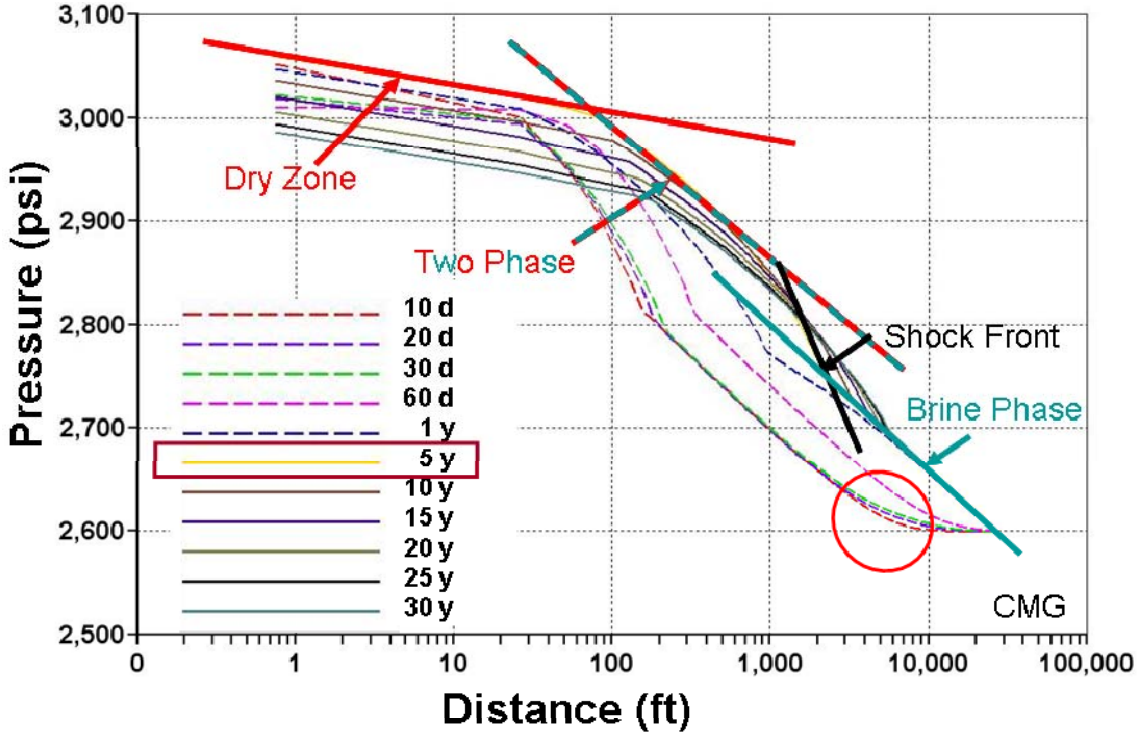

Fig. 4.4—Pressure profiles vs radial distance for CO_2 injection well. CO_2 is injected for 30 years at 52 million scf/D (~1 million T/yr). The initial hydrostatic pressure of the reservoir is 2,600 psi. The fracture pressure of the reservoir is 4,200 psi.

For steady-state flow, well bottomhole flowing pressure is given by

$$P_{wf} = P_e - \frac{141.2qB\mu}{kh}\left(\ln\frac{r_e}{r_w} + s\right), \quad \text{..... (4.8)}$$

where

P_e = initial reservoir pressure (psi)

q = flow rate (bbl/Day)

B = formation volume factor (bbl/STB)

μ = viscosity (cp)

k = permeability (md)

h = thickness (ft)

r_e = well radius (ft)

r_w = drainage radius (ft)

s = skin

The slope, *m,* of the curve at any point is given by

$$m = \frac{141.2qB}{\lambda h}, \quad \text{..... (4.9)}$$

where λ is the mobility of the reservoir fluid. It is the ratio of effective permeability to viscosity.

$$\lambda_{dry} = \frac{k_{r,S_{g=1}}}{\mu_w} \quad \text{..... (4.10)}$$

is the mobility of the single phase CO_2 zone.

$$\lambda_{2\phi} = \left(\frac{k_{rg}}{\mu_g} + \frac{k_{rw}}{\mu_w} \right)\Bigg|_{s_{g,avg}} \quad \text{..... (4.11)}$$

is the total mobility of the two-phase region.

$$\lambda_{brine} = \frac{1}{\mu_w} \quad \text{..... (4.12)}$$

is the mobility of the brine zone.

In Fig. 4.4, the lines illustrate that the pressure gradient is a linear function of the logarithm of radial distance from the well. Near the well the pressure gradient is lower or the mobility is higher because only CO_2 is flowing, and it has a much lower viscosity than brine. In the two-phase zone, the pressure gradient is higher than the dry zone or the mobility is relatively lower than the dry zone because both CO_2 and brine are flowing together. Between this zone and the outer single-phase zone is seen a much higher pressure gradient for the shock zone that will be explained later. The pressure gradient in the brine zone is higher than either the dry or the two-phase zone. This means its mobility is the lowest. One important observation here is that the pressure gradient in the single-phase zone is similar to that observed in the two-phase zone. The slopes of the two lines are almost parallel.

4.6 Pressure Derivative Plot

Fig. 4.5 shows a log-log plot of the pseudopressure function (Al-Hussainy et al. 1966) and its derivative with elapsed time on the Y axis. The pseudopressure change is shown during the falloff test as the upper symbols (red), and its derivative as the lower symbols trend (green). The pressure data has been simulated for a falloff test after 20 days on injection. The duration of the fall of is 5 days. A three-zone radial composite model (Acosta and Ambastha 1994) was tried to fit to the simulated pressure transient data. The pore space for the composite model was divided into three heterogeneous regions presenting a radial symmetry around the (vertical) wellbore. Mobility and diffusivity of the first region are defined by the time and pressure matches, and parameters of the two other zones are defined through their respective mobility and diffusivity ratios. The circular outer limit can be no-flow or constant pressure. The analytical model for the simulated data is also shown in Fig. 4.5 with solid lines. This

shows that the three-zone radial composite models are suitable to fit the pressure transient data. The derivative shows level trends that are directly proportional to the line slopes shown in Fig. 4.4. In Fig. 4.5, the behavior as time increases reflects pressure gradients at increasing radial distance from the well. The level of the flat trend in the derivative is inversely proportional to the product of the mobility and thickness (λh). Mobility is the ratio of effective permeability to the flowing fluid viscosity. Thickness refers to the aquifer thickness. The early low level corresponds to the low pressure gradient in the dry zone that results from the high mobility of the flowing CO_2. On the log-log plot, the intermediate pressure derivative data right after the dry zone is falling on a straight line, whose slope begins less than unity and then goes into an intermediate radial flow, the level corresponding to that of the two-phase zone. This is caused by continuously changing mobility and storativity.

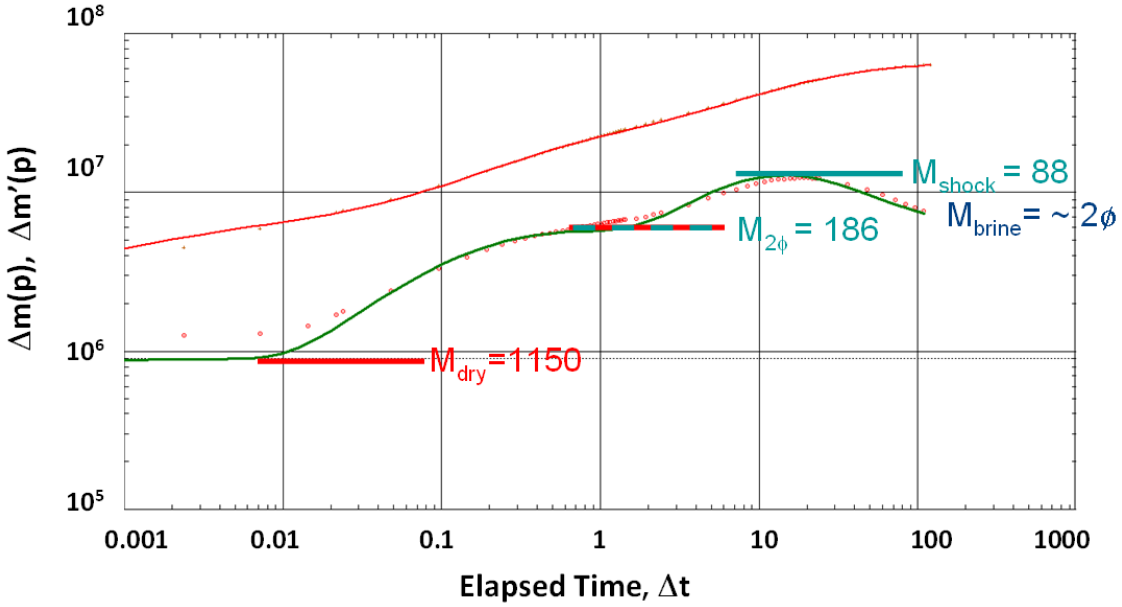

Fig. 4.5—Simulated injection falloff test after 20 days on injection. CO_2 is injected for 30 years at 52 million scf/D (~1 million T/yr). The initial hydrostatic pressure of the reservoir is 2,600 psi. The fracture pressure of the reservoir is 4,200 psi. The falloff was taken over a period of 5 days. The analytical model for the simulated data is also shown with solid lines.

Still later is a level corresponding to the shock zone. It is also known as the dispersive mixing zone, as discussed in Section 4.4. This discontinuity is happening because of the significant variation in fluid properties in a short distance. A fixed value of mobility is difficult to define in this region because it is constantly changing. M_{shock} in Fig. 4.5 corresponds to the mobility calculation from the slope at the last point of the shock front in Fig. 4.4. The shock front marks the end of the transition zone. At the end of transition region, towards the reservoir outer boundary, exists a single-phase brine zone, uninvaded by the injected CO_2. This zone has lowest mobility and storativity values. However, in this case the single-phase brine zone is too far away to be sensed by the falloff test, which is already 5 days long, but the derivative trend is returning to the lower level associated with the pressure gradient in that zone. The brine derivative level is masked by the shock front. It may be possible to detect the brine derivative level for a much longer falloff.

However, taking a really long falloff may not be possible during the early life of a sequestration project for the obvious reason of not interrupting CO_2 injection operations for significant duration. We envision a much longer falloff after the permanent cessation of injection, which corresponds to life of the power plant. In this case, we consider a 30-year injection period followed by a 1.5-year-long falloff. Fig. 4.6 shows a simulated pressure falloff test for 1.5 years after 30 years on injection. As can be seen, the shock front did not reach the brine derivative level rather the pressure derivative plot dives down as a consequence of the drainage boundary. Fig. 4.4 shows that the pressure disturbance after 30 years of injection has reached the simulation boundary at about 25,000 ft from the well. As a consequence of the boundary interference, it is not possible to see the brine derivative level.

Fig. 4.7 shows a simulated pressure falloff test for 1.5 years after 30 years on injection for an infinite-acting boundary condition. All other simulation parameters are kept constant. Clearly, the pressure transient reaches the brine derivative level in 1.5 years.

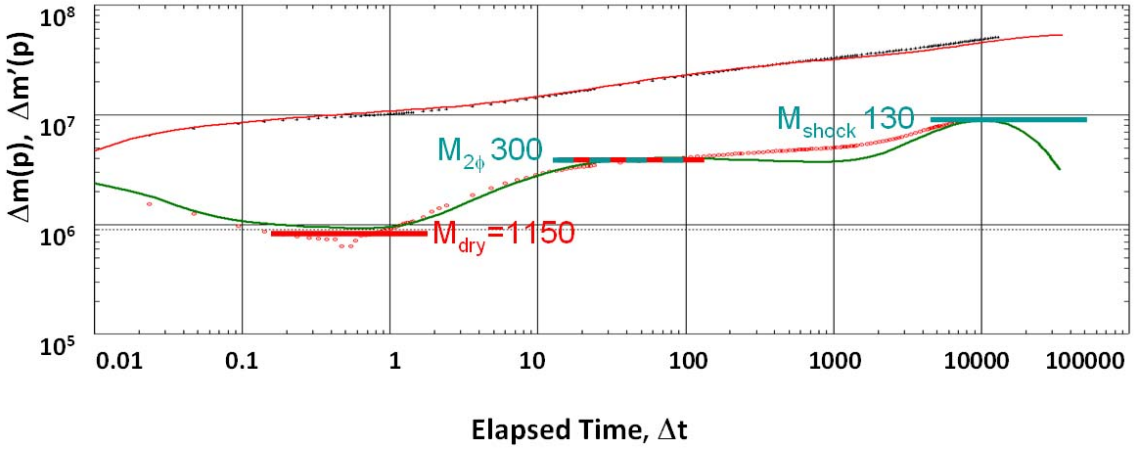

Fig. 4.6—Plot shows simulated injection falloff test after 30 years on injection. CO_2 was injected for 30 years at 52 million scf/D (~1 million T/yr). The falloff was taken for a period of 1.5 years. The simulation boundary is about 25,000 ft from the injection well. The analytical model for the simulated data is also shown with solid lines.

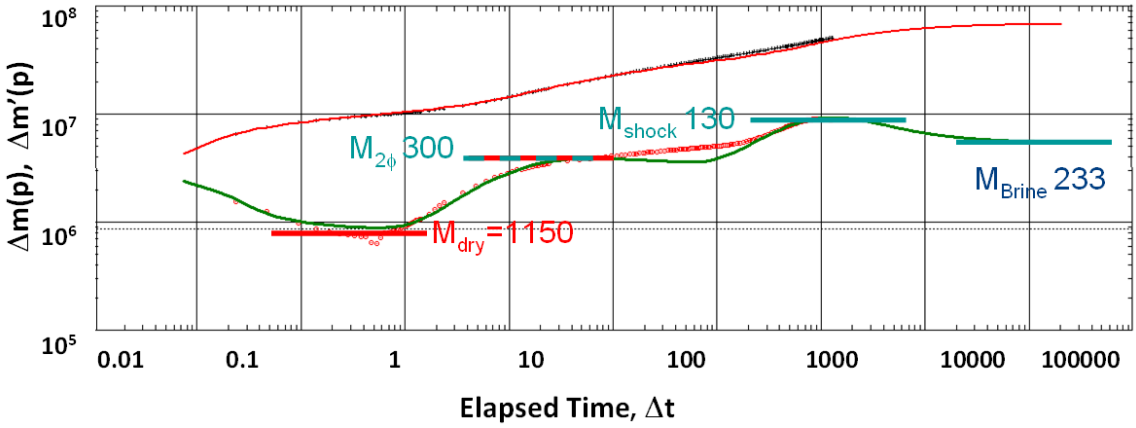

Fig. 4.7—Plot shows simulated injection falloff test after 30 years on injection. CO_2 was injected for 30 years at 52 million scf/D (~1 million T/yr). The falloff was taken for a period of 1.5 years. The simulation boundary is at infinite distance from the injection well. The analytical model for the simulated data is also shown with solid lines.

Consequently, it is practically impossible to see the brine derivative level unless the drainage boundaries are too far off from the injection well or a longer falloff is taken very early in the life of a sequestration project. For commercial sequestration projects

at practical injection rates (>3 million T/yr), multiple injection wells will be required to be able to put the target amount of CO_2 in the ground. The pressure interference between the wells located in the same aquifer causes significant injection losses and severely limits the drainage area, thus making boundary effects dominant in a pressure falloff test.

Lake (1989) shows that a dispersive mixing zone grows in proportion to square root of time. This means that with subsequent falloff tests, it will be more and more difficult to see the brine-derivative level beyond the shock front.

4.5.1 Successive Pressure Falloff Tests

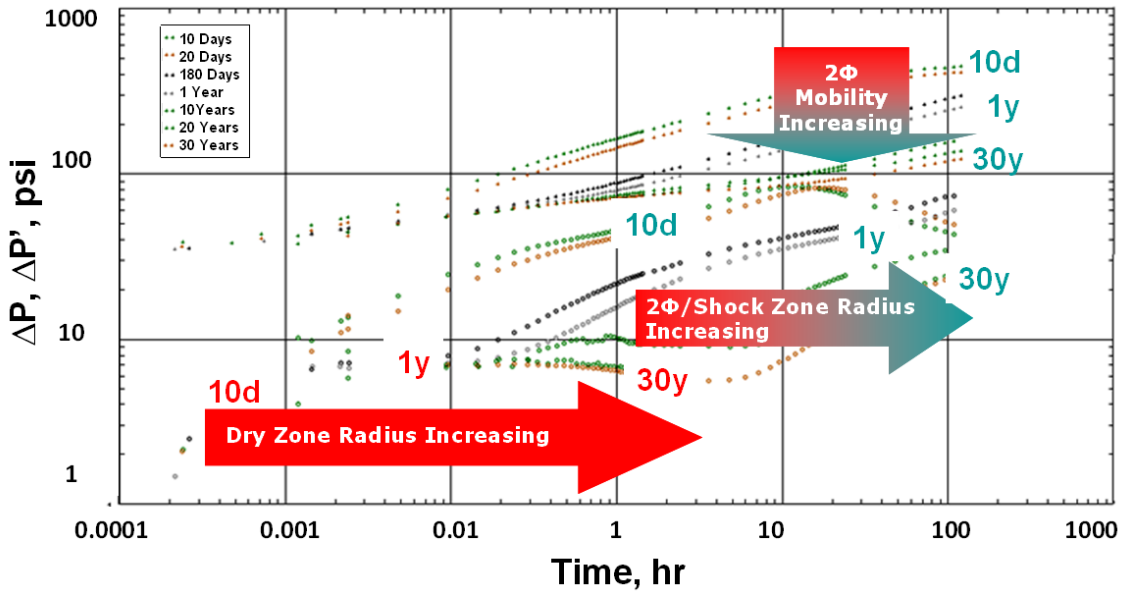

Fig. 4.8—Succession of injection falloff tests showing advance of dry and two-phase zones.

Fig. 4.8 shows a succession of injection falloff tests like the one shown in Fig. 4.5. Marked in red are upward departures in the pressure derivative from the first level trend corresponding to the dry zone mobility. Timing of this departure is proportional to the square of the dry zone radius. Likewise, marked in cyan are departure times from the two-phase level trend that are related to the position of the shock front. Also shown is gradual reduction in the pressure change trends. This corresponds to

increasing injectivity resulting from the expanding zone of higher dry-zone mobility around the well. Dry-zone radius can be calculated with reasonable accuracy at different times using the time-of-departure concept. The radius of the dry zone can be written as

$$r_{dry} = \sqrt{\frac{kt}{948\phi\mu c_t}}, \quad \text{..... (4.13)}$$

where k = permeability (md)

t = time of departure from the first radial flow (hr)

ϕ = porosity

μ = viscosity (cp)

c_t = total compressibility (psi^{-1})

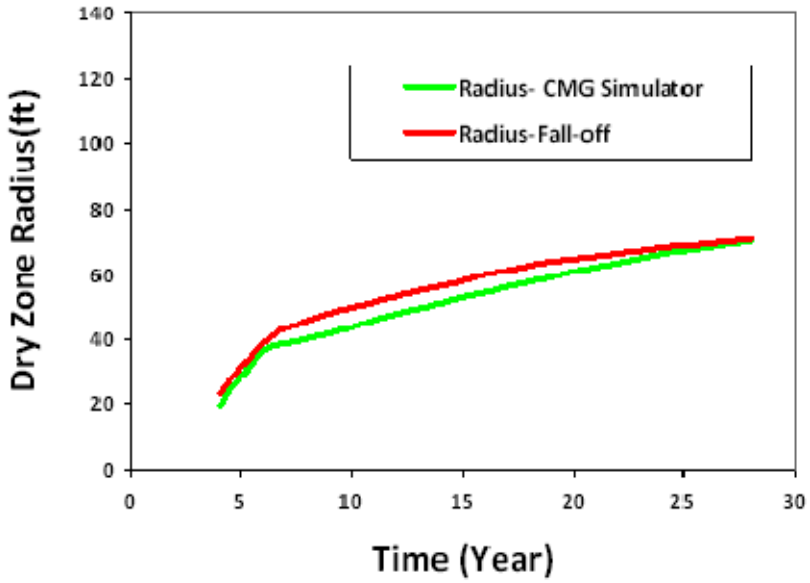

Fig. 4.9—A comparison of the radius of dry zone obtained from CMG simulator and pressure falloff test at different injection time. CO_2 was injected for 30 years at 52 million scf/D (~1 million T/yr).

Fig. 4.9 shows a comparison of the dry zone radius computed from CMG numerical simulation and from the successive falloff tests using the time of departure concept. The mobility values from the numerical simulator are calculated using the pressure profile around the CO_2 injection well (Fig. 4.4). Using the procedure explained in Section 4.5, a close match is obtained with the radius obtained from numerical simulator.

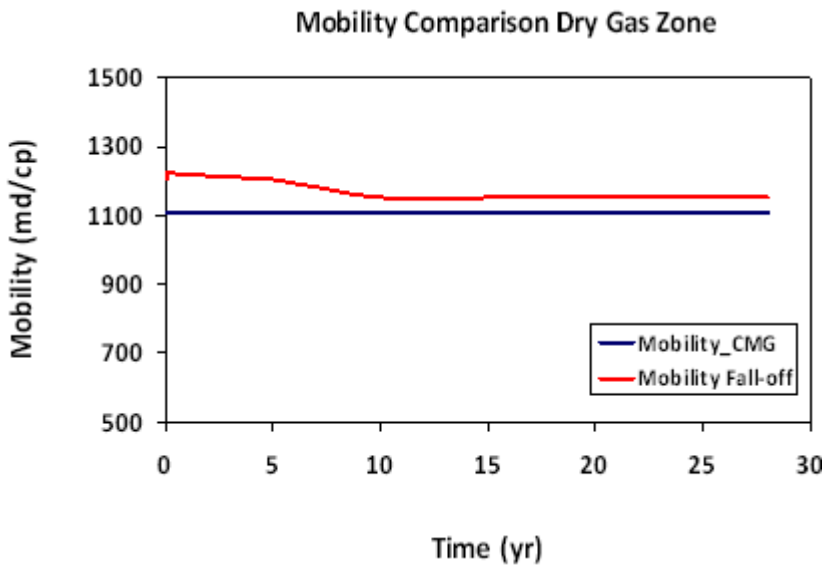

Fig. 4.10—Comparison of the mobility of the dry zone obtained from the numerical reservoir simulator and pressure falloff test at different injection times. CO_2 was injected for 30 years at 52 million scf/D (~1 million T/yr).

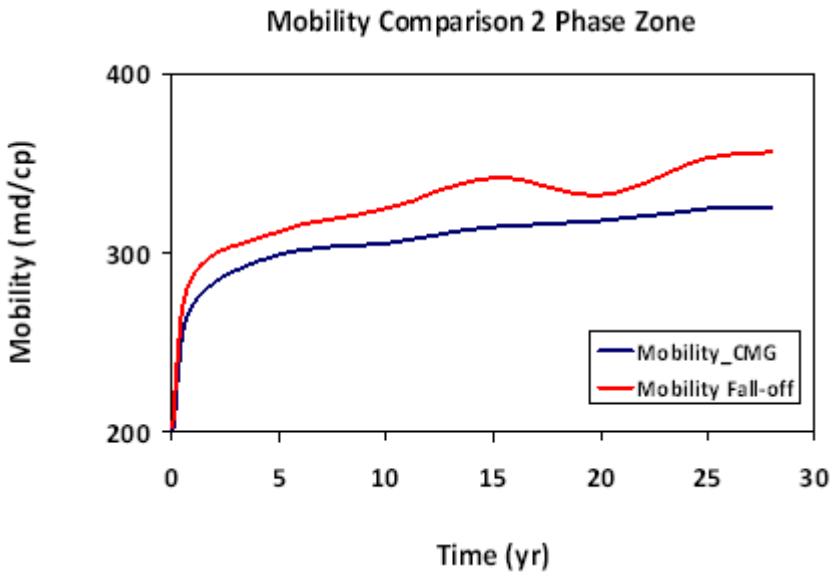

Fig. 4.11—Comparison of the mobility of two-phase zone obtained from numerical reservoir simulator and pressure falloff test at different injection time. CO_2 was injected for 30 years at 52 million scf/D (~1 million T/yr).

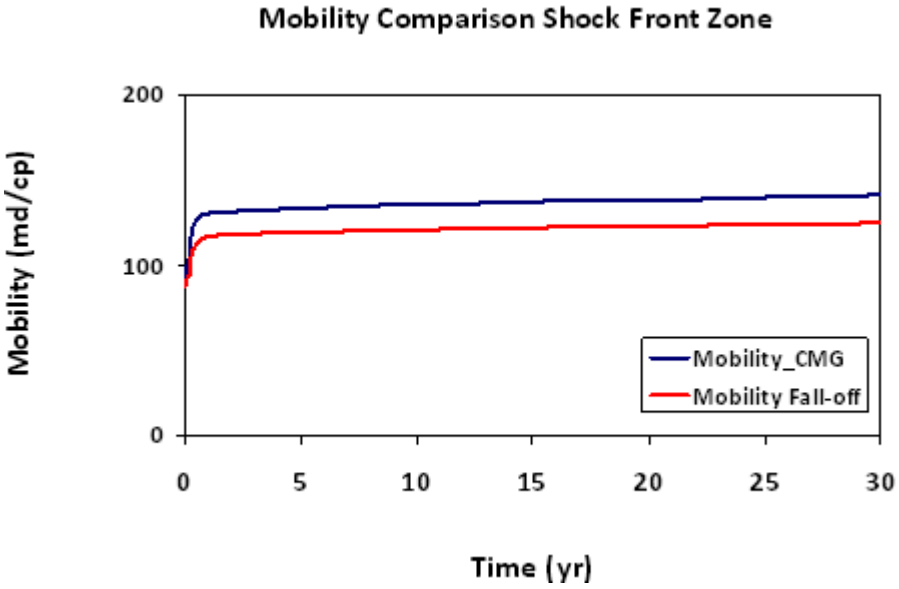

Fig. 4.12—Comparison of the mobility of shock front obtained from numerical reservoir simulator and pressure falloff test at different injection time. CO_2 was injected for 30 years at 52 million scf/D (~1 million T/yr).

Fig. 4.10 through Fig. 4.12 shows a comparison of the mobilities of different zones (dry, two-phase, shock) computed from CMG numerical simulation and from the successive falloff tests. A procedure for computing the mobilities of different zones from the numerical simulator was discussed in Section 4.5 and from pressure falloffs was discussed in Section 4.6 of this section. A close match was obtained between the mobilities computed from pressure falloff tests and the numerical simulator.

The physics of CO_2 sequestration is clearly visible from the successive pressure falloff tests. Planning falloff tests at regular intervals for a commercial scale CO_2 projects can provide significant insights into the real-time movement of saturation fronts and mobility behavior in the aquifer. The information obtained can also be integrated to constrain and refine numerical simulation models.

4.7 Determination of Average Aquifer Pressure

Horner analysis is the usual way to determine reservoir pressure. The Horner time function is given by the ratio of total time divided by the elapsed time since injection is stopped (the start of the pressure falloff). The total time is approximated as the sum of the material balance time and elapsed time since the start of the falloff. Material balance time is given by the cumulative injection divided by the last injection rate before injection is stopped.

When the injection pressure falloff is graphed against the logarithm of the Horner time function, a linear trend is normally observed for ranges of time that show a level pressure derivative. The usual Horner analysis approach would extrapolate the portion of the data showing the level derivative response corresponding to the single-phase brine to infinite shut-in time, which corresponds to unit value in the Horner time function. However, Fig. 4.8 shows that none of the falloffs, not even those after only a few days on injection, end with this response. This would normally discourage Horner analysis.

What enables Horner analysis to work is the observation that the pressure gradient in the two-phase zone has a similar value to that in the single-phase zone. Therefore, if the trend seen for the two-phase zone is extrapolated to the unit Horner time function value, the resulting extrapolated pressure will be nearly what would be determined with an extrapolation based on a rigorous analysis of the trend for the brine zone. However, this is very sensitive to the inputs of the relative permeability curves and may not work if the two-phase mobility is not close enough to the brine mobility in magnitude.

Fig. 4.13 illustrates the point. Each of the lines shown in the figure are drawn through the portion of the data that flatten at the two-phase level on a log-log diagnostic plot like that in Fig. 4.5 for a given injection falloff test. The extrapolated pressures determined for each of these lines are shown in Fig. 4.14. Also shown in Fig. 4.14 are actual average reservoir pressure values from the CMG numerical simulation compared to the average pressure obtained from pressure falloffs, and it is evident that this approach provides a very reasonable approximation to the average reservoir pressure trend.

Figs. 4.4 through 4.14 all relate to a simulation with the outer boundary of the reservoir held at a constant pressure. While many CO_2 injection models use this outer boundary condition because is runs much faster and requires much lower CPU resources than with a no-flow outer boundary, the no-flow outer boundary is appropriate if the aquifer volume is compartmentalized by either structural or stratigraphic limits, or if the well volume is effectively bounded by interference with other injection wells.

Fig. 4.15 shows the simulated succession of injection falloff analyses for a bounded aquifer. The reservoir reaches a quasisteady state much like what is called pseudosteady state for primary production of a single-phase fluid. While for

pseudosteady-state production the pressure profile remains the same and pressure drops everywhere at the same rate, for CO_2 injection the established behavior continues to change as the various saturation zones expand in time. Apart from these rather subtle changes, the overall effect is analogous to pseudosteady-state behavior.

From Fig. 4.16, the trend for the extrapolated pressures from the Horner analysis again matches the trend determined from the simulation, but the trend is quite unlike that observed for the open aquifer simulated with a constant pressure outer boundary. In this case the average reservoir pressure rises linearly with time as long as CO_2 injection continues at a constant rate. The pore volume of the closed aquifer can easily be estimated from the linear pressure increase by the following simple material balance equation:

$$V_{CO_2} = c_t(\Delta p)V_p \quad \text{..... (4.14)}$$

where V_{CO_2} is the total volume of CO_2 to be injected over the life of the sequestration project, V_p is pore volume available for CO_2 storage, c_t is the total compressibility discussed in Eq. 3.19, and Δp is the difference between average aquifer pressure determined from the Horner plot and the initial aquifer pressure. This equation is not applicable to open aquifers because the native brine is moving out of the system.

The gas injection rate for the closed drainage area in this case is 10 million scf/D for 30 years. Using Eq. 3.19, the compressibility of the system can be estimated as 6.5E-6 psi^{-1}. The pressure rise of the system after 5 years is 80 psi, and the volume injected is 18,250 million scf, or 22.8 million reservoir cu ft. From this, the pore volume is estimated as 4.38E+10 ft^3. For the given thickness of 250 ft and porosity of 0.2, the dimension of the square drainage area can be estimated as 5.2 miles X 5.2 miles. This is very close to the actual dimension of 5 miles X 5 miles. Accurate estimation of compressibility is very important for the accuracy of this analysis.

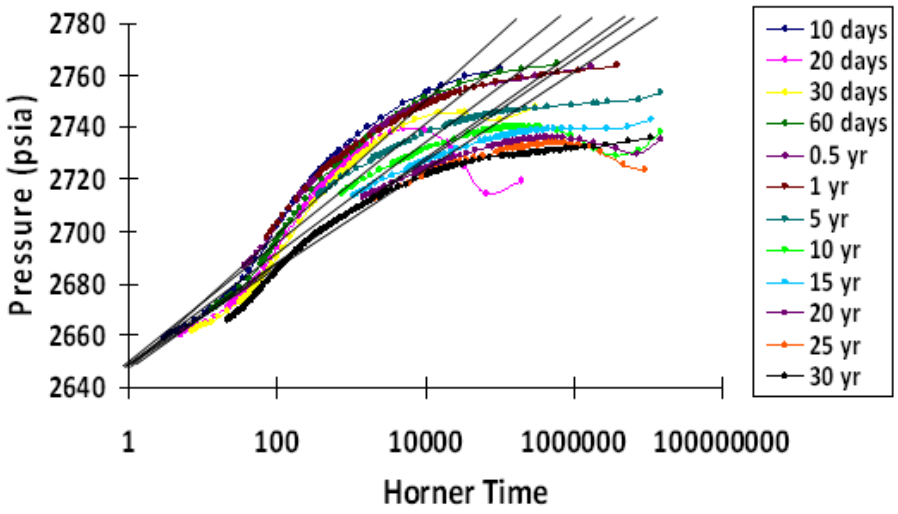

Fig. 4.13—Horner analysis for estimation of average aquifer pressure, open aquifer case. CO_2 was injected for 30 years at 10 million scf/D (~0.2 million T/yr). The initial hydrostatic pressure of the reservoir was 2,600 psi. The fracture pressure of the reservoir is 4,200 psi.

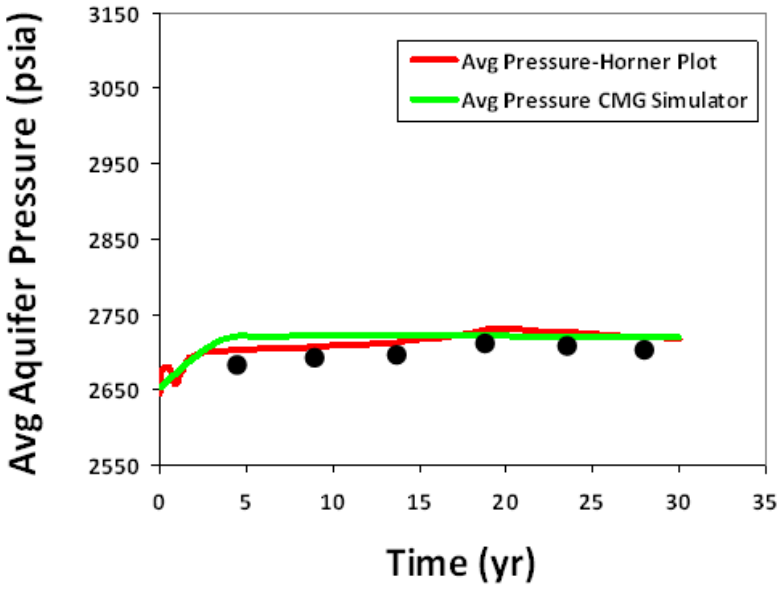

Fig. 4.14—Trend from extrapolated pressures values determined from Horner analysis compared to values determined from the CMG numerical, open aquifer case. CO_2 was injected for 30 years at 10 million scf/D (~0.2 million T/yr). The initial hydrostatic pressure of the reservoir was 2,600 psi. The fracture pressure of the reservoir is 4,200 psi.

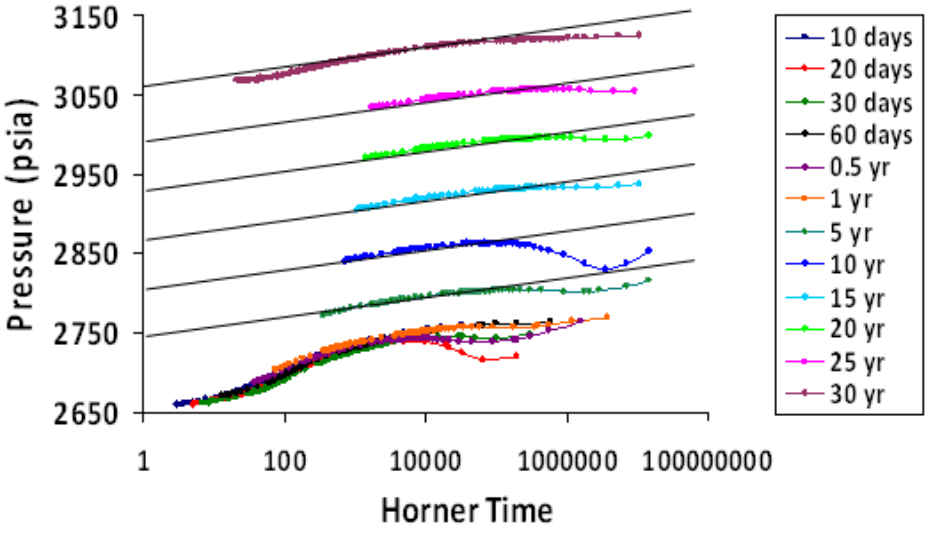

Fig. 4.15—Horner analysis for estimation of average aquifer pressure-bounded aquifer case. CO_2 was injected for 30 years at 10 million scf/D (~0.2 million T/yr). The initial hydrostatic pressure of the reservoir was 2,600 psi. The fracture pressure of the reservoir is 4,200 psi.

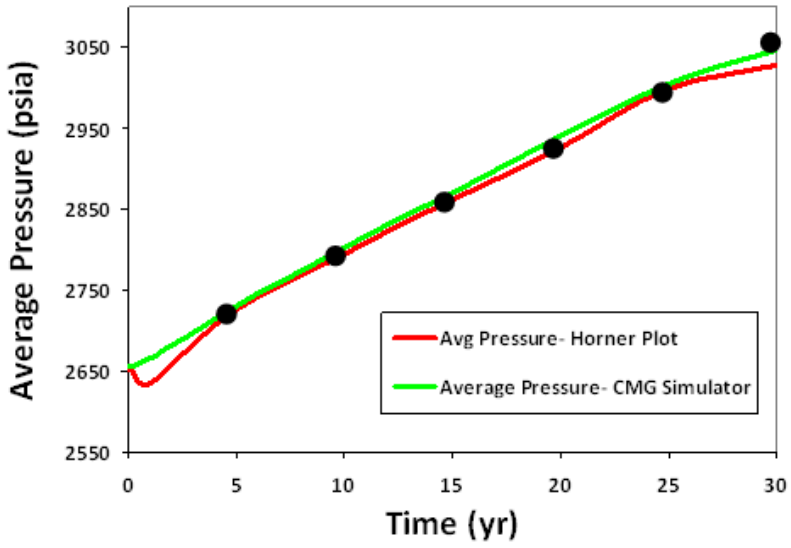

Fig. 4.16—Trend from extrapolated pressure values determined from Horner analysis compared to values determined from the CMG numerical simulation, bounder aquifer case. CO_2 was injected for 30 years at 10 million scf/D (~0.2 million T/yr). The initial hydrostatic pressure of the reservoir was 2,600 psi. The fracture pressure of the reservoir is 4,200 psi.

4.8 Detection of an Aquifer Leak

One major requirement for the commercial application of geologic sequestration is accurate leak detection through continued monitoring. The small expected concentration of the leaking CO_2 above the aquifer as well as the large background of CO_2 present in the atmosphere makes it extremely challenging to implement surface monitoring techniques.

The continuous diffusion of CO_2 from the soil into the atmosphere due to plant and microbial respiration further exacerbates the situation. Any leak of CO_2 from a reservoir would have to be differentiated from these other processes. Surface monitoring includes the detection of injected tracer molecules, direct measurement of CO_2 soil flux, soil gas analysis, and carbon isotope analysis from soil gas (Strazisar et al. 2003). A range of technologies exists to measure CO_2 concentrations and fluxes in the shallow subsurface and the atmospheric surface layer (Oldenburg et al. 2003). These measurements, in conjunction with a parallel modeling effort and deep seismic surveys, will provide an accurate measure of the leakage rate of CO_2 to the surface.

Current literature insists on monitoring the leakage from the reservoir quantitatively by measuring the surface fluxes (IPCC 2008). However, an understanding of the leakage behavior from the subsurface standpoint is critical to assessing the realized benefit of sequestration in geologic formations. A substantial leak of CO_2 can be easily seen through ongoing monitoring of the average pressure behavior. To show this, simulations were performed using the three leak positions shown in Fig. 4.17. The first case is for a leak in the dry zone, then a leak in the two-phase zone, and finally a leak in the brine zone. The leaks were modeled using long horizontal wells with a threshold BHP of 2,900 psi. The initial reservoir pressure is 2,600 psi. The horizontal well starts leaking fluid out of the reservoir as the reservoir pressure rises

and reaches a threshold value of 2,900 psi. The idea is to simulate a breach in the seal that cracks open when the pressure of the reservoir rises above a certain value.

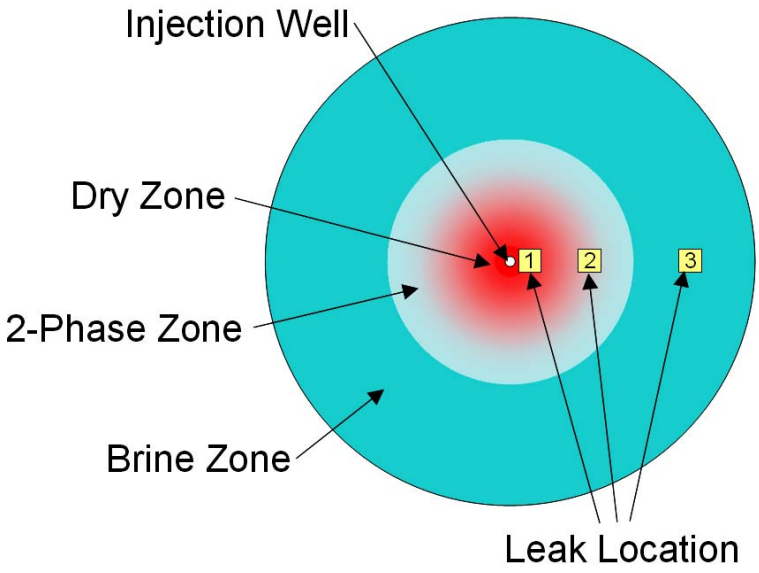

Fig. 4.17—Simulated leak positions.

4.8.1 Dry Zone Leak

Fig. 4.18 shows Horner graphs of successive injection falloff tests for the case with a leak in the dry zone. The falloffs are taken every two years after the second year. The leak location is at a distance of 1,000 ft from the wellbore. The behavior is clearly distinct from that seen in either Fig. 4.13 or Fig. 4.15, and the average pressure behavior is also different, as seen in Fig 4.19. The Horner plot for the case with no leakage in Fig. 4.15 shows a classic quasisteady-state behavior where the average reservoir pressure rises linearly with time as long as CO_2 injection continues at a constant rate, whereas in this case the pressure is leveling out as in the case of a constant-pressure boundary, but at a higher average aquifer pressure. This is also highlighted from the clustering of pressure falloffs on the Horner plot in late time. Because this is a simulation, the fluid phase leaking from the aquifer can be determined, and Fig. 4.20 shows that mainly CO_2 is leaking out once the dry zone radius reaches this position.

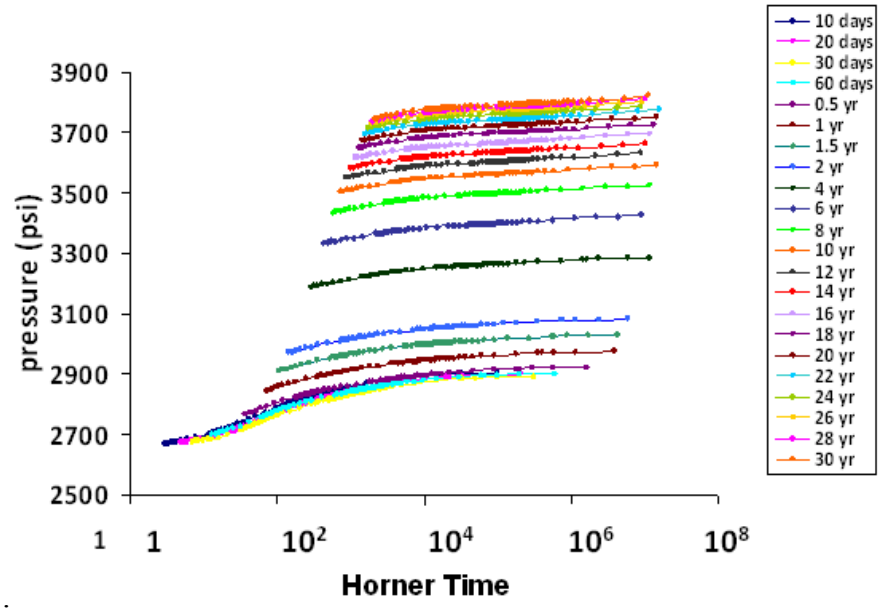

Fig. 4.18—Horner analysis for estimation of average aquifer pressure, bounded aquifer with leak in the dry zone. CO_2 was injected for 30 years at 25 million scf/D (~0.5 million T/yr). The initial hydrostatic pressure of the reservoir was 2,600 psi. The fracture pressure of the reservoir is 4,200 psi. The leak is is located at a distance of 1,000 ft from the wellbore.

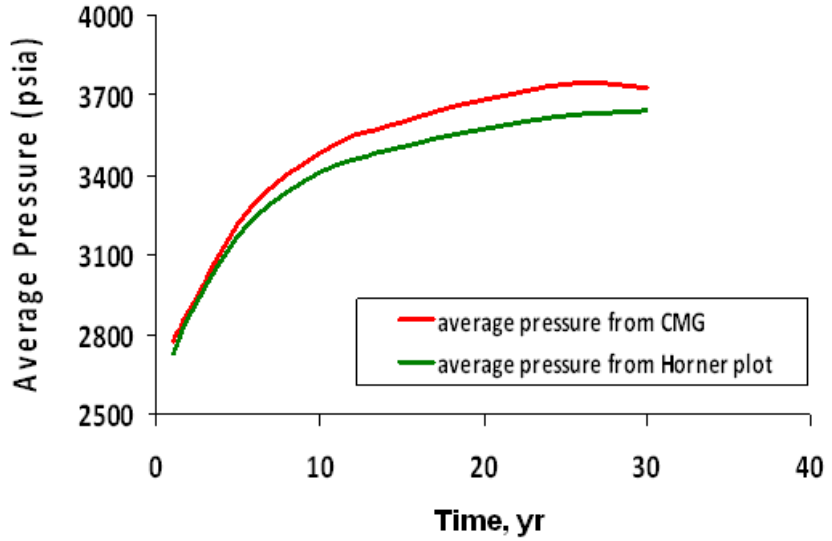

Fig. 4.19—Trend from extrapolated pressure values determined from Horner analysis compared to values determined from the simulation, bounded aquifer with leak in the dry zone. CO_2 was injected for 30 years at 25 million scf/D (~0.5 million T/yr). The initial hydrostatic pressure of the reservoir was

2,600 psi. The fracture pressure of the reservoir is 4,200 psi. The leak is located at a distance of 1,000 ft from the wellbore.

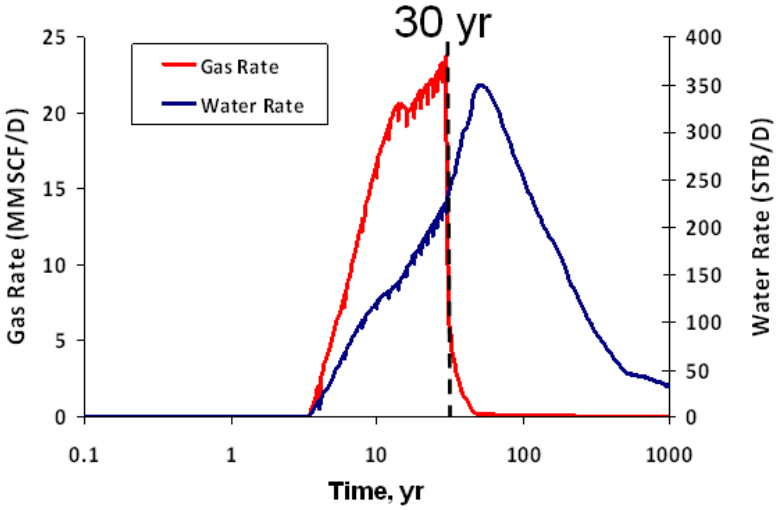

Fig. 4.20— Simulated fluids leaking from the dry zone. CO_2 was injected for 30 years at 25 million scf/D (~0.5 million T/yr). The initial hydrostatic pressure of the reservoir was 2,600 psi. The fracture pressure of the reservoir is 4,200 psi. The leak is located at a distance of 1,000 ft from the wellbore.

4.8.2 Two-phase Zone Leak

Fig. 4.21 shows Horner graphs of successive injection falloff tests for the case with a leak in the two-phase zone. The leak is located at a distance of 7,000 ft from the wellbore. The behavior is clearly distinct from that seen in either Fig. 4.13 or Fig. 4.15. Fig. 4.22 shows average pressure behavior for a leak in the two-phase zone. After leveling for some time, eventually the average pressure again goes into quasisteady state behavior. Once again, the Horner plot looks quite different from the classic quasisteady state behavior shown in Fig. 4.15 highlighting no leak. Interestingly, the clustering of pressure falloffs on the Horner plot has shifted its position. This indicates that the rate and quantity of fluid leaking out of the reservoir is not same as the case when the leak was 1,000 ft away from the wellbore. Fig. 4.23 shows that mainly brine is leaking out of the aquifer with small amount of CO_2, once the two-phase zone radius reaches this position.

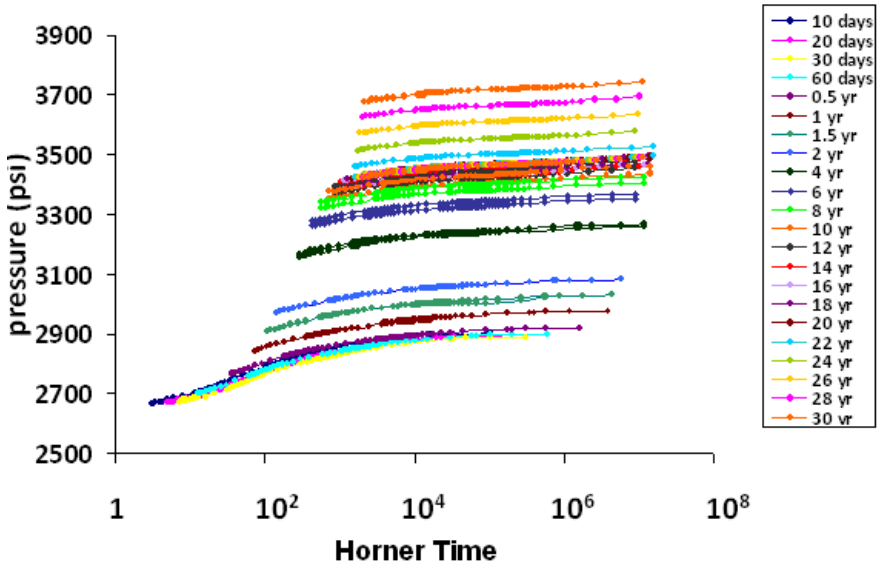

Fig. 4.21—Horner analysis for estimation of average aquifer pressure — bounded aquifer with leak in the two-phase zone. CO_2 was injected for 30 years at 25 million scf/D (~0.5 million T/yr). The initial hydrostatic pressure of the reservoir was 2,600 psi. The fracture pressure of the reservoir is 4,200 psi. The leak is located at a distance of 7,000 ft from the wellbore.

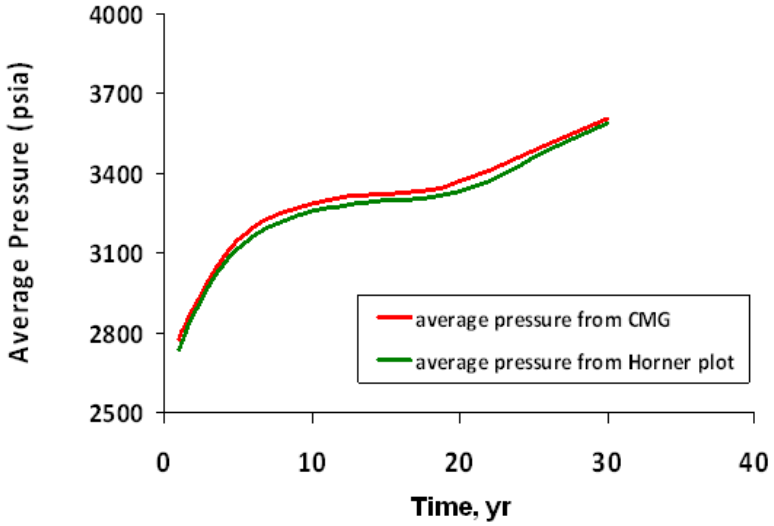

Fig. 4.22— Trend from extrapolated pressure values determined from Horner analysis compared to values determined from the simulation, bounded aquifer with leak in the two-phase zone. CO_2 was injected for 30 years at 25 million scf/D (~0.5 million T/yr). The initial hydrostatic pressure of the

reservoir was 2,600 psi. The fracture pressure of the reservoir is 4,200 psi. The leak is located at a distance of 7,000 ft from the wellbore.

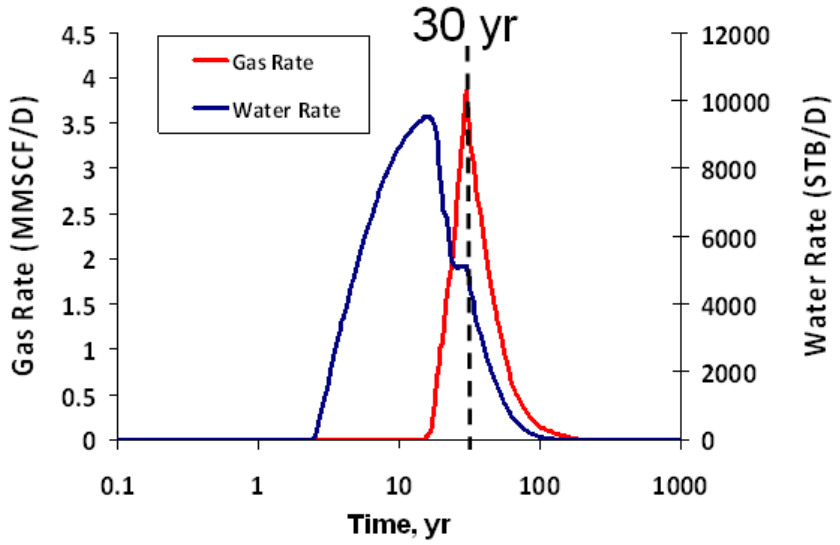

Fig. 4.23—Simulated fluids leaking from the two-phase zone. CO_2 was injected for 30 years at 25 million scf/D (~0.5 million T/yr). The initial hydrostatic pressure of the reservoir was 2,600 psi. The fracture pressure of the reservoir is 4,200 psi. The leak is located at a distance of 7,000 ft from the wellbore.

4.8.3 Brine Zone Leak

Fig. 4.24 shows Horner graphs of successive injection falloff tests for the case with a leak in the brine zone. The leak is located at a distance of 15,000 ft from the wellbore. The behavior is clearly distinct from that seen in either Fig. 4.13 or Fig. 4.15. Fig. 4.25 shows average pressure behavior for a leak in the brine zone. After initial quasisteady- state behavior, the pressure is leveling out as in the case of a constant-pressure boundary, but at a higher average aquifer pressure. Once again, the Horner plot looks quite different from the classic quasisteady-state behavior shown in Fig. 4.15, which had no leak. Interestingly, the clustering of pressure falloffs on the Horner plot has shifted its position again. This indicates that the rate and quantity of fluid leaking out of the reservoir is not same as the case when the leak was 1,000 ft or 7,000

ft away from the wellbore. Fig. 4.26 shows that only brine is leaking out of the aquifer.

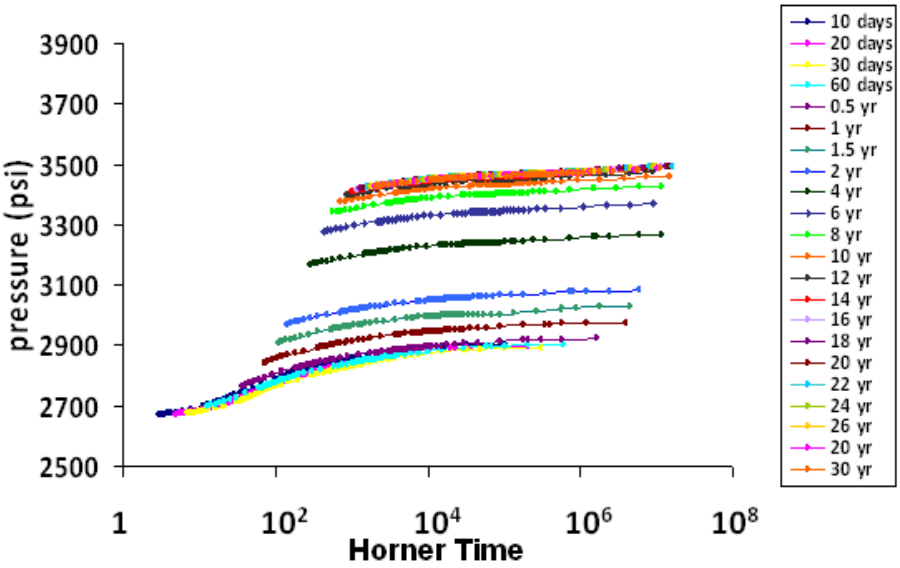

Fig. 4.24—Horner analysis for estimation of average aquifer pressure, bounded aquifer with leak in the brine zone. CO_2 was injected for 30 years at 25 million scf/D (~0.5 million T/yr). The initial hydrostatic pressure of the reservoir was 2,600 psi. The fracture pressure of the reservoir is 4,200 psi. The leak is located at a distance of 15,000 ft from the wellbore.

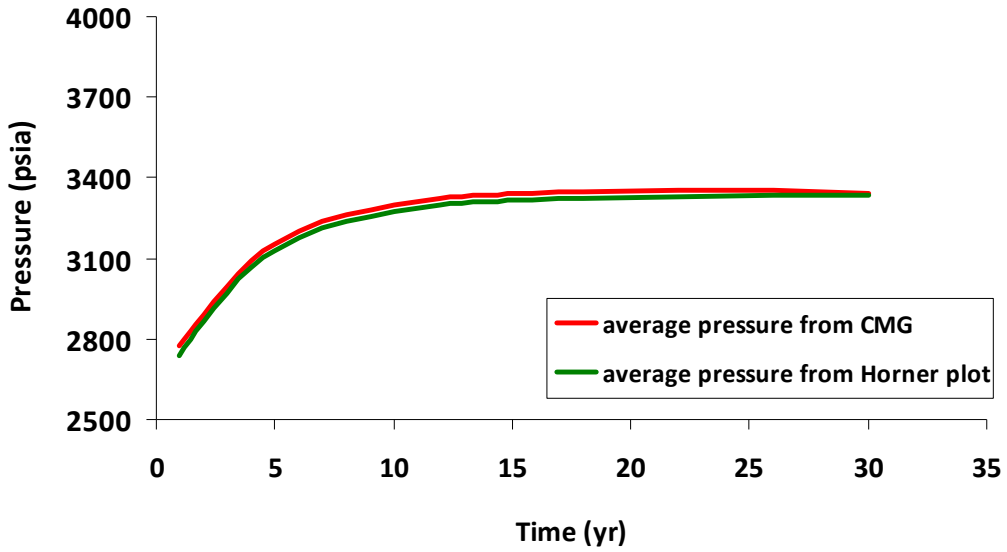

Fig. 4.25—Trend from extrapolated pressure values determined from Horner analysis compared to values determined from the simulation, bounded aquifer with leak in the brine zone. CO_2 was injected for 30 years at 25 million scf/D (~0.5 million T/yr). The initial hydrostatic pressure of the reservoir was 2,600 psi. The fracture pressure of the reservoir is 4,200 psi. The leak is located at a distance of 15,000 ft from the wellbore.

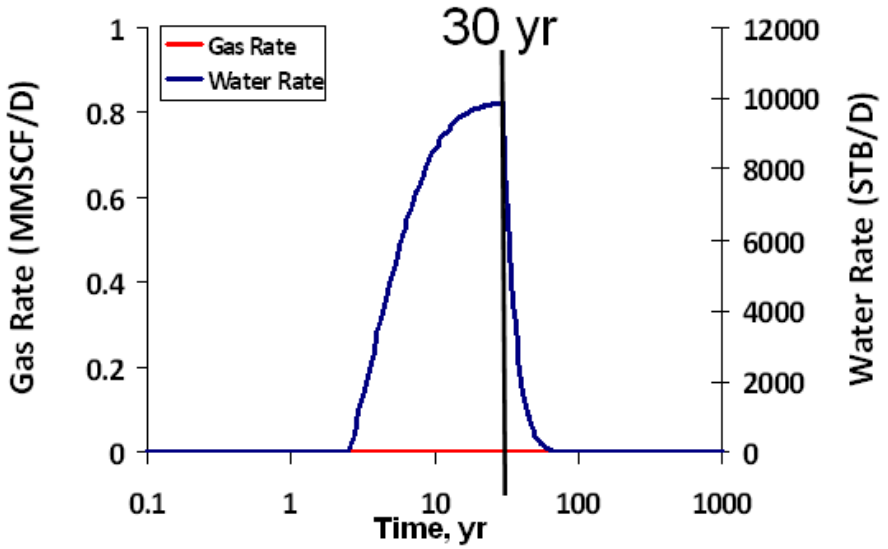

Fig. 4.26—Simulated fluids leaking from the brine zone. CO_2 was injected for 30 years at 25 million scf/D (~0.5 million T/yr). The initial hydrostatic pressure of the reservoir was 2,600 psi. The fracture pressure of the reservoir is 4,200 psi. The leak is located at a distance of 7,000 ft from the wellbore.

The behavior of Horner plot depends on the location and amount of fluid leaking out of the system. It is very difficult to characterize the location of the leak with the Horner plots. However, if the size of the aquifer or the rate of the leakage any one of them is known then the distinctive differences in average pressure behavior can be analyzed using material balance. The next section will briefly discuss the application of material balance for quantification of leaks.

4.8.4 Quantification of Leakage

The total volume of the fluid leaking out of the aquifer can be calculated using material balance. Fig. 4.27 shows the average pressure behavior of the case with a leak in the brine zone. The trend line shows the pseudosteady-state behavior of the aquifer with no leak. If there is no leak, the average pressure should continue to follow this trend as long as constant rate injection continues.

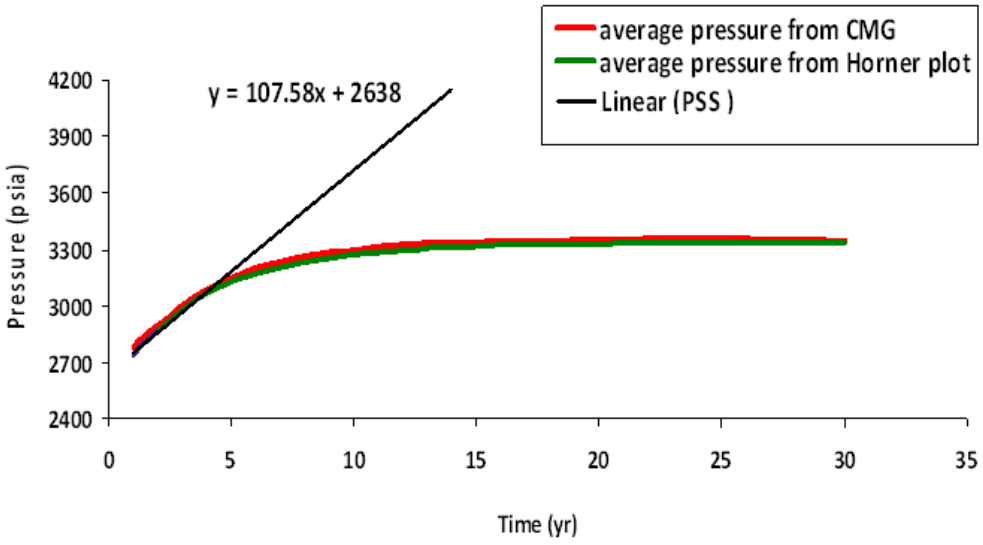

Fig. 4.27—Simulated fluids leaking from the brine zone. CO_2 was injected for 30 years at 25 million scf/D (~0.5 million T/yr). The initial hydrostatic pressure of the reservoir was 2,600 psi. The fracture pressure of the reservoir is 4,200 psi. The leak is located at a distance of 7,000 ft from the wellbore.

The difference between the average pressure determined from successive falloff tests and the pseudosteady state trendline can provide an estimation of the total fluid leaking out of the aquifer.

$$V_{leak} = c_t(\overline{p}_{pss} - \overline{p}_{leak})V_p, \quad \text{..... (4.14)}$$

where V_{leak} is the total volume of fluid leaking out of the aquifer, V_p is pore volume determined as previously from the early linear trend in average pressure with time, c_t is the total compressibility calculated from Eq. 3.19 in Section 3, $\overline{p}_{pss}$ is the pressure from the pseudosteady-state trendline, and $\overline{p}_{leak}$ is the average pressure for the leaking aquifer. Fig. 4.28 shows a comparison of simulated fluids leaking from the brine zone and prediction from Eq. 4.14.

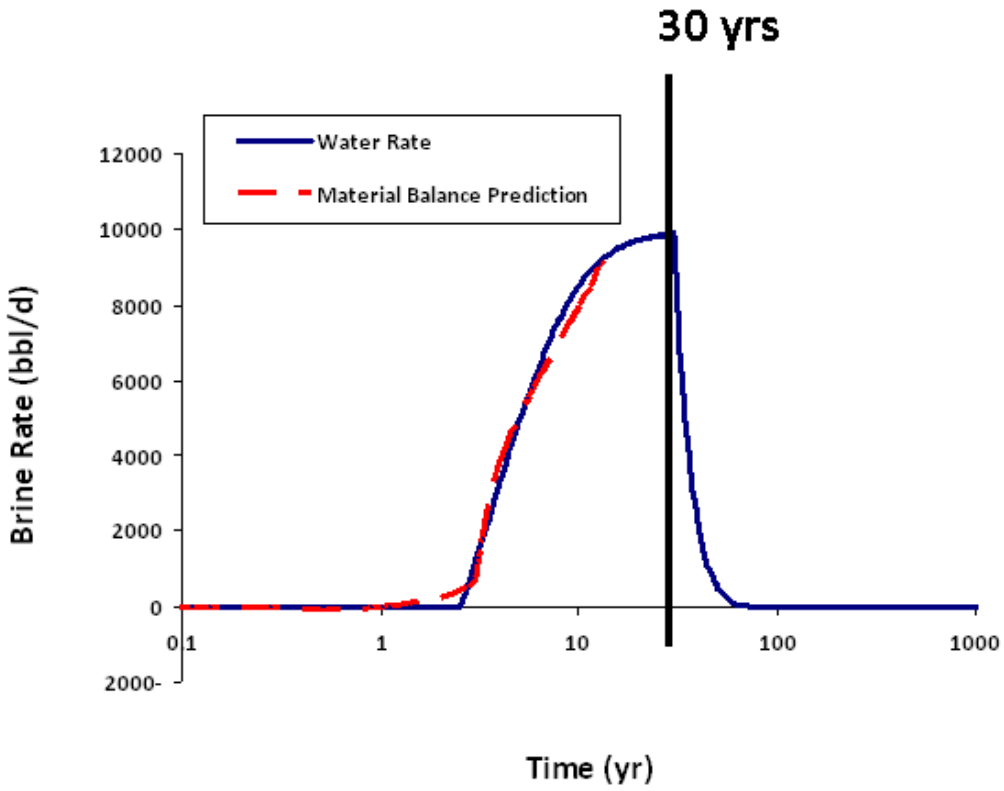

Fig. 4.28—Comparison of simulated fluids leaking from the brine zone and prediction from simple material balance. CO_2 was injected for 30 years at 25 million scf/D (~0.5 million T/yr). The initial hydrostatic pressure of the reservoir was 2,600 psi. The fracture pressure of the reservoir is 4,200 psi. The leak is located at a distance of 7,000 ft from the wellbore.

4.9 Section Conslusions

This section shows results of simulations of bulk CO_2 injection from a vertical well. The physics of CO_2 sequestration is clearly visible from the successive pressure falloff tests. Planning falloff tests at regular intervals for commercial-scale CO_2 projects can provide significant insights into the real-time movement of saturation fronts and mobility behavior in the aquifer. The observation that mobilities of the two-phase zone and the single-phase brine zone are similar enables a reasonable estimation for the average aquifer pressure using Horner analysis. Horner analysis of simulated falloffs showed that the behavior of average pressure easily distinguishes whether a well drains a limited volume exhibiting quasisteady-state behavior, an open aquifer with constant pressure support, or an effectively infinite aquifer; it is also sensitive to the presence of a leak in the aquifer seal. Further, simple material balance analysis on the average pressure trend enables estimation of the aquifer volume and estimation of the volume of total fluid leaking from the aquifer in the case that leaking behavior is observed. Our results show that regular injection falloff testing in CO_2 injection wells is an effective way to detect a leak in an aquifer intended for CO_2 storage. More work is needed to investigate falloff test behavior for horizontal CO_2 injection wells.

5. BRINE PRODUCTION FOR PRESSURE CONTROL

5.1 Introduction

The storage capacity of CO_2 in a closed aquifer is greatly limited by aquifer pressurization during injection. The inability of water to move out of the system because of compartmentalization, structural or stratigraphic limits, or by interference with other injection wells is the main reason for rapid pressure increase. As discussed in Section 3, closed systems would be ideal for CO_2 containment because low-permeability barriers would prevent leakage of CO_2 from the formation, but since the displaced brine cannot escape, the capacity for CO_2 storage is rather small. Producing extra brine out of the reservoir can greatly relieve the increased pressure and increase the storage potential of the aquifer. Strategic placement of the production wells at optimal locations will decrease the risk of CO_2 breakthrough at the production well.

The lower pressure buildup and large storage potential of "open" aquifers might be a desirable choice for CO_2. However, in continents like Australia, most of the desirable basins lie far from the required stationary CO_2 sources (Rigg et al. 2001). Sometimes the lack of a large aquifer near a high CO_2 emission site necessitates relatively smaller and closed aquifers for CO_2 storage. In this section, Section 5.2 describes how these simulations were done, and Section 5.3 discusses how pressurization greatly reduces the risk of CO_2 leak and greatly increases the storage potential and briefly addresses how produced brine may be handled.

5.2 Reduction of Aquifer Pressurization Risk

As discussed in the previous section, pressure contours above the hydrostatic pressure extend much farther into the aquifer than the saturation contours in the case of an infinite-acting aquifer and extend throughout a limited aquifer volume, whether it is modeled as open or closed. The situation worsens in closed and partially confined aquifers (Oruganti et al. 2009). Shallower freshwater resources may be in hydraulic communication to the deep saline aquifer through local high-permeability flow paths

such as faults and abandoned wellbores. The pressurization at depth would then provide a driving force for upward migration of either CO_2 , fresh brine, or carbonated brine.

A risk factor was defined at the location of the +50-psi pressure contour above the hydrostatic pressure. Such a parameter should be included in any certification framework for geological storage (Oldenburg et al. 2008; Oruganti et al. 2009). This value varies on a case-by-case basis, depending on the aquifer properties and formation characteristics. However, for this thesis we assume it to be +50 psi.

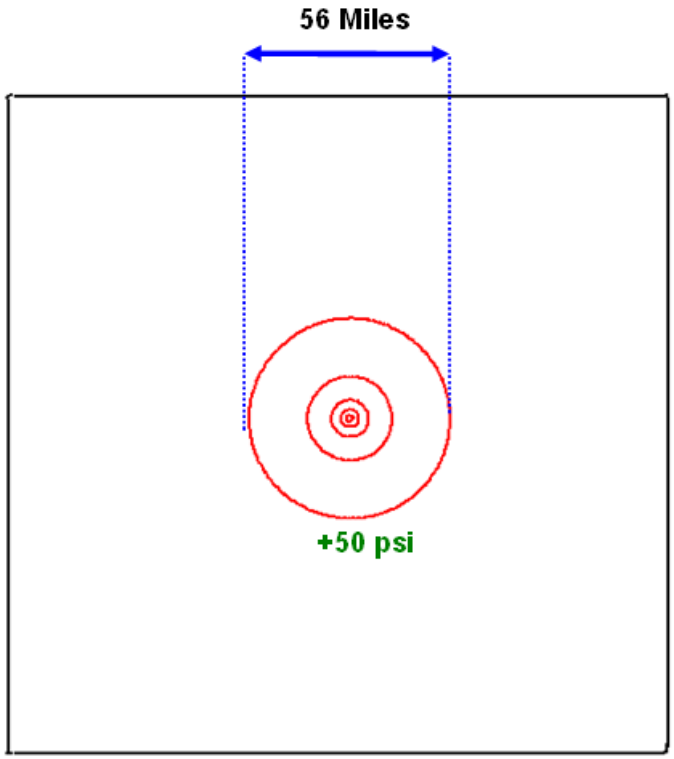

Fig. 5.1—The + 50 psi overpressure contour for the bulk injection case with no brine production. The contour extends for a radial distance of 23 miles from the injection well. The boundaries of the reservoir are at 100 miles from the center of the well. CO_2 is injected for 30 years at 52 million scf/D (~1 million T/yr). The initial hydrostatic pressure of the reservoir is 2,600 psi. The fracture pressure of the reservoir is 4,200 psi.

Fig. 5.1 shows the +50-psi overpressure contour for bulk injection in an effectively infinite aquifer with no brine production. The simulation domain is 250 ft thick with a square drainage area with 100-mile sides. CO_2 was injected for 30 years at 52 million scf/D (~1 million T/yr). The initial hydrostatic pressure of the reservoir was 2,600 psi. The fracture pressure of the reservoir is 4,200 psi. The rest of the reservoir properties are same as the base case discussed in Section 2. The overpressure contour extends for a radial distance of 23 miles from the injection well. The area of influence of this pressure contour is extremely large (~1650 sq mi). For comparison purposes, 1,650 square miles of area of influence is more the area of the USA state of Rhode Island. The footprint area of elevated pressure indicates the extremely large subsurface volumes where such pressure impacts might be expected. This may have important implications on large-scale connectivity assessment, reservoir characterization, and overall economics of the project. Such a huge area of influence clearly makes a case for brine production for pressure relief.

Fig. 5.2 shows the +50-psi overpressure contour for the case with two brine producers. The simulation domain is 250 ft thick with a square drainage area with 100-mile sides. CO_2 is injected for 30 years at 52 million scf/D (~1 million T/yr). The distance between the vertical production wells (10,000 ft) is decided on the CO_2 breakthrough criteria. The initial hydrostatic pressure of the reservoir was 2,600 psi. The average pressure of the reservoir is kept constant by producing brine equal to the volume of injected CO_2 at reservoir conditions. The rest of the reservoir properties are the same as the base case discussed in Section 2. The overpressure contour only extends for a radial distance of 0.25 miles from the injection well. This is an astronomical reduction in the area of influence to only 0.2 sq mi. This area of influence is 0.06% of the area without brine production. Hence, water production wells should be used to ensure that pressure is maintained within safe operating limits. With brine production, less aquifer space is required to sequester an equal amount of CO_2. Brine production significantly increases the storage potential of the aquifer.

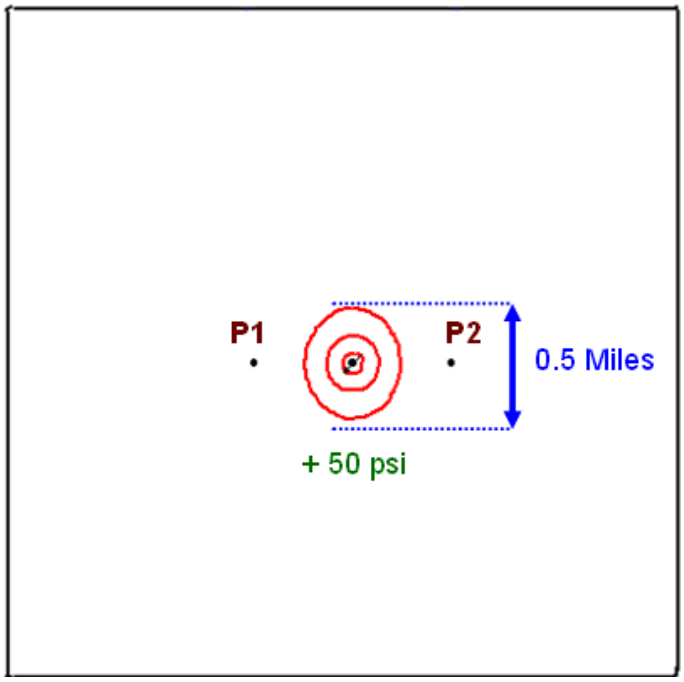

Fig. 5.2—The + 50 psi overpressure contour for the bulk injection case with two brine producers (P1 and P2). The contour extends for a radial distance of 0.5 miles from the injection well. The boundaries of the reservoir are at 100 miles from the center of the well. CO_2 is injected for 30 years at 52 million scf/D (~1 million T/yr). The initial hydrostatic pressure of the reservoir is 2,600 psi. The fracture pressure of the reservoir is 4,200 psi.

5.2.1 Breakthrough Control

For the injection production scenario, one of the main concerns is the production of CO_2 from the drainage well. The brine production wells should be as far as possible away from the injection well. The injected CO_2 has a tendency to migrate toward the producer. A simple but rigorous way to control this is to inject as low as possible and produce as low as possible. The "inject-low-and-let-rise" strategy (Kumar et al. 2005) helps in increasing residually trapped gas in the reservoir. With this approach, vertical movement toward the seal is retarded. Producing the brine as deep as possible will stall breakthrough of CO_2 rising under gravity. Drilling horizontal wells at the bottom

of the aquifer for brine production can be one of the ways to implement this technique efficiently.

5.2.2 Handling Produced Brine

Produced water treatment would be costly using current desalination and treatment technologies; alternatives like solar-driven technology for freshwater production (Khatib and Verbeet 2002), advanced vapor-compression desalination technology (Ruiz 2005), and coupling carbon dioxide sequestration and extracted water for treatment and use in a power plant (Kobos et al. 2008) may be feasible.

5.3 Section Conclusions

Brine production reduces the energy requirement for CO_2 injection by reducing the required injection pressures and greatly reduces the footprint of the overall CO_2 sequestration operation. However, simulations showed that while it greatly reduces risks of CO_2 leakage by reducing aquifer pressurization, brine production does not prevent accumulation of free CO_2 at the top of the aquifer. The next section offers a novel approach that avoids both risks.

6. AQUIFER MANAGEMENT TO ACCELERATE CO_2 DISSOLUTION AND TRAPPING

6.1 Introduction

The risk associated with aquifer pressurization was dealt with in Section 5. However, a risk of free gas saturation below the top seal still exists. This section specifically addresses that. The CO_2 injected in bulk form into a deep aquifer is typically 5 to 50% less dense than the resident brine. In this situation, buoyancy forces will drive the injected CO_2 upwards in the aquifer until a geological seal is reached. The performance of bulk CO_2 injection schemes highly depends on the seal integrity assessment and presence of thief zones. The accumulated pocket of free CO_2 would readily leak through a breach in an aquifer seal. Ideally, the aquifer should be monitored as long as the free CO_2 is present, but the CO_2 is expected to remain for more than 1,000 years. Long-term monitoring of the seal integrity and avoiding leakage will be very costly.

Since the main risk of leakage arises from mobile free-phase CO_2, we have investigated a technique to eliminate buoyancy-driven accumulation of a mobile free-phase CO_2 below the top seal.

In this section, we adopt a well-balanced view to the problem by combining the inject-low-let-rise strategy (Kumar 2008) with strategically designed brine recirculation to accelerate CO_2 dissolution and trapping. We try to engineer the system in a way that addresses simultaneously the risks of the mobile free-phase CO_2 and aquifer pressurization due to CO_2 injection. Section 6.2 discusses the design specifics of the proposed engineered system. Gravity number is an important indication of the sequestration efficiency; it is discussed in detail in Section 6.3. In Section 6.4, we apply the engineered system to sequester the CO_2 output from a standard 500-MW coal-fired power plant. Field-scale reservoir simulation sensitivity studies provide

additional insights into the problem. Since the real subsurface formations are not , we show the application of the concept in heterogeneous permeability fields and dipping aquifer systems in Section 6.5.

6.2. System Design: Adressing Risks

Fig. 6.1 shows a comparison of the engineered system with the base case. The base case is the bulk CO_2 injection scenario with a single, horizontal CO_2 injector. The engineered system can be designed to address the two kinds of risk discussed in the previous section. In the subsequent discussion we deal with individual risks one by one.

6.2.1 Addressing Risk from Free CO_2 below Aquifer Seal

To decrease the time for the CO_2 plume to hit the top seal, it is important to decrease the plume velocity in the vertical direction. The following discussion will address an engineering design that increases the areal sweep of CO_2 in the horizontal direction and decreases the velocity in the vertical direction. A single pattern of the engineered system consists of drilling and completing one horizontal brine injection well (I_B) relatively near the top of the reservoir and exactly above the horizontal CO_2 injector (I_{CO_2}). Two brine production wells (P_B) are employed on either side of the horizontal CO_2 injector at the bottom of the reservoir.

The aim of the top brine injection well (I_B) is to decrease the vertical velocity of CO_2 rising towards the reservoir seal, and the brine producers on the sides increase the velocity of CO_2 in the horizontal direction. Decreasing the velocity of CO_2 in the vertical direction delays the time for the plume to hit the reservoir seal. Increasing the velocity of CO_2 in the horizontal direction results into a better sweep efficiency of CO_2 in the aquifer. We recommend the use of horizontal wells for CO_2 injection. Distributing the total flow along the length of horizontal wells substantially reduces the vertical velocity of the plume and delays the time of the plume to hit the reservoir seal.

Recirculating the brine by producing it through the horizontal brine producers and injecting it back through the top brine injector helps in creating a curtain of falling brine. CO_2 is then injected inside the falling curtain of brine to expose it to as much fresh brine as possible. The brine curtain will gradually widen as it falls under inclined pressure gradients (downwards) between the top brine injector and bottom brine producers. The injected brine has a high density; without the brine producers, it tends to fall quickly through the reservoir and fails to achieve significant areal coverage. Thus, the use of brine producers on the sides helps in expanding the size of the falling curtain. Fig. 6.2 (a) and (b) shows the top view and 3D view of the streamlines traced from the sources (injectors) to sinks (producers).

As can be seen, the brine tries to form an envelope or curtain around the CO_2 injector. The width of the curtain is also increasing from the top brine injector to brine producers. The perforations on the side of the top injector will provide width to the curtain, and perforations on the bottom will prevent the flow of rising CO_2 from the injector I_{CO_2}. Any top perforations on the top injector I_B should be avoided. Perforations on production wells P_B towards the CO_2 injector I_{CO_2} will help provide better areal sweep of CO_2. The flow from the top perforation on the brine producers will connect to the brine injector I_B to provide a downward gradient to rising CO_2. As a design criterion, the length of the production wells should be sufficiently less than the length of CO_2 injector. This helps in maintaining sufficiently high horizontal velocity of CO_2 towards the production wells, thus providing a better sweep in the aquifer. One important point to note here is that the brine recirculation is stopped as soon the CO_2 injection stops.

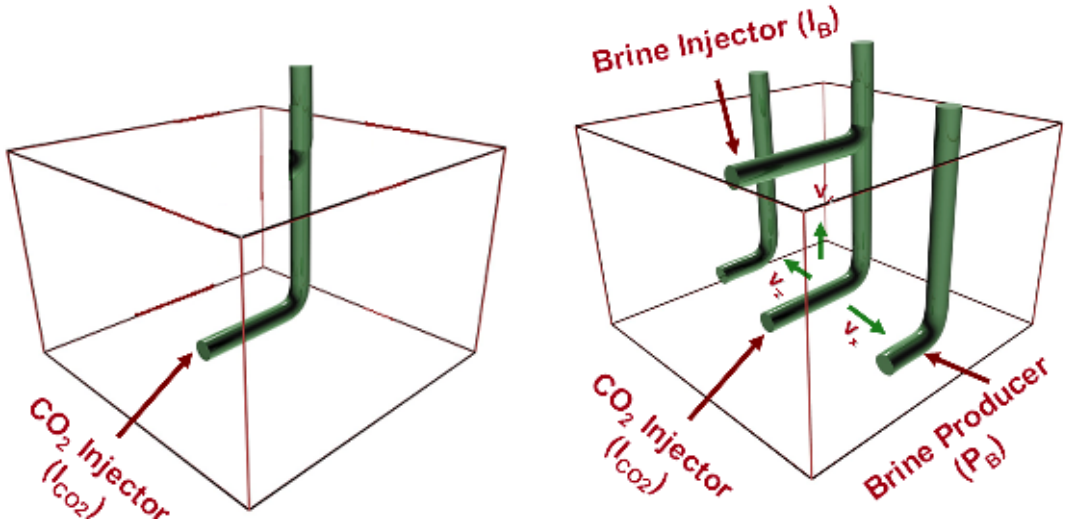

(a) **(b)**

Fig. 6.1—(a) Base case with one horizontal CO_2 injector. (b) Engineered case with a horizontal CO_2 and a brine injector and two horizontal brine producers.

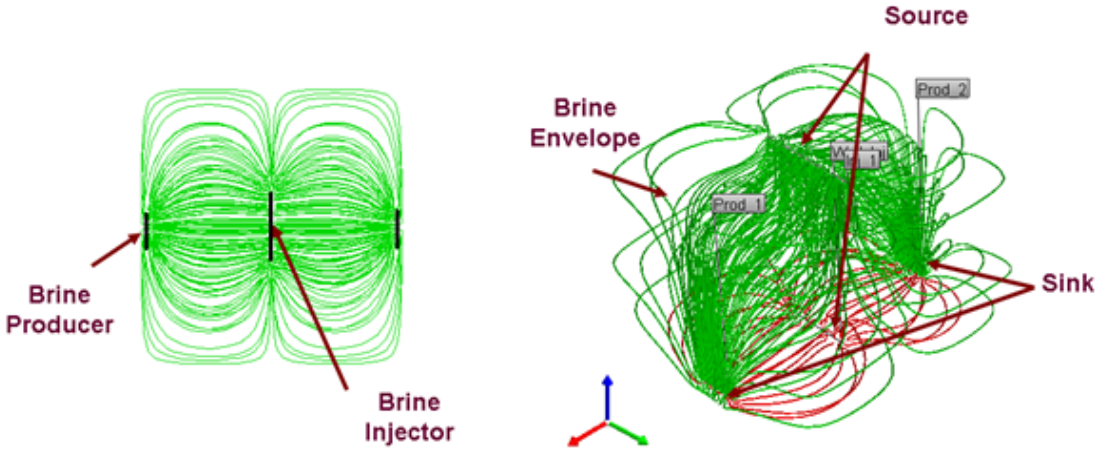

(a) **(b)**

Fig. 6.2—(a) Top view of the streamlines originating from the brine injector (source) to brine producer (sink). **(b)** 3D view of the streamlines originating from brine injector (source) to brine producer (green) and CO_2 injector (source) to brine producer (red).

For the engineered system, CO_2 is injectedto in a stream of fresh brine injected from the top injector, exposing it to fresh, undersaturated brine. Contrary to this, the injected CO_2 in the base case forms a dense gas cloud around the injection well, which

makes it difficult for the fresh, undersaturated brine to contact the injected CO_2. A single pattern of the engineered system discussed above is analogous to pattern waterflooding of oil reservoirs for pressure maintenance and displacing the residual oil. Generally, several patterns are required to manage a field. One of the first steps in designing a waterflooding project is flood pattern selection and design. The design depends on reservoir permeability, heterogeneity, thickness, depth, lithology, fluid saturations and drive mechanisms. Each pattern has its own water injection and oil production rates. Analogous to that, in each engineering pattern a specific amount of gas can be injected to attain zero mobile gas saturation below the top seal throughout the life of a sequestration project. The rate associated with this can also be called the optimal injection rate. The amount of gas for each pattern depends on aquifer thickness, permeability, anisotropy, brine injection rates, and available pore volume. Several patterns may be required depending on a specific power-plant CO_2 output. Fig. 6.3 shows engineering patterns aligned side by side. For every two CO_2 injectors, there are three brine producers. Each pattern can take a specific amount of gas, and the number of patterns can be calculated as

$$n = \frac{\text{Power-plant } CO_2 \text{ output (MMSCFD)}}{\text{Gas injected in each pattern (MMSCFD)}} \quad \text{.....(6.1)}$$

where n is total number of patterns needed to sequester a target amount of CO_2.

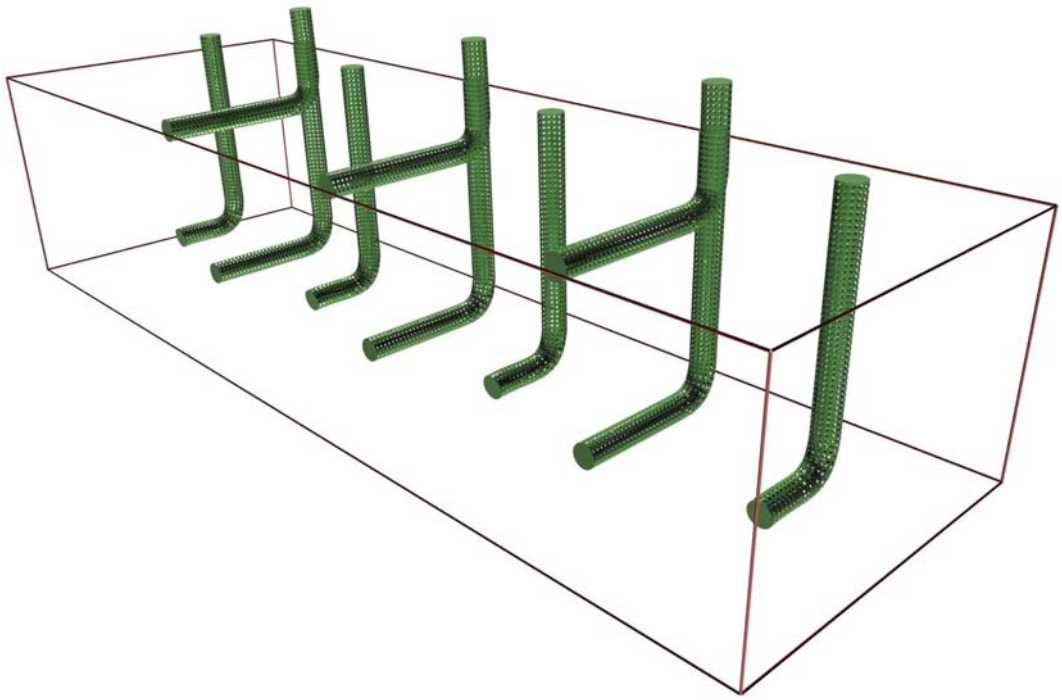

Fig. 6.3—Three engineered patterns place side by side.

6.2.2 Addressing Risk from Aquifer Pressurization

As discussed in the previous section, producing additional brine out of the reservoir can address the risks associated with aquifer pressurization due to CO_2 injection. The engineered system addresses the risk of pressurization by producing additional brine out of the system through the horizontal brine producers. A simple material balance of the system suggests the amount of brine produced in reservoir barrels. It should be equal to the sum of injected brine and CO_2. It can be written as

$$Q + Q_{\text{brine in}} = Q_{\text{brine out}} \cdot \quad \text{.....(6.2)}$$

As described in Fig.6.3, often several patterns will be required to sequester a target amount of CO_2. For n injection wells n+1 brine producers will be required. The brine production rate for a set of n patterns can be written as

$$nq_{Co_2} + nq_{\text{brine in}} = (n+1)q_{\text{brine out}} \quad \text{.....(6.3)}$$

$$q_{\text{brine out}} = \frac{n}{(n+1)}\left(q_{CO_2} + q_{\text{brine in}}\right), \quad \text{.....(6.4)}$$

where

$q_{\text{brine out}}$ = brine production rate from each brine producer (bbl/D)

$q_{\text{brine in}}$ = brine injection rate from each brine injector (bbl/D)

q_{CO_2} = gas injection rate from each CO_2 injector (bbl/D)

The remaining brine ($q_{\text{brine out}}$ - $q_{\text{brine in}}$) that is not injected back into the formation should be disposed off or send back to the power-plant for utilization. Inexpensive treatment options of the brine are mentioned in Section 5.3 in this thesis.

6.3 Gravity Number

Gravity number is defined as the ratio of gravity forces to viscous forces. Ide et al. (2006) investigated the interplay of viscous and gravity forces and capillary trapping of CO_2. They showed that the gravity number determines the shape of the CO_2 plume in the aquifer. They also concluded that the gas injection processes in which gravitational forces are weak compared to viscous forces (and thus have a low gravity number) trap significantly more CO_2 than do flows with high gravity numbers.

In high gravity number displacements, stronger buoyant movement of CO_2 drives the gas towards the top seal as soon as the gas is injected. Since it is not in contact with much of the brine and rock during its gravity-dominated flow, the trapping is less. In low-gravity-number displacements, CO_2 is carried away horizontally by the high viscous forces. Once viscous forces diminish, the gas travels vertically upwards under gravity. This way CO_2 contacts more brine and rock volume, resulting into greater trapping. Low-gravity-number displacements have a better sweep.

Ide et al. (2006) also showed that although high-gravity-number displacements trap significantly less CO_2 than low-gravity-number displacements, the rate at which the final trapped gas saturation is reached is much higher in high-gravity-number systems.

Many different expressions can be found in the literature for gravity number, but the basic concept is the same. All are ratios of gravity forces to viscous forces. We use the expression of gravity number as defined by Kumar et al. (2008),

$$N_{gv} = \frac{k_v \Delta\rho g \cos\alpha}{\mu u}, \quad \text{..... (6.5)}$$

where k_v = vertical permeability

$\Delta\rho$ = density difference between brine and CO_2 at reservoir conditions

α = dip angle

μ = CO_2 viscosity

u = total velocity of CO_2 at the sandface

$$u = \frac{q}{2\pi r_w h_p}, \quad \text{..... (6.4)}$$

where r_w is the radius of the well and h_p is the perforation interval.

Fig. 6.4 shows a comparison of the 2D gas saturation profile for low- and high-gravity displacement scenarios. The well is perforated through the bottom quarter of the formation. The aquifer is 500 ft thick and the horizontal permeability in both the cases is 100 md. The gas was injected for a period of 30 years. The gravity number was altered by changing the vertical permeability and CO_2 injection rates. For Case (a), the injection rate is 5 million scf/D and vertical permeability is 50 md. The gravity number for this case is 0.19. In Case (b) the injection rate is 10 million scf/D and

vertical permeability is 5 md. The gravity number for this case is 0.01. Clearly, for a high gravity number, strong buoyant forces drive the gas toward the top seal as soon as the gas is injected, whereas for low gravity numbers, CO_2 seems to traverse more horizontal distance due to viscous forces. Kumar et al. (2008) carried out a large number of simulations and used gravity number to characterize the size of the plume and sequestration efficiency. Hold onto this concept for now. We will use this in Section 6.4.3 to compare the gravity numbers of the base case with the engineered case to characterize the plume behavior.

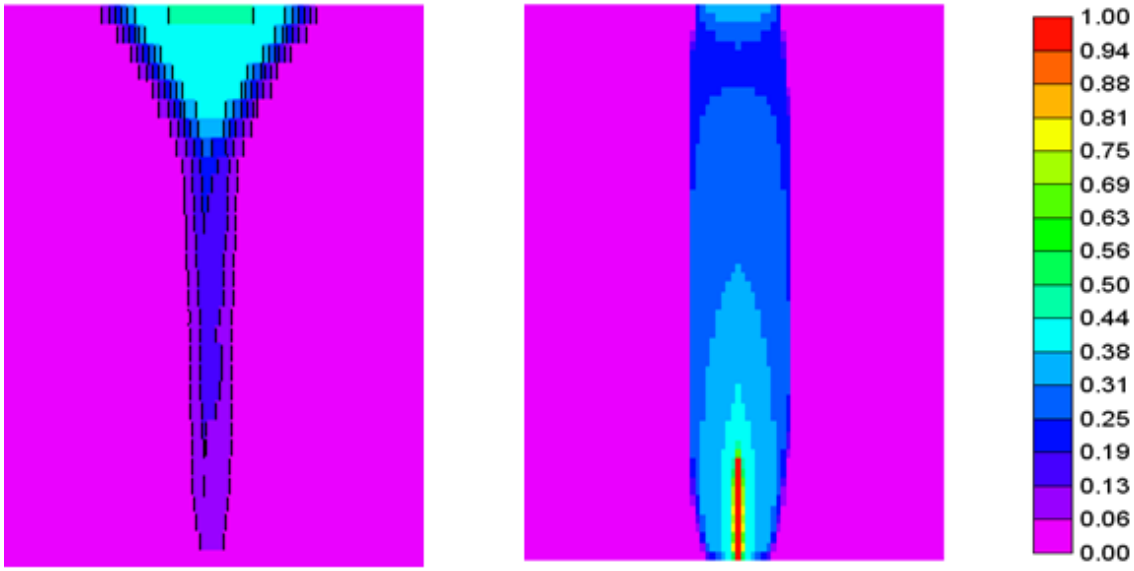

(a) **(b)**

Fig. 6.4—(a) Shape of the plume for the high gravity number (0.19) after 30 years of injection. Strong buoyant movement drives the gas towards the top seal as soon as the gas is injected. (**b)** Shape of the plume for the low gravity number (0.01) after 30 years of injection. CO_2 seems to travel more horizontal distance due to high viscous forces.

6.4. System Design for 500-Mw Power Plant

A modern commercial 500-MW coal power plant generates about 3 million metric tons of CO_2 per year. Assuming it is captured as a pure CO_2 stream, how should the system be designed to accelerate dissolution and trapping mechanisms substantiality? What will be the required water circulation rate? How many well patterns will be needed if the plant life is assumed to be 30 years? Suppose an aquifer exists in the vicinity of the plant with thickness 1,000 ft and other properties are the same as the base case model discussed in Section 2. Land's model is used for modeling residual trapping. Using the Holtz (2002) correlation, for a porosity value of 0.25 for the base case, the maximum residual gas saturation is approximately 0.3.

6.4.1 Pattern Dimensions

Several simulation runs were made by systematically changing the horizontal injector and producer well lengths, water circulation rate, and distance between the CO_2 injector and brine producers until a specific combination of the system variables were obtained to achieve zero free gas saturation below the top seal. The distance of the brine producer from the CO_2 injector is decided on the criterion of breakthrough of CO_2. This distance determines the pattern size for a particular thickness and CO_2 injection rate. Fig. 6.5 shows the required pattern size needed for injecting 3 million T of gas per year for a 1,000-ft thick interval for 30 years. Through a combination of brine recirculation, horizontal wells, and buoyancy-driven upward migration, all of the CO_2 was trapped and dissolved before it could reach the top seal. Brine was recirculated for a period of 30 years, and it was stopped along with CO_2 injection.

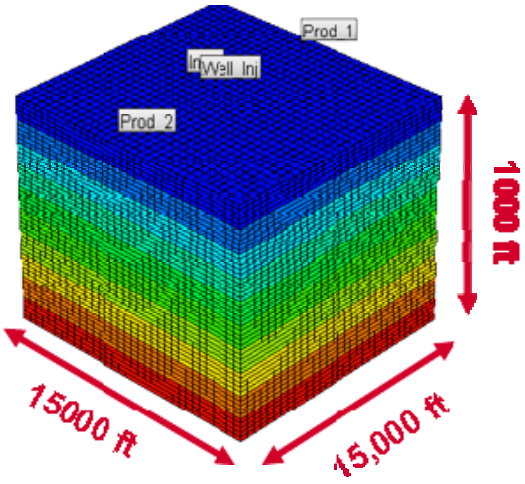

Fig. 6.5—Size of the required pattern for Case 1. 3 million T/yr of gas was injected for a 1,000-ft-thick interval for 30 years. (The plot is not to scale. It has been enlarged in the Z direction for better visibility)

6.4.2 Velocity Fields

Fig. 6.6 (a) and (b) compares velocity fields in the vertical directions for the base case and the engineered case respectively. Approximately 3 million T/yr (~156 million scf/D) of gas is injected over a period of 30 years. Brine injection rate from the top injector is approximately 340,000 bbl/D and brine production from each producer is 200 bbl/D. An extra 60,000 bbl/D of brine is produced to control aquifer pressurization.

The length of the CO_2 injector is 4,000 ft. It can be clearly seen that the vertical velocity (*Vz* in Fig 6.1) of the gas for the engineered case at any particular injection time is as low as 0.01 ft/D as compared to 0.03 ft/D for the base case. The brine injection well reduced the velocity of rising plume by 3-fold over the CO_2 injection well. Fig. 6.7 (a) and (b) compares velocity fields in the horizontal directions (Vx in Fig 6.1) for the base case and the engineered case respectively. At any particular time, the horizontal velocity for the base case is 0.01 ft/D as compared to 0.03 ft/D for the engineered case. Also, the gas has a velocity up to 4,000 ft away from the injection well as compared to only 1,000 ft for the base case. This indicates the increased sweep efficiency of the gas in the horizontal direction.

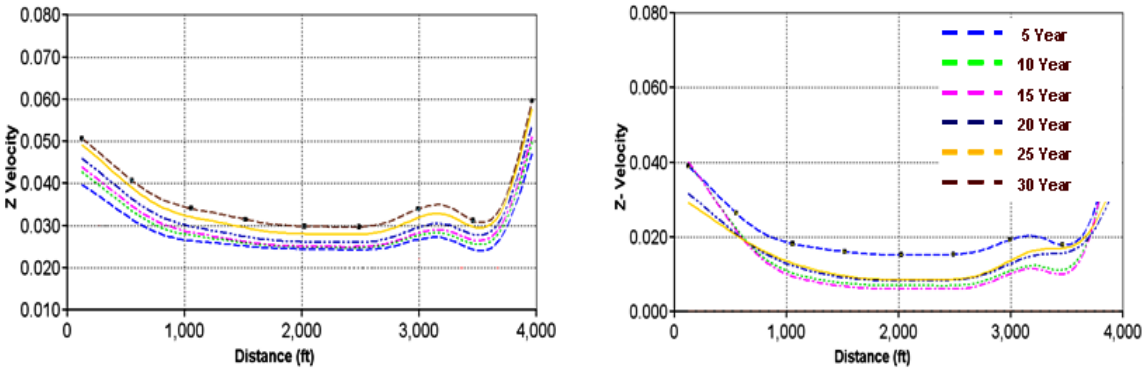

(a) **(b)**

Fig. 6.6—Vertical gas velocity from horizontal well. (a) Base case. (b) Engineered case. Approximately 3 million T/yr (~156 million scf/D) of gas is injected over a period of 30 years. Brine injection rate from the top injector is approximately 340 bbl/D and brine production from each producer is 200 bbl/D. An extra 60 bbl/Day of brine is produced to control aquifer pressurization. The length of the CO_2 injector is 4000 ft.

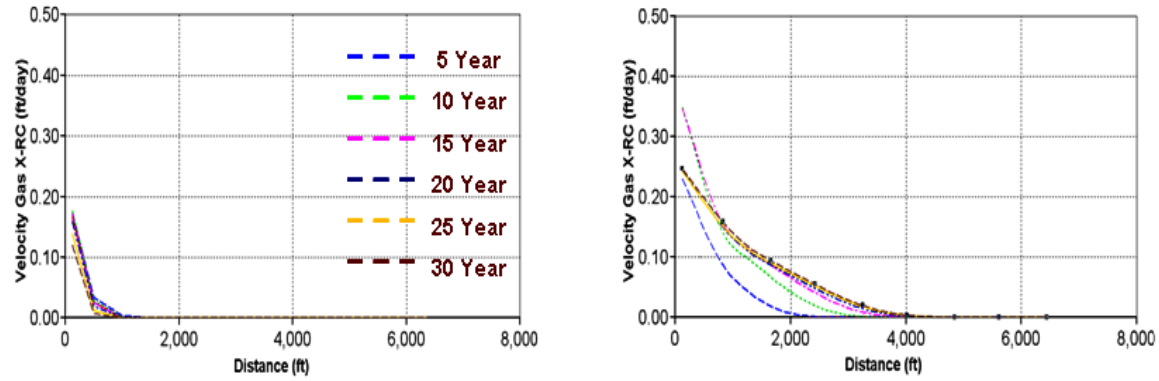

(a) **(b)**

Fig. 6.7— Horizontal gas velocity away from horizontal well (a) Base case (b) Engineered case. Approximately 3 million T/yr (~156 million scf/D) of gas is injected over a period 30 years. Brine injection rate from the top injector is approximately 340 bbl/D and brine production from each producer is 200 bbl/D. An extra 60 bbl/Day of brine is produced to control aquifer pressurization. The length of the CO_2 injector is 4,000 ft.

6.4.3 Gas Saturation

Table 6.1 shows the parameters values for obtaining zero gas saturation below the top seal. Fig. 6.8 shows the free-gas saturation of the base case and the engineered case just below the reservoir seal. As can be seen, after 1,000 years almost all of the free gas is accumulated below the top seal for the base case due to significant buoyancy contrast between the brine and the injected gas. After 1,000 years, the areal extent of gas saturation for the base case is approximately 25 sq mi. This is a substantial area of influence. In the case of the open aquifer, this estimate does not include the water displaced, which could easily double or triple the area of influence. Thus, the ultimate area of influence for the bulk injection approach could be huge. However, engineering the system renders the CO_2 immobile during the injection phase of storage. The engineered system is successful in dissolving and trapping all of the CO_2 in a very small volume. Hence, there is no free gas saturation below the top layer for the engineered case in Fig. 6.8 (b), even after 1,000 years.

Table 6. 1—Parameter values for obtaining zero gas saturation below the top seal

Parameter	Value
Gas Injection Rate	156 million scf/D (~ 3 million T/yr)
Length of CO_2 Injector	4000 ft
Length of Water Injector	6000 ft
Length of Water Producers	2500 ft
Brine Injection Rate	340,000 bbl/Day
Brine Production Rate	200,000 bbl/Day
Material Balance Brine Production	60,000 bbl/Day
Size of One Pattern	15,000 ft X 15,000 ft X 1,000 ft

The average pressure of the reservoir for the engineered case is more or less close to the initial hydrostatic pressure due to additional brine production. This addresses the risk associated with pressurization due to CO_2 injection. The strategy seems counter-

intuitive as the simulation studies using the same reservoir model imply that only around 1% of the pore space will contain CO_2 if it is injected alone. Engineering the system increases aquifer utilization since more gas is stored in less volume. Fig. 6.9 shows a comparison of capillary trapped gas between the base case and the engineered case after 1,000 years. Capillary trapping is one of the most rapid methods for CO_2 immobilization. A significant amount of increase in trapping is obtained for the engineered case since the injected gas in the engineered system efficiently contacts the undersaturated brine away from the CO_2 injector.

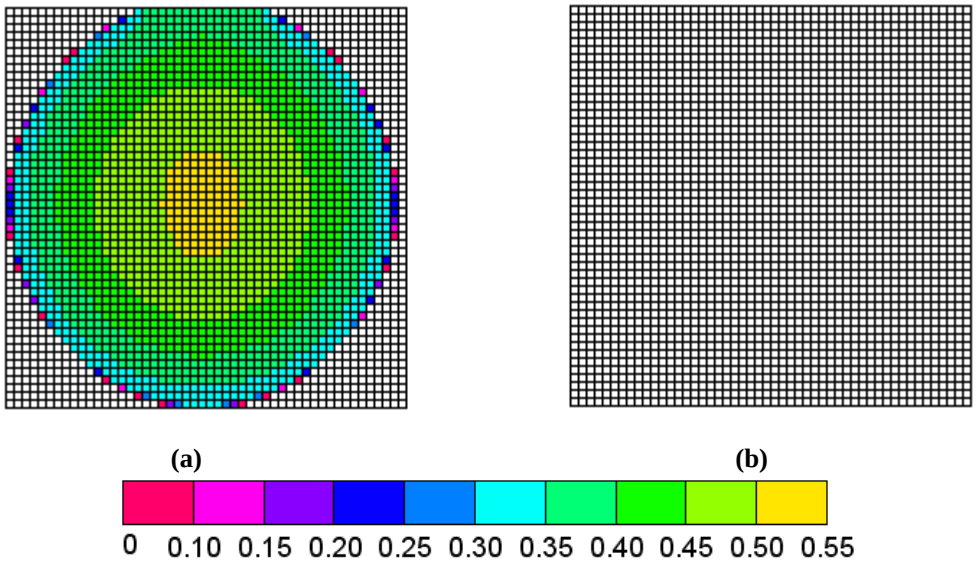

Fig. 6.8—(a) Top view of free gas saturation for the base case after 1,000 years. **(b)** Top view of free gas saturation for the engineered case after 1,000 years. 3 million T/yr of gas was injected along with brine recirculation for the 30 years.

D View X-Z view

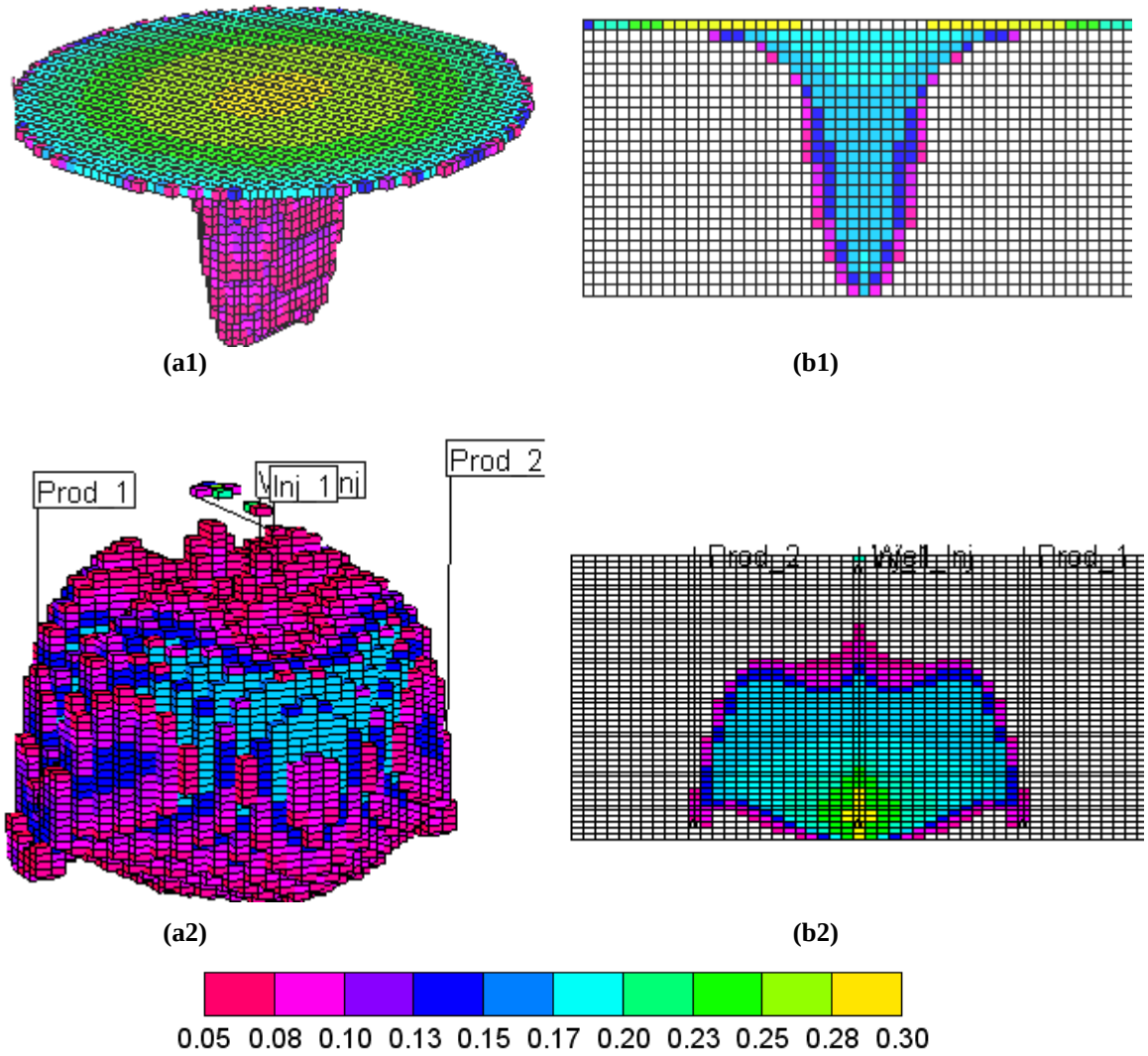

Fig. 6.9—Comparison of trapped gas saturation for the base case and engineered case after 1,000 years. 3 million T/yr of gas was injected for the 30 years. **(a1)** 3D view of trapped gas saturation for the base case. **(a2)** 3D view of trapped gas saturation for the engineered case **(b1)** X-Z view of trapped gas saturation for the base case (Ngv=1.25). **(b2)** X-Z view of trapped gas saturation for the engineered case (Ngv=0.5).

The gravity number for the base case is 1.25, whereas the gravity number for the engineered case is 0.5. The gravity number of the system has decreased due to the engineering. This means sweep efficiency of the engineered system should increase.

This is also evident from Fig. 6.9 (b1) and (b2), which shows trapped gas saturation. Clearly, the engineered case shows a better sweep of CO_2 in the aquifer over the base case. For the engineered case, some top layers do not contain the trapped gas; this means that the CO_2 was immobilized before hitting the top seal.

6.4.4 Dissolution and Trapping

Fig. 6.10(a) and (b) compares the increase in dissolution and capillary trapping over the base case. A two-fold increase in dissolution and 1.5 times increase in trapping is quite evident, although the scale on the Y axes of Figs. 6.10 (a) and (b) are significantly different. The dissolution of CO_2 in brine is extremely low (Burton and Bryant 2007). Thus, the amount of gas trapped for any injection scheme case far exceeds the number of moles of the dissolved gas. These results are in agreement with some of the previously published research (Spiteri et al. 2005; Ide et al. 2007; Nghiem et al. 2009). Note that these results are very sensitive to the value of maximum residual gas saturation.

Fig. 6.11 compares the total mobile CO_2 (in billion moles) at different times for the base case and the engineered case. It also shows the cumulative gas injected in billion moles. Some free gas remains in the aquifer for the engineered case after the injection ends. However, the free gas in the aquifer is much lower for the engineered case than for the base case. The free gas left in the system will be dissolved and trapped before it ever gets to the top of the aquifer seal. In fact, 90% of the gas is rendered immobile (dissolved and trapped) for the engineered case as early as 50 years after starting injection, thus reducing the tendency of the free gas to leak back to the atmosphere through an imperfect caprock, imperfectly sealed wellbore, or conductive fault. Contrary to this, a significant amount of the gas still exists in the mobile free phase for the base case even after 1,000 years. The cost of inventory verifications and monitoring for such an elongated period could be prohibitive. The aim of a sequestration project should be to decrease the residence time of free CO_2. Eliminating the dependence on long-term storage mechanisms like mineral trapping and

leveraging the short-term mechanisms like dissolution and mineral trapping could be the key to avoiding long-term monitoring costs and securing the storage.

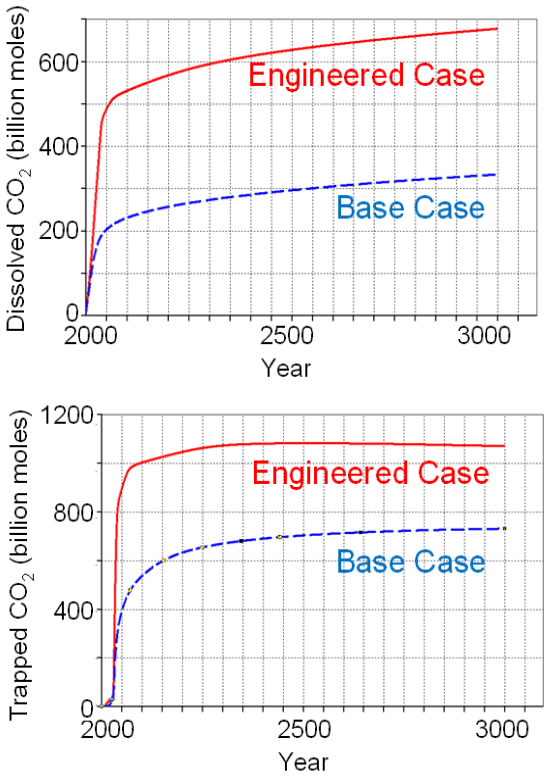

(a) **(b)**

Fig. 6.10—(a) Plot comparing dissolved CO_2 with time for the base case (blue) and the engineered case (red). **(b)** Plot comparing trapped CO_2 with time for the base case and the engineered case. 3 million T/yr of gas was injected for the 30 years in a 1,000-ft-thick interval.

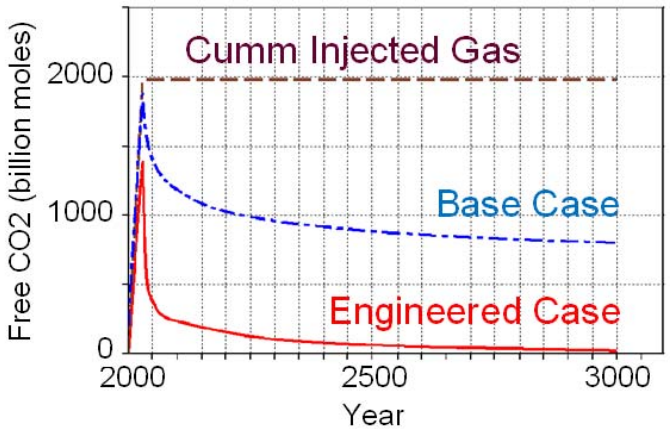

Fig. 6.11—Plot comparing mobile CO_2 with time for the base case (blue) and the engineered case (red). The brown curve shows the total gas injected for 30 years at the rate of 3 million T/yr.

6.4.5 Carbonated Brine Production

One of the prime concerns for the engineering design would be breakthrough of CO_2-saturated brine at the production wells and producing CO_2-saturated brine. The treatment of carbonated brine could be prohibitive to sequestration project economics. The "inject-low-and-produce-low" strategy was proposed in Section 5.3 to avoid any gas breakthrough in the production wells. Producing the brine as deep as possible will avoid breakthrough of CO_2 rising under gravity. However, since the top brine injector is providing a downward gradient to rising CO_2, there are high chances of carbonated brine production in the production wells due to improved dissolution from the efficient engineering of the system. One way to control this is to keep a safe distance between the CO_2 injector and the brine production well. A second reassuring argument could be based on the extremely low solubility of CO_2 at surface conditions. Fig. 1.5 shows the solubility of CO_2 in brine (in mole percent) for various aquifer depth and salinity ranges. As can be seen, the solubility is 0.05% by mole fraction. Clearly, this is a very small amount of CO_2 as compared to the injected quantity. Any produced CO_2 from the brine injector will be flashed out of the solution as soon as it reaches the surface. We anticipate a flash tank for the brine before re-injecting it back into the ground from the top brine injector. Fig. 6.12 shows the gas rate from the brine production wells (red curve). CO_2 breakthrough occurs at the end of 20 years, and the gas rate through the brine producer rises slowly. By the end of 30 years, the cumulative gas production from the brine producer is approximately 4% the total injected gas. However, the remaining 96% of the injected gas is dissolved and trapped securely as early as 50 years.

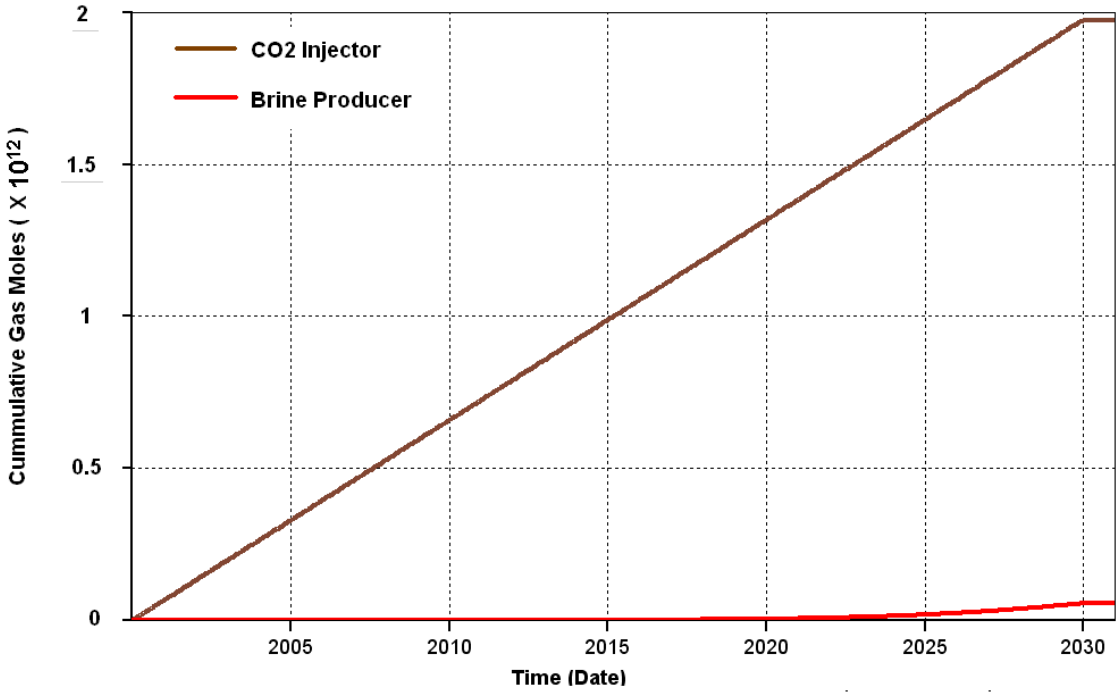

Fig. 6.12—Cumulative gas production rate (gmole) from the brine producers (red curve). The brown curve shows the cumulative gas injection (gmoles) through the CO_2 injector.

6.4.6 Sensitivity Studies

This section discusses the sensitivity of CO_2 injection rate to aquifer properties and pattern geometry. Fig. 6.13 shows a curve (red) for the amount of gas that can be injected in a single base case engineering pattern for different vertical permeability values. The thickness of the aquifer is 1,000 ft and the horizontal permeability is 100 md. The amount of gas that can be injected in each pattern is very sensitive to the vertical permeability. The efficiency of the system severely decreases for a vertical permeability greater than 25 md. With an increase in vertical permeability, increases the vertical velocity of the CO_2 plume rises under buoyancy. After a certain threshold value of vertical permeability, it is almost impossible to eliminate gas saturation below the top seal. As the vertical permeability increases, the rate of brine injection from the top injector should increase to provide a strong downward gradient to buoyant CO_2. The brown curve in Fig.6.13 shows an increasing trend with increasing

vertical permeability. The engineered system is very sensitive to vertical permeability of the system and works best for vertical permeability values less than 20 to 25 md.

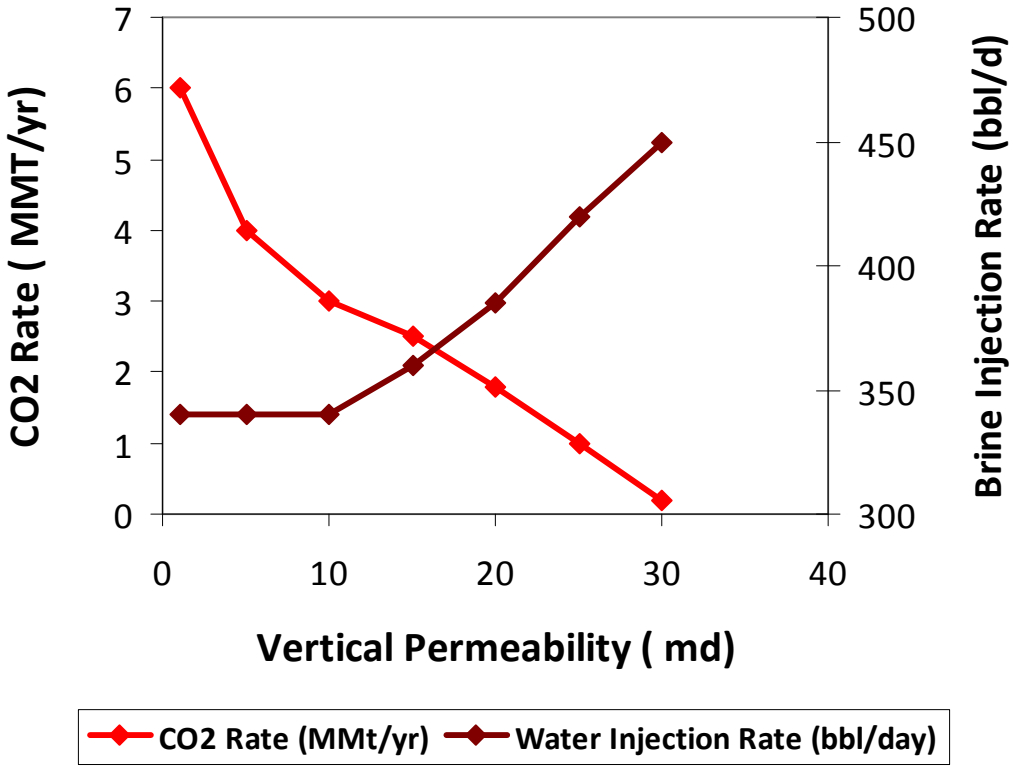

Fig. 6.13—CO_2 injection rate (million T/yr) for the base case engineered pattern for different vertical permeability values (red curve). The brown curve shows the water injection rate for a specific vertical permeability. The thickness of the base case aquifer is 1,000 ft.

Fig. 6.14 shows the effects of horizontal permeability on the optimal amount of gas that can be safely injected in each base case engineering pattern for zero mobile gas saturation below the top seal. The thickness of the pattern is 1,000 ft and the vertical permeability is kept constant at 10 md. As can be seen, the optimal CO_2 injection rate for each pattern is independent of horizontal permeability. In Fig.6.14 the red curve shows that this amount is 3 million T/yr for different values of horizontal permeability. However, as the horizontal permeability increases, the horizontal velocity of the CO_2 from the CO_2 injector to brine producer increases. This leads to an early breakthrough of CO_2 at the brine production well. To avoid this, the well

spacing between the gas injector and the brine producer should be increased to make the design more efficient and avoid producing CO_2 with the brine. The brown curve in Fig.6.14 shows the well spacing between the CO_2 injector and brine producer for different values of horizontal permeability.

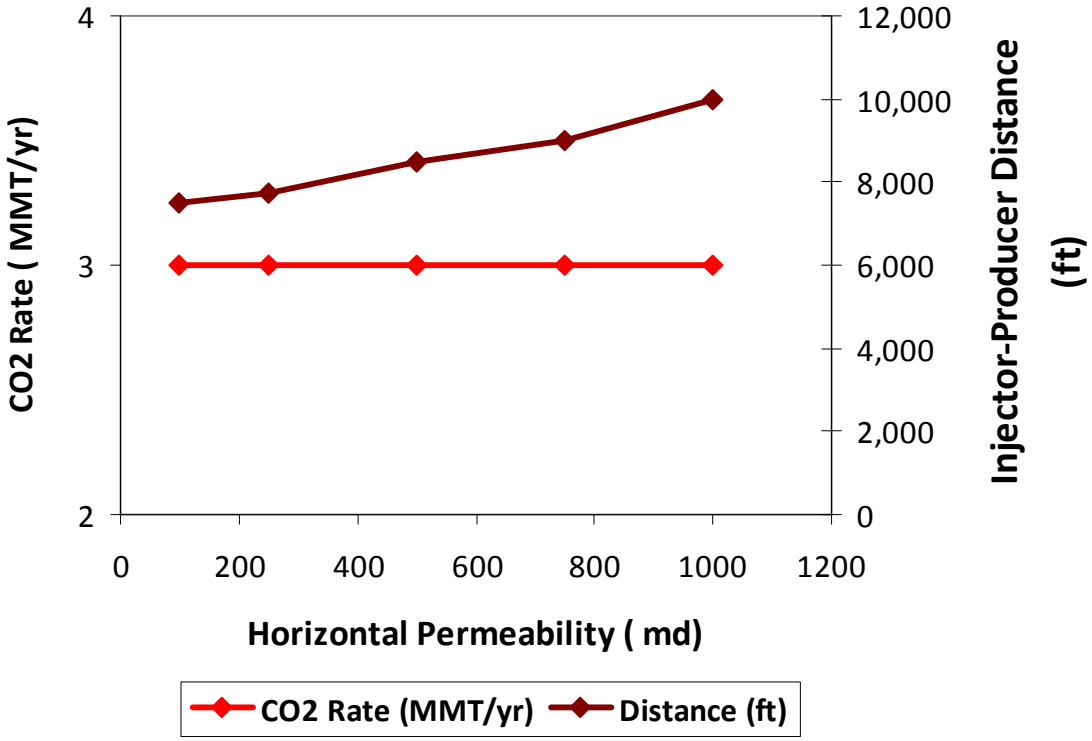

Fig. 6.14—CO_2 injection rate (million T/yr) for the base case engineered pattern for different horizontal permeability values (red curve). The brown curve shows the distance between the CO_2 injector and the brine producer in ft. The thickness of the base case aquifer is 1,000 ft.

Fig. 6.15 shows the amount of CO_2 injection vs aquifer thickness (red curve). As the aquifer thickness decreases, the optimal injection rate of CO_2 decreases. Injecting more than the suggested amount may lead to mobile gas saturation below the top aquifer seal. As the thickness decreases, the optimal gas injection rate decreases, and the number of patterns required to sequester a target amount of CO_2 (3 million T/yr for 30 yrs in this case) increases (brown curve). For example, for a 750-ft-thick aquifer, the optimal injection rate for each pattern is 1.5 million T/yr and 2 patterns will be

required to inject 3 million T of CO_2 per year for 30 years. If the injection rate of CO_2 exceeds 1.5 million T/yr/pattern, then the project operators may experience mobile free gas saturation below the top seal, unless substantial changes have been made to the engineering—not to mention that this curve was generated for the base case aquifer model with 10-md vertical permeability. Any changes to reservoir properties and thickness may change the results significantly.

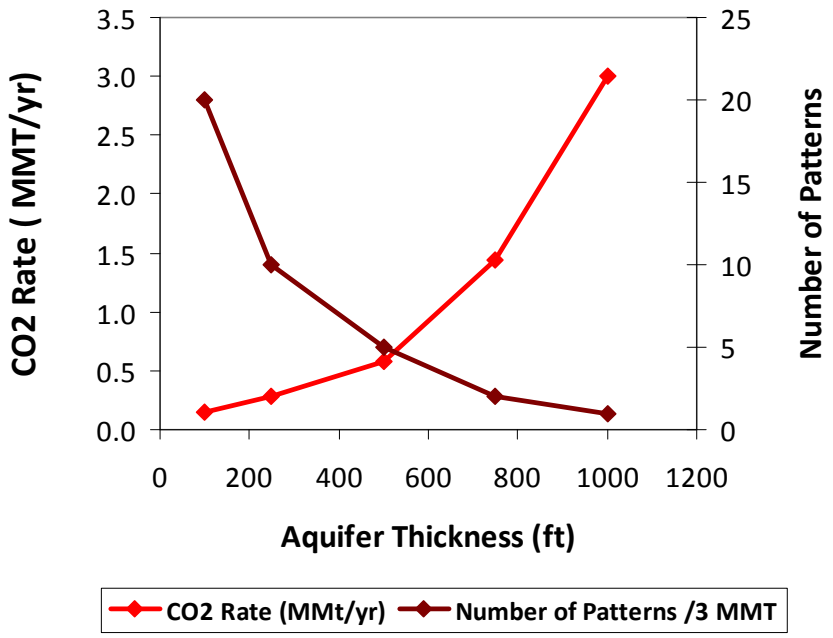

Fig. 6.15—CO_2 injection rate (million T/yr) for varying aquifer thickness (red curve). The brown curve shows the number of patterns required to sequester 3 million T/yr of CO_2 in an aquifer for a particular aquifer thickness.

6.4.7 Storage Potential

Storage potential as discussed in previous sections is the percentage of pore volume that can be occupied by CO_2. In the case of closed aquifers, this factor is limited by the available pore volume and aquifer pressurization. As discussed earlier, a closed system would be ideal for CO_2 containment because the low permeability barriers will not allow the injected supercritical CO_2 to leak back to the atmosphere. However, it is

important to produce brine out of the closed system for pressure relief and to increase the storage potential of the system. The engineering system discussed in the previous section of this section increases the volume of CO_2 that can be stored in a closed aquifer volume. For the engineered case discussed in Section 6.4, 3 million T/yr of CO_2 was injected for 30 years in a 15,000 ft X 15,000 ft X 1,000 ft pattern. This corresponds to a storage potential of 8.5%. This is approximately *4 times* higher than the storage potential for the bulk injection approach injecting the same amount in an aquifer with similar pressure and temperature conditions. Moreover, the accelerated dissolution and trapping of CO_2 renders 90% of the gas immobile by the end of 50 years.

The injection dynamics of the system is controlled, and it prevents CO_2 from migrating toward potential outlets or sensitive areas. It is easier to characterize a small portion of the aquifer with greater confidence than to characterizie miles and miles of aquifer extensions. A high-resolution characterization of a smaller, closed aquifer volume can build greater confidence in engineering design and in evaluating the target formation for suitability for CO_2 storage.

Although this technique requires additional drilled wells, the engineered case significantly reduces the reservoir volume required to effectively sequester a given volume of CO_2. Since the free gas saturation in the reservoir is reduced early on, the increase in the cost due to additional wells is compensated for by the dramatic reduction in monitoring cost. In analogy to improved recovery in pattern well waterflooding, engineered aquifer management improves aquifer storage potential, thereby reducing the underground footprint of the CO_2 sequestration operation. It has potential to reduce the uncertainty about the long-term fate of the injected CO_2.

6.5 Applications of Engineered Case

In reality, aquifers are rarely homogeneous. Since the results of the engineered case are encouraging with homogeneous permeability and porosity fields, in the following section, we discuss the application of the engineered case to horizontal and dipped aquifers with stochastic permeability and porosity fields. Again, 3 million T/yr of gas was injected for 30 years along with 30 years of brine recirculation.

Case 1: Modification of Homogeneous Case to Stochastic Permeability Field

In this section, a stochastic property field was generated as shown in Fig. 6.16. The permeability in the field varies from 1 md to 200 md with a mean permeability estimate of 100 md. The mean of the permeability was kept constant as the permeability of the homogeneous base case field. The vertical permeability is 0.1 times the horizontal permeability. The conditional permeability realization was generated using the sequential Gaussian simulation (SGSIM) geostatistical algorithm that has been implemented into Stanford geostatistical modeling software (SGEMS). A random permeability data set was used to condition the Gaussian simulation. Each realization is discretized into a 50 X 50 X 50 (500 ft X 500 ft X 20 ft) gridblock system. The porosity field was correlated to the randomly generated permeability field with the Holtz (2002) correlation discussed in Section 2.4. The average porosity of the field is 23%.

The maximum residual gas saturation and residual water saturation was again correlated to the random porosity field using the Holtz (2002) correlation. For each gridblock, different values of porosity, permeability, capillary pressure, maximum residual saturation, and residual water saturation were assigned in GEM-GHG. Kumar et al. (2004) defined different types of rock curves with porosity as independent variables. The value of porosity and permeability for each grid block will determine its rock type, which in turn determines its values of residual gas saturation and residual water saturation.

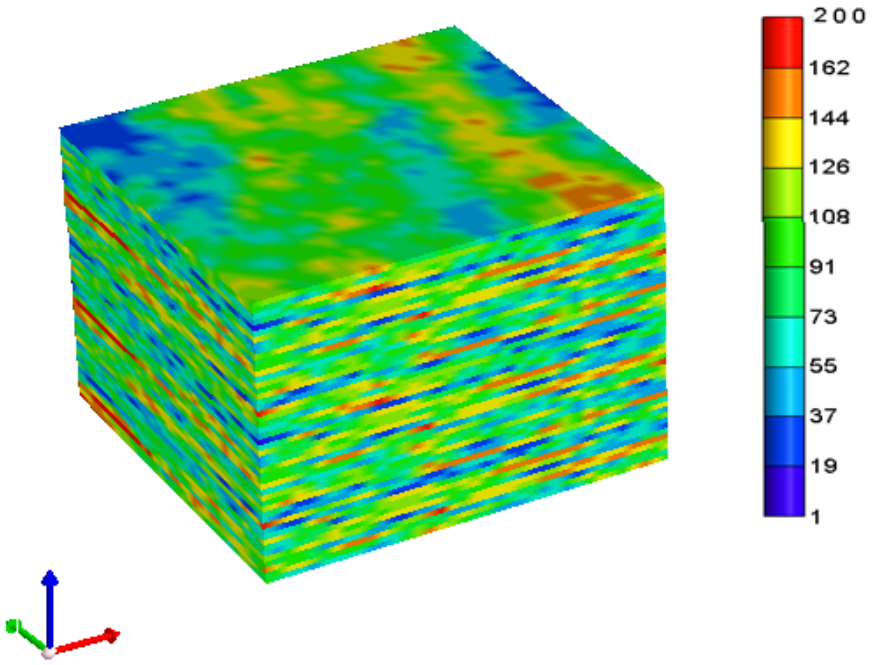

Fig. 6.16—Horizontal permeability in md for heterogeneous case.

The drainage capillary pressure curves for any rock type were modeled using the Brooks-Corey function. Kumar et al. (2004) also scaled the capillary pressure curves for each rock type to average permeability (Table 6.2). Without going into further detail, the relative permeability and capillary pressure curves used in the simulations are shown for each of the rock types.

Table 6.2—Values used in different relative permeability tables (Kumar et al. 2002)

Rock Type	Porosity	Average Porosity	S^{max}_{gr}	Average Permeability	S_{wirr}	k_{rg}
	(fraction)	(fraction)	(fraction)	(md)	(fraction)	(fraction)
1	0.16- 0.195	0.18	0.373	4.192	0.628	0.13
2	0.195-0.225	0.21	0.344	21.594	0.276	0.52
3	0.225-0.255	0.24	0.315	77.877	0.194	0.62
4	0.225-0.285	0.27	0.286	241.423	0.161	0.68

Figs. 6.17 through 6.20 show the drainage relative permeability and capillary pressure curves for four different rock types. The capillary entry pressure varies for different rock types, and this leads to preferential gas flow into high-permeability rocks. The gas relative permeability curves shown in the plots are extended beyond the endpoint to maximum gas saturation 1 for correct mobility calculation of the fluid in the dry zone. The water relative permeability does not change during this extension (Kumar et al. 2008).

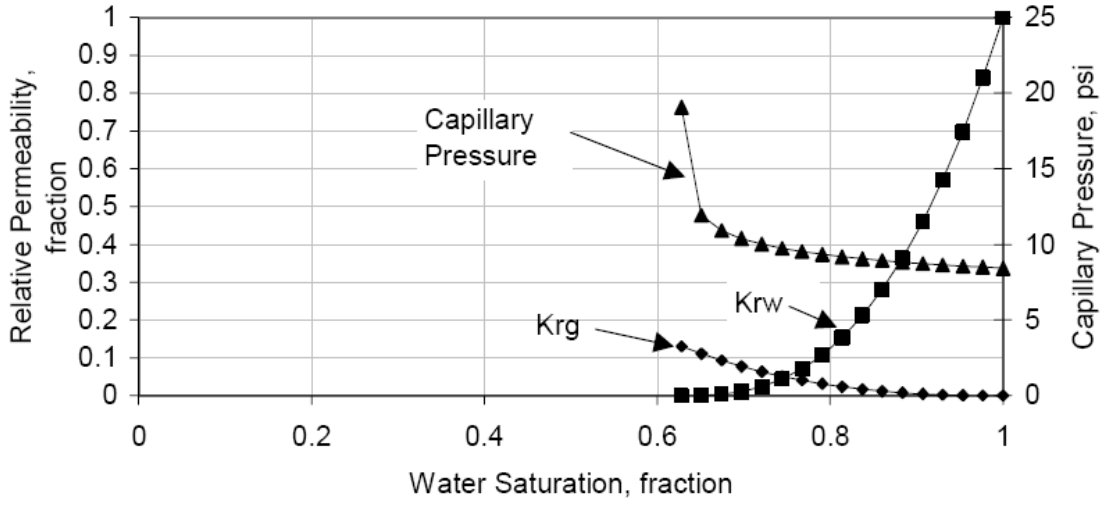

Fig. 6.17—Relative permeability and capillary pressure curves for Rock Type 1 (Kumar et al. 2002).

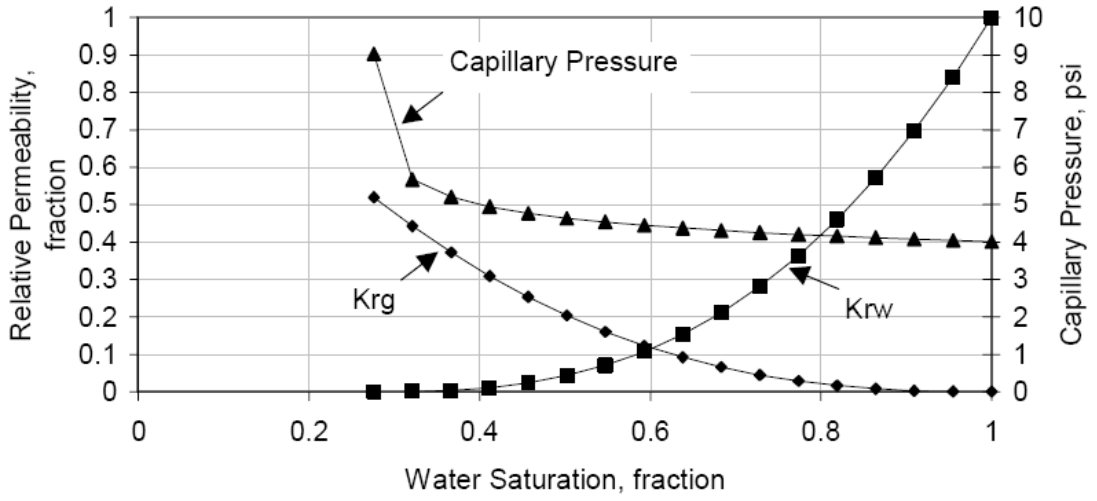

Fig. 6.18—Relative permeability and capillary pressure curves for Rock Type 2 (Kumar et al. 2002).

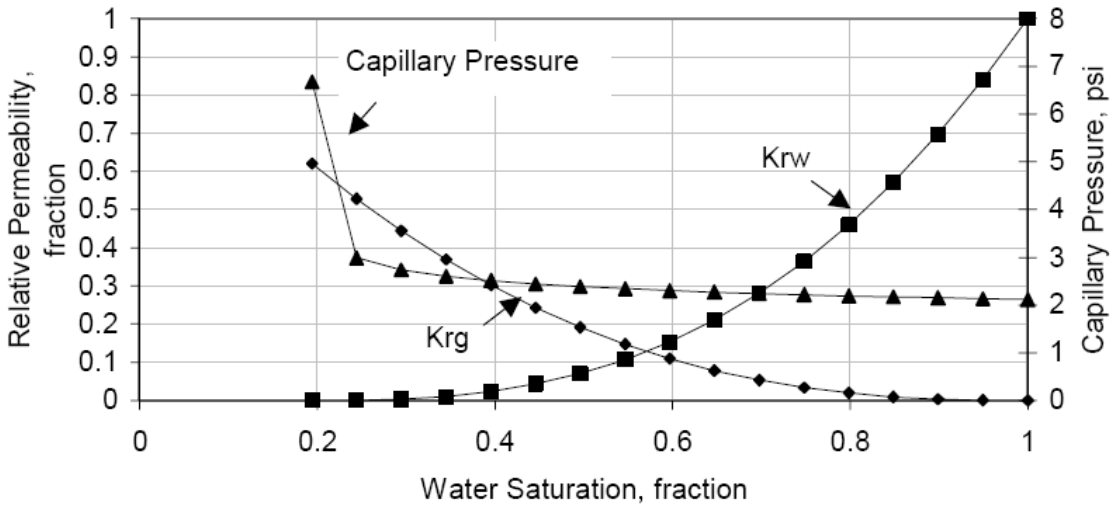

Fig. 6.19—Relative permeability and capillary pressure curves for Rock Type 3 (Kumar et al. 2002).

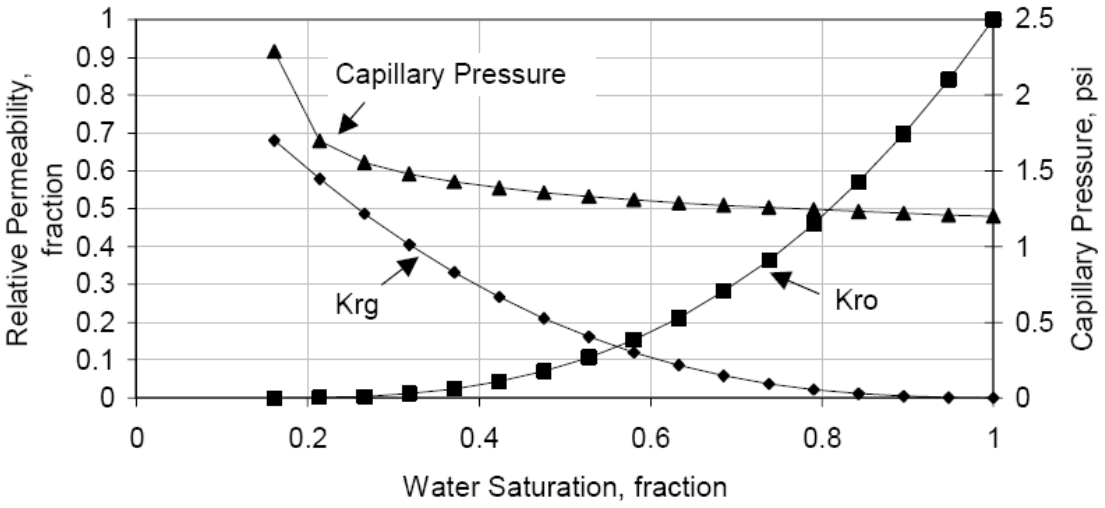

Fig. 6.20—Relative permeability and capillary pressure curves for Rock Type 4 (Kumar et al. 2002).

Fig. 6.21 shows the free gas saturation just below the top seal after 1,000 years. As can be seen, the free gas was rendered immobile before it could reach the top seal. Fig. 6.22 and 6.23 show the trapped gas saturation after 1,000 years for the heterogeneous case. It is quite clear from Fig. 6.24 that heterogeneous permeability field has an effect on the shape of the trapped gas saturation.

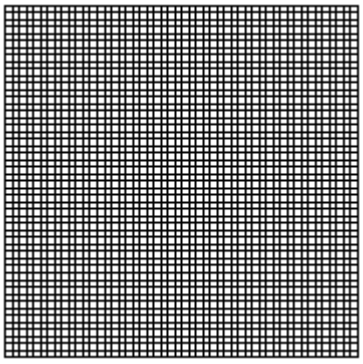

Fig. 6.21—Free gas saturation for the heterogeneous case just below the top seal after 1,000 years.

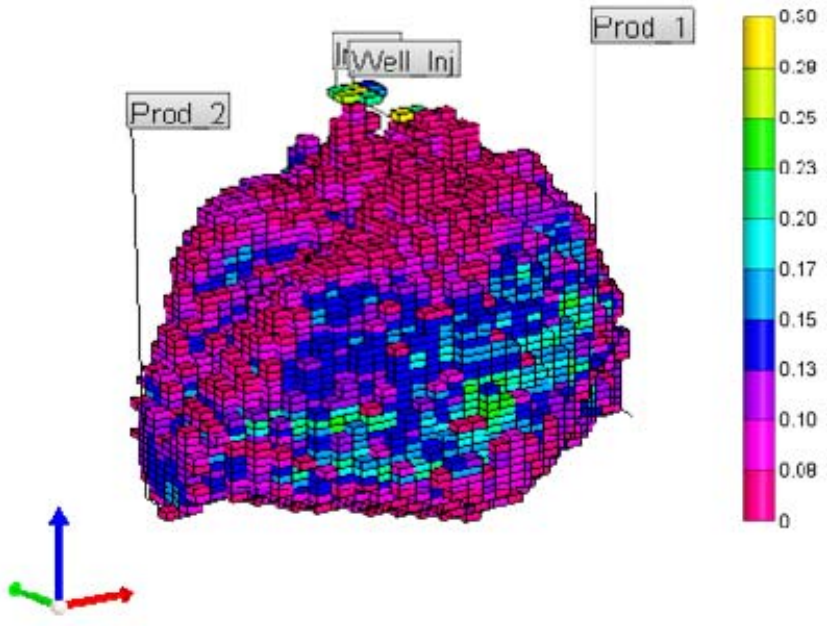

Fig. 6.22—3D view of trapped gas saturation for the heterogeneous engineered case after 1,000 years. 3 million T/yr of gas was injected for the 30 years. Brine recirculation was stopped along with CO_2 injection.

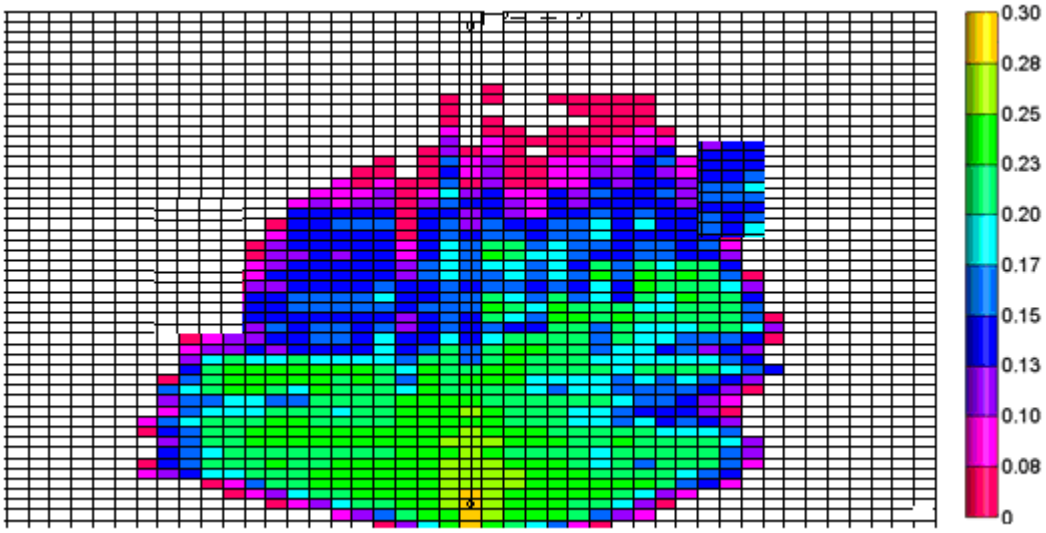

Fig. 6.23— X-Z view of trapped gas saturation for the heterogeneous engineered case after 1,000 years. 3 million T/yr of gas was injected for the 30 years. Brine recirculation was stopped along with CO_2 injection.

Velocity Fields

One very unique feature of engineering the system in heterogeneous field is the velocity field generated between the top injector and the bottom producer. The reason the engineered system works so well under heterogeneous conditions is the direct correlation between the water velocity from the top brine injector and the gas velocity from the bottom CO_2 injector. The velocity of the CO_2 rising under the buoyancy will be higher in the gridblock with higher permeability, which has less capillary entry pressure. Similarly, the velocity of brine from the top injection falling downwards under gravity will have a higher velocity in the high permeability gridlocks because it has less capillary entry pressure. This indicates that in the gridblock in which the Z velocity is higher, the velocity of brine falling from top will also be higher. As can be seen in Fig. 6.24, if the Z velocity of the CO_2 is higher at any point on along the horizontal length of the wellbore, the velocity of the brine from the top injector is also higher. The velocity profiles from both the injectors more or less follow the same trend. The preferential movement of injected brine in gridblocks with higher permeability helps in suppressing the movement of rising CO_2 from the high-permeability gridblocks under buoyancy.

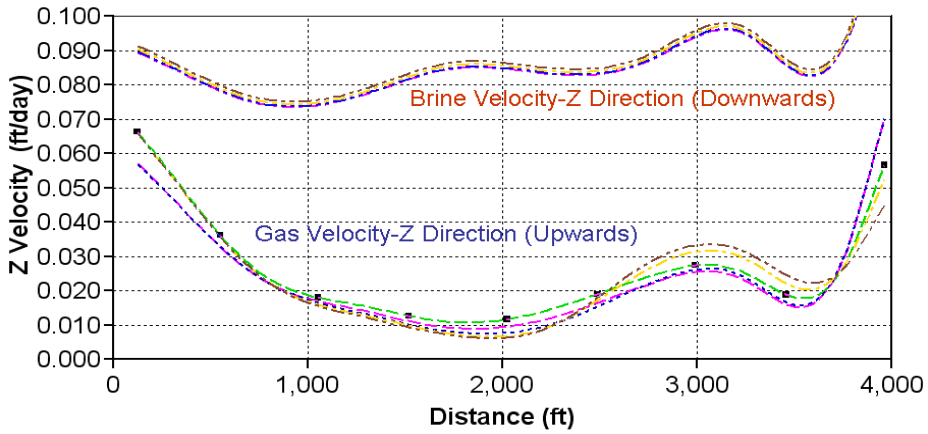

Fig. 6.24—Plot showing the Z velocity profile along the horizontal well direction in ft/D. The top plot shows the water velocity flowing downwards from the top brine injector and the bottom plots show the Z velocity of the gas rising upwards.

Mobile Gas

Fig. 6.25 shows the total mobile CO_2 (in billion moles) at different times for the heterogeneous engineered case. It also shows the cumulative gas injected in billion moles. As expected, almost 85 to 90% of the gas is rendered immobile (dissolved and trapped) as early as 50 years after starting injection, thus reducing the tendency of the free gas to leak back to the atmosphere through an imperfect caprock, imperfectly sealed wellbore, or conductive fault.

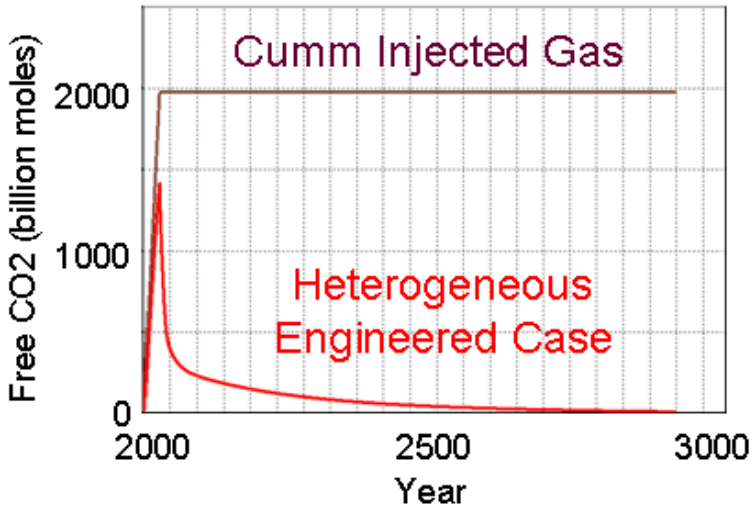

Fig.6.25—Mobile CO_2 with time for the heterogeneous engineered case (red). The brown curve shows the total gas injected for 30 years at the rate of 3 million T/yr.

Case 2: Heterogeneous Permeability Field with Dipping formation

In this section, a stochastic property field is shown from Case 1. The formation has a geological dip of 4^o with the rest of the properties the same as the base case discussed in Section 2. Again, 3 million T/yr of gas was injected for 30 years and brine was recirculated for 30 years (Fig. 6.26).

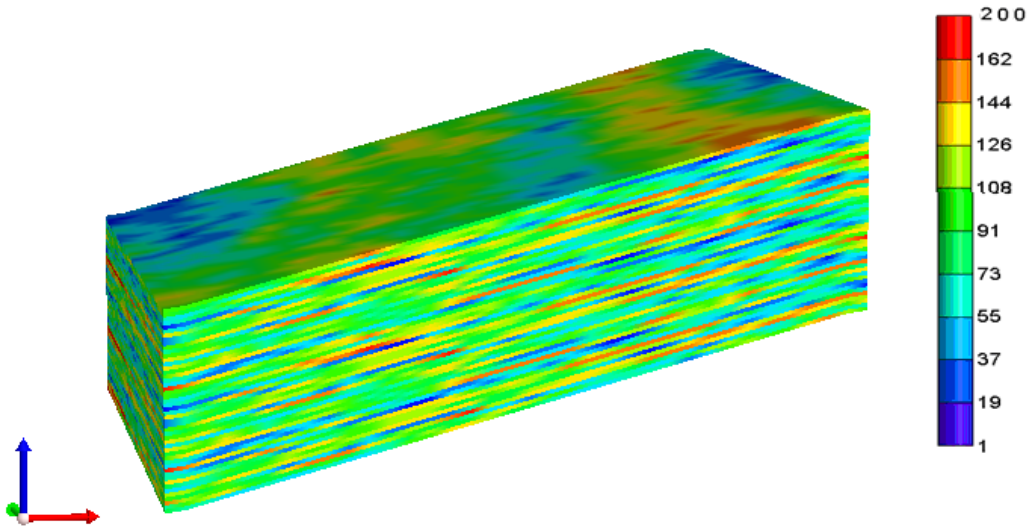

Fig. 6.26—Horizontal permeability in md for the heterogeneous dipping aquifer.

During the injection period, the flow of the gas is mostly pressure driven, while after the injection it is mostly gravity driven due to density contrast. The CO_2 travels updip and travels a much farther distance in dipping aquifers. Since the flow behavior of CO_2 and water is different in inclined aquifers as compared to horizontal aquifers, some modifications have to be made to regular engineering design.

Some salient features of engineering the system in dipped aquifers:

- Since the CO_2 has a tendency to rise updip, the production well updip should be farther away from the CO_2 injector than the production well downdip to avoid early breakthrough.
- The production rate from the two production wells is not equal. The rate from the well updip is lower than the rate from the well downdip to avoid early breakthrough in the producer updip and to give CO_2 a better sweep in the downward direction.
- For a large aquifer dip (>4^o), the top brine injector should be placed slightly updip as compared to the CO_2 injector. Since the CO_2 has a tendency to rise updip, a stronger gradient is required between the top brine injector and top brine producer to avoid any contact of the CO_2 with the top aquifer seal. The reduced distance between the two wells (top brine injector and producer) will provide a stronger gradient to keep the CO_2 inside the falling brine curtain.

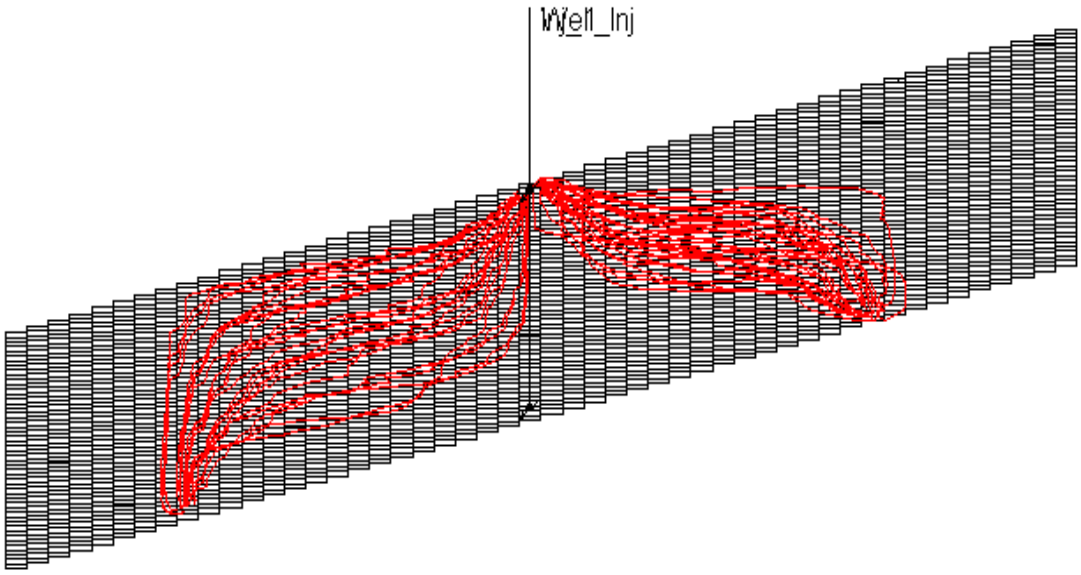

Fig. 6.27—X-Z view of the streamlines originating from the top brine injector to the bottom brine producers.

Fig. 6.27 shows the streamlines traced from the source (top brine injector) to sinks (brine producers). As can be seen, the brine tries to form an envelope or curtain around the CO_2 injector. The width of the curtain is different in two directions from the CO_2 injector. (updip and downdip). The width of the curtain is smaller updip because the brine producer updip is more close to top brine injector. This works to the benefit of the engineering design because it gives a stronger downward gradient between the top brine injector and brine producer keeping the rising CO_2 away from the top seal.

Fig. 6.28 shows the free gas saturation just below the top seal after 1,000 years. As can be seen, the free gas was rendered immobile before it could reach the top seal. Fig. 6.29 and 6.30 shows the trapped gas saturation after 1,000 years for the heterogeneous dipped aquifer. It is quite clear from Fig. 6.30 that heterogeneous permeability and aquifer dip has an effect on the shape of the trapped gas saturation. The engineering of the system provides a good sweep in the direction downdip from the CO_2 injector.

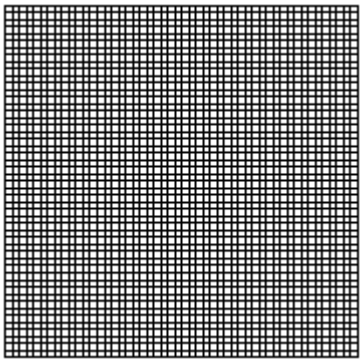

Fig. 6.28—Free gas saturation for the heterogeneous dipping aquifer just below the top seal after 1,000 years.

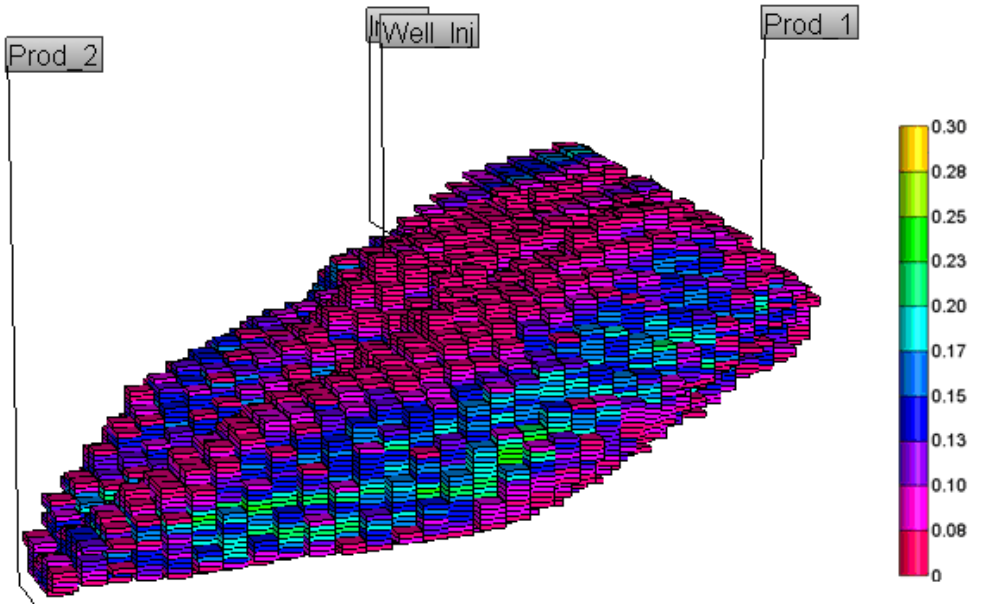

Fig. 6.29— 3D view of trapped gas saturation for the heterogeneous dipping aquifer after 1,000 years. 3 million T/yr of gas was injected for the 30 years.

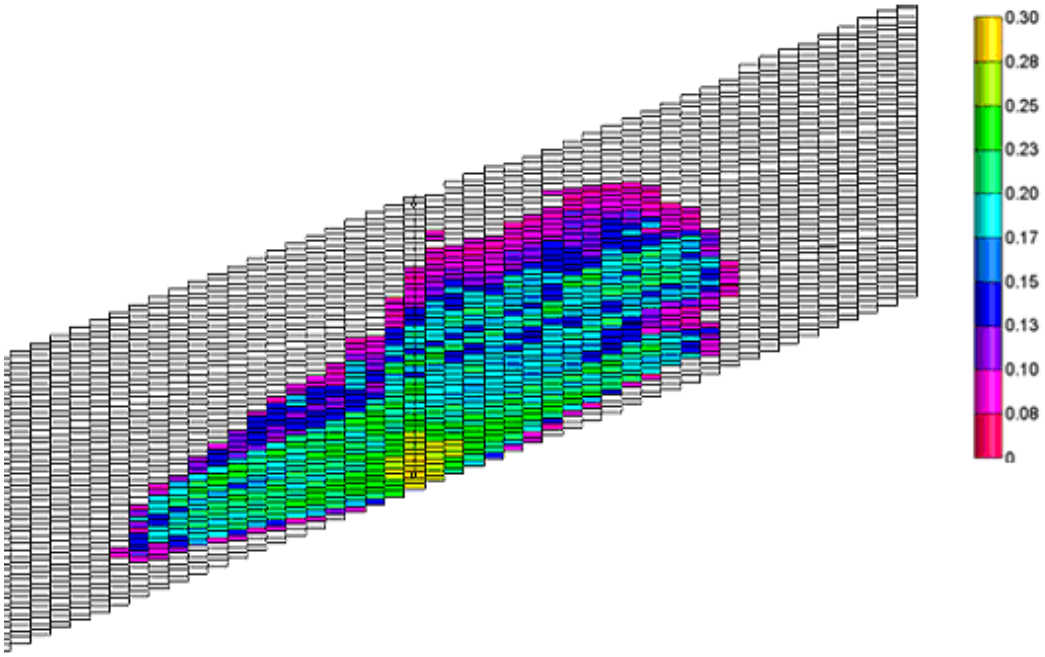

Fig. 6.30— X-Z view of trapped gas saturation for the heterogeneous dipping aquifer after 1,000 years. 3 million T/yr of gas was injected for the 30 years

Mobile Gas

Fig. 6.31 shows the total mobile CO_2 (in billion moles) at different times for the heterogeneous dipped aquifer case. It also shows the cumulative gas injected in billion moles. As expected, almost 90% of the gas is rendered immobile (dissolved and trapped) as early as 40 years after starting injection. The dissolution and trapping of CO_2 for the dipped aquifer is faster than for the horizontal aquifers because the CO_2 travels a greater distance in the aquifer and comes in contact with more fresh brine. The same amount of free CO_2 is realized in the system 10 years earlier for the dipping aquifer case. The engineering design for the dipped aquifer case is highly effective, thus reducing the tendency of the free gas to leak back to the atmosphere through an imperfect caprock, imperfectly sealed wellbore and conductive fault.

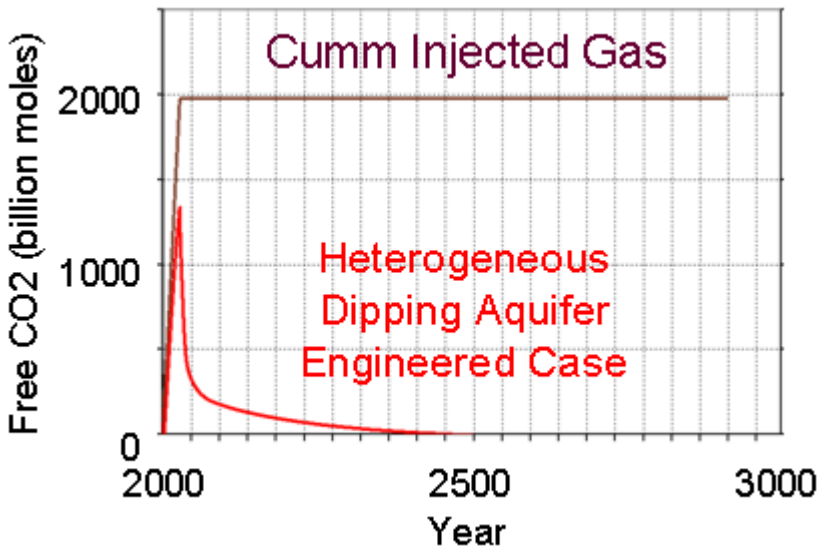

Fig. 6.31—Mobile CO_2 with time for the heterogeneous dipped aquifer engineered case (red). The brown curve shows the total gas injected for 30 years at the rate of 3 million T/yr.

6.6 Section Conclusions

This section presents a method for accelerating CO_2 dissolution in saline aquifers by re-circulating brine in a strategically designed engineered system. Relevant risk arising from aquifer pressurization due to injection and free CO_2 below the aquifer

seal is addressed. Simulation studies for homogeneous and heterogeneous permeability fields suggest that almost 90% of the CO_2 is rendered immobile as early as 20 years after the cessation of injection. This is much lower than the free gas saturation in the bulk injection scenario even 1,000 years after stopping the injection. Further, the storage potential is 8%. This is four times more than the storage potential for the bulk injection scenario. Consequently, it will not increase the number of wells required to sequester the CO_2. Design for a given thickness, depth, and aquifer properties includes optimization of the aquifer geometry, well lengths, well spacing, CO_2 injection rates, and number of patterns. Sensitivity studies show that the maximum amount of gas that can be immobilized in a particular aquifer decreases as vertical permeability increases and formation thickness decreases. Horizontal permeability has a minimal effect on the efficiency of the system.

Eliminating the dependence of CO_2 storage operations on long-term dissolution and mineralization mechanisms provides security to the storage and significantly reduces long-term monitoring costs. From a practical standpoint, dissolution and residual trapping are two low-risk modes of storages that could be designed and manipulated to increase the storage security and reduce risk. Thus, it is important to explore engineering techniques to eliminate buoyancy-driven accumulation of free gas and accelerate its dissolution and capillary trapping in the system. Once the gas is dissolved, risk assessment may ignore the leakage pathways owing to very slow movement of CO_2-saturated brines.

Using current multilateral well technology, the suggested engineering design could be easily implemented for real field-scale applications. Enough experience exists in the oil and gas industry for injecting and producing saline water for pressure maintenance and waterflooding operations. Applying such techniques can greatly reduce risks related to aquifer pressurization and free mobile gas. The increased storability expands the range of reservoirs that are acceptable for CO_2 storage.

Preliminary results are encouraging and demonstrate potential to accelerate CO_2 dissolution and trapping, virtually eliminating the risk of mobile free-phase CO_2 leakage from the storage site.

7. CONCLUSIONS AND RECOMMENDATIONS

Large quantities of CO_2 should be sequestered for geologic CO_2 storage to make an impact on the environment. Many previous studies have shown simulations of CO_2 sequestration in deep saline aquifers. This thesis is specifically focused on addressing the risk of CO_2 leakage from an aquifer, its monitoring, and mitigation. The likelihood of CO_2 leakage from an aquifer is aggravated by two factors: pressurization of the aquifer and accumulation of free CO_2 at the top of the aquifer just below the seal. Ways to address these risks are considered in this thesis. Section 7.1 discusses the specific findings of this research and Section 7.2 identifies future research opportunities related.

7.1 Conclusions

Many published studies have used an open (constant pressure) boundary for simulations that focused on CO_2 dissolution and trapping for thousands of years following the end of CO_2 injection. The focus of this research is on the behavior of the aquifer during CO_2 injection. After successfully simulating published results for bulk CO_2 injection with a vertical well, this study showed that a closed aquifer boundary greatly affects simulation results during the time of injection. This research investigated three approaches to geologic CO_2 sequestration in saline aquifers: bulk CO_2 injection, brine production to avoid aquifer pressurization and increase CO_2 storability, and an engineered system designed to accelerate CO_2 dissolution and trapping. The objective was to consider sequestration of CO_2 captured from a 500-MW coal power plant operating for 30 years.

Conclusions for bulk CO_2 injection include the following:

1. Simulations clearly indicated that bulk CO_2 injection into a single well could rarely inject the volume of CO_2 produced by the power plant in a typical aquifer and that multiple wells would be required. In an array of injection wells, the

aquifer volume allotted to each injection well is limited by interference with other injection wells. Therefore, modeling of CO_2 injection must consider a closed outer boundary, and bulk injection in a closed system will pressurize the aquifer. Simulations confirm this conclusion.

2. An analytical model developed for this study extends a previously published analytical model for the open aquifer to a closed aquifer. A spreadsheet model provides very similar results to detailed simulation in a fraction of the time and enables systematic determination of the aquifer volume and the number of wells required to sequester the target amount of CO_2. Results indicate that depending on the aquifer properties, the sequestration operation would require thousands of square miles of aquifer area or hundreds of wells or both. In any case, the aquifer must be pressurized, and CO_2 accumulates at the top of the aquifer, leading to an unacceptable risk of CO_2 leakage.

3. Simulations over 30 years on injection demonstrated the value of regular pressure falloff monitoring of CO_2 injection wells. Pressure falloff responses provide ongoing indications of the dry zone and two-phase zone radii over time and quantification of the zone mobility values. For the case studied, the falloff responses also provided reasonable estimates for the ongoing average aquifer pressure that can be used for material balance analysis. In turn, analysis of average pressure over time can indicate whether the behavior is that of an open or closed aquifer and an estimation of the aquifer size. Alternatively, average pressure behavior over time can signal presence of an aquifer leak and provide an estimation of how much fluid may be leaking from the aquifer and whether the leak is predominantly CO_2 or brine.

These results suggest that bulk CO2 injection is neither economically nor environmentally acceptable.

To avoid pressurizing the aquifer and reduce the number of wells required to sequester the CO2, brine should be produced from the aquifer as a volume equal to that of the injected CO2. This approach addresses the pressurization risk, but does not address the problem of CO2 accumulating at the top of the aquifer.

An engineered system is proposed to both avoid aquifer pressurization and accelerate CO2 dissolution and trapping. This system would position a horizontal brine injection well above and parallel to a horizontal CO2 injection well with horizontal brine production wells drilled parallel to the CO2 injection well at a specified lateral spacing. Simulations showed that this configuration prevents CO2 accumulation at the top of the aquifer during injection and that 90% of the CO2 is permanently dissolved or trapped during injection after 50 years, including the 30 years of injection. This approach would greatly reduce the risk of CO2 leakage both during and forever after injection.

7.2 Recommendations

1. Bulk phase CO_2 injection can provide substantive reduction in CO_2 emissions only if additional brine is produced out of the system to address relevant risks arising from aquifer pressurization. Treatment of produced brine is extremely costly using current desalination and treatment technologies. Inexpensive alternative technologies for freshwater production should be explored to enable this option.

2. The sensitivity of pressure transient measurements to detect significant leakage from the storage formation and detection limits for pressure gauges should be thoroughly investigated.

3. The fundamentals underlying the proposed CO_2 injection scheme need to be formalized and generalized. The countercurrent engineering scheme proposed in this thesis is an unstable displacement and thus difficult to express through analytical solutions, and further investigations are needed into stream-function and streamline-based analytical solutions. In particular, expressions like gravity number should be modified to capture the dynamics of the engineered system. The new expression should be capable of comparing the efficiency of engineered systems based on the well lengths and brine injection/production rates.

REFERENCES

Acosta, L.G. and Ambastha, A.K. 1994. Thermal Well Test Analysis Using an Analytical Multi-Region Composite Reservoir Model. Paper SPE 28422 presented at the SPE Annual Technical Conference and Exhibition, New Orleans, 25-28 September. DOI: 10.2118/90149-MS.

Albritton, D.L. and Meira-Filho, L.G. 2001. Climate Change 2001: The Scientific Basis: Contribution of Working Group I to the *Third Assessment Report of the Intergovernmental Panel on Climate Change—Technical Summary.* IPCC: Geneva, Switzerland, 2001.

Arts, R., Eiken, O., Chadwick, A., Zweigel, P., van der Meer, L., and Zinszner, B. 2002. Monitoring of CO_2 Injected at Sleipner Using Time Lapse Seismic Data. Paper presented at the Sixth International Conference on Greenhouse Gas Control Technologies (GHGT-6), Kyoto, Japan, 1-4 October.

Bakker, R.J. 2003. Package FLUIDS 1. Computer Programs for Analysis of Fluid Inclusion Data and for Modelling Bulk Fluid Properties. *Chemical Geology* **194**: 3-23.

Baklid, A., Korbøl, R. and Owren, G. 1996. Sleipner Vest CO_2 Disposal, CO_2 Injection into a Shallow Underground Aquifer. Paper SPE 36600 presented at the SPE Annual Technical Conference and Exhibition, Denver, Colorado, 6-9 October. DOI: 10.2118/36600-MS.

Becker, E.M., Burruss, R.C., Freeman, P.A, Merrill, M.D., Brennan, S.T., and Ruppert, L.F. 2009. Use of Formation Pressure Data to Determine the Limitations to Storage Volumes and Injectability of CO_2 in the Frio Formation of the Texas Gulf Coast. Paper presented at the 2009 AAPG Annual Convention and Exhibition, Denver, Colorado, 7-10 June.

Benson, S.M., Hepple, R., Apps, J., C.F. Tsang, C.F., and Lippmann, M. 2002. Lessons Learned from Natural and Industrial Analogues for Storage of Carbon Dioxide in Deep Geologic Formations, Lawrence Berkeley National Laboratory Report LBNL-51170.

Benson, S. 2006. Monitoring Carbon Dioxide Sequestration in Deep Geological Formations for Inventory Verification and Carbon Credits. Paper SPE 102833 presented at the SPE Annual Technology Conference and Exhibition, San Antonio, Texas, 24-27 September.

Braunt, R.G., Celia, M.A., Peters, C.A., and Guswa, A.J. 2002. Safe Storage of CO_2 in Deep Saline Aquifers. *Environmental Science and Technology* **36** (11): 240-245.

Bryant, S.L., Lakshiminarasimhan, S., and Pope, G.A. 2006. Buoyancy-Dominated Multiphase Flow and Its Impact on Geological Sequestration of CO_2. Paper SPE 99938 presented at SPE/DOE Symposium on Improved Oil Recovery, Tulsa, Oklahoma, 22-26 April.

Buckley, S.E., and Leverett, M.C. 19492. Mechanism of Fluid Displacement in Sands. *Trans.*, AIME **146**, 107-116.

Burton, M. and Bryant, S.L. 2007. Eliminating Buoyant Migration of Sequestered CO_2 Through Surface Dissolution: Implementation Costs and Technical Challenges, paper SPE 110650, presented at the 2007 SPE Annual Technical Conference and Exhibition, 11-14 November 2007, Anaheim, California, U.S.A.

Burton, M., Kumar, N., and Bryant, S.L. 2008. Time-Dependent Injectivity during CO_2 Storage in Aquifers. Paper SPE 113937 presented at the SPE/DOE Improved Oil Recovery Symposium, Tulsa, Oklahoma, 19-23 April.

Carroll, J.J., Slupsky, J.D., and Mather, A.E. 1991. The Solubility of Carbon Dioxide in Water at Low Pressure. *J. of Physical and Chemical Reference Data* **20** (6): 1201-1209.

Celia, M.A. and Bachu, S. 2003. Geological Sequestration of CO_2: Is Leakage Unavoidable and Acceptable? Proc. of the 6th International Conference on Greenhouse Gas Control Technologies. Amsterdam, The Netherlands, **I:** 477—482.

Chalaturnyk, R. and Gunter W.D. 2004. Geological Storage of CO_2: Time Frames, Monitoring and Verification. Proc. of the Greenhouse Gas Control Technologies Conference (GHGT7), Vancouver, **I:** 623-31.

Damen, K., Faaij, A., and Turkenbur, W. 2006. Health, Safety and Environmental Risks of Underground CO_2 Storage—Overview of Mechanisms and Current Knowledge. *Climatic Change* **74:** 1—3.

DEFRA. 2003. The Scientific Case for Setting a Long-Term Emission Reduction Target. Department for Environment, Food and Regional Affairs, UK.

Duan, Z. and Sun, R. 2003. An Improved Model Calculating CO_2 Solubility in Pure Water and Aqueous NaCl Solutions from 273 to 533 K and from 0 to 2000 bar, *Chem. Geol.,* **193:** 257-271.

Economides, M. and Ehlig-Economides, C. *(Submitted).* Sequestering Carbon Dioxide in Closed Underground Volume. Paper SPE 124430 to be presented at the SPE Annual Technical Conference and Exhibition, New Orleans, 4-7 October 2009.

Garcia, J.E. 2001. *Density of Aqueous Solutions of CO_2*. Berkeley, California: Lawrence Berkeley National Laboratory.

Gunter, W.D. and Perkins, E. 2001. Geochemical Monitoring of CO_2 Enhanced Oil Recovery. Proc. of the NETL Workshop on Carbon Sequestration Science, http://www.netl.doe.gov/.

Gunter, W.D., Perkins E.H., and McCann, T.J. 1993.Aquifer Disposal of CO_2-Rich Gases: Reaction Design for Added Capacity. *Energy Conversion and Management* **34:** 941—8.

Gunter, W.D., Wong, S., Cheel, D.B., and Sjostrom G. 1998. Large CO_2 Sinks: Their Role in the Mitigation of Greenhouse Gases from an International, National (Canadian) and Provincial (Alberta) Perspective. *Appl Energy* **61**(4):209-227.

Hangx, S.J.T. 2005. Behavior of the CO_2-H_2O System and Preliminary Mineralisation Model and Experiments. CATO Workpackage WP 4.1, Deliverable WP 4.1-3-05.

Hesse, M., Tchelepi, H., and Orr, F.M. Jr. 2006. Scaling Analysis of the Migration of CO_2 in Saline Aquifers. Paper SPE 102796 presented at the SPE Annual Technical Conference and Exhibition, San Antonio, Texas, 24-27 September.

Holloway, S. 2001. Storage of Fossil Fuel-Derived Carbon Dioxide Beneath the Surface of the Earth. *Annual Reviews of Energy and the Environment* **26:** 145-166.

Holloway, S. 1996. The Underground Disposal of Carbon-Dioxide. Final report JOULE II Project No.CT92-0031, British Geological Survey, Keyworth, Nottingham, 335.

Holtz, M.H. 2002. Residual Gas Saturation to Aquifer Influx: A Calculation Method for 3D Computer Model Construction. Paper SPE 75502 presented at the SPE Gas Technology Symposium, Calgary, 30 April-2 May.

Hoversten, G.M. and Myer, L.R. 2000. Monitoring of CO_2 Sequestration Using Integrated Geophysical and Reservoir Data. Proc. of the 5th International Conference on Greenhouse Gas Control Technologies, Collingwood, Victoria, Australia 305-310.

Hoversten, G.M., Gritto, R. Daley, T.M., Majer, E.L., and Myer, L.R. 2002. Crosswell Seismic and Electromagnetic Monitoring of CO_2 Sequestration. Proc. of the Sixth International Conference on Greenhouse Gas Control Technologies (GHGT-6), Kyoto, 1-4 October.

Hovorka, S. D., Benson, S. M., and Doughty, C. K. 2006. Measuring Permanence of CO_2 Storage in Saline Formations−the Frio Experiment. *Geosciences* **13** (2): 105-121.

Ide, T., Jessen, K., and Orr, F.M. Jr. 2007. Storage of CO_2 in Saline Aquifers: Effects of Gravity, Viscous, and Capillary Forces on Amount and Timing of Trapping. *International Journal of Greehouse Gas Control* **1** (4): 481-491.

EIA. 2006. International Carbon Dioxide Emissions and Carbon Intensity Database http://www.eia.doe.gov/emeu/international/carbondioxide.html.

IPCC. 2008. Special Report on Carbon Dioxide Capture and Storage, Metz, B., Davidson, O., de Coninck, H., Loos, M., Meyer, L.A., editors. Cambridge University Press: New York.

Izpec, O., Demiral, B., Bertin, H., and Akin, S. 2006. Experimental and Numerical Modeling of Direct Injection of CO2 into Carbonate Formations. Paper SPE 100809 presented at the at the SPE Annual Technical Conference and Exhibition, San Antonio, Texas, 24–27 September.

Jarrel, P.M., Fox, C.E., Stein, M.H., and Webb, S.L. 2002. *Practical Aspects of CO_2 Flooding.* Society of Petroleum Engineers: Richardson, Texas. **22**. ISBN 1-55563-096-0.

Juanes, R., Spiteri, E.J., Orr, F.M. Jr. and Blunt, M.J. 2006. Impact of Relative Permeability Hysteresis on Geological CO_2 Storage. *Water Resources Research* **42:** W12418, 1-13.

Khatib, Z. and Verbeek, P. 2003. Water to Value-Produced Water Management for Sustainable Field Development of Mature and Green Fields, *J. Petrol. Technol.* **55** (1): 26.

Kikuta, K., Hongo, S., Tanase, D. and Ohsumi, T. 2005. Field Test of CO_2 Injection in Nagaoka, Japan. Proc. of the 7th International Conference on Greenhouse Gas Control Technologies, Oxford **2:** 1367-1372.

Kobos, P.H., Cappelle, M.A., Krumhans, J.L., Dewers, T., Borns, D.J., Brady, P.V., and McNemar, A. 2008. Using Saline Aquifers for Combined Power Plant Water Needs and Carbon Sequestration. Paper presented at the 28th USAEE/IAEE North American Conference, New Orleans, 3 – 5 December.

Kumar, A., Noh, N.H., Sepehrnoori, K., Pope, G.A., Bryant, S.L., and Lake, L.W. 2005. Reservoir Simulation of CO_2 Storage in Deep Saline Aquifers. SPE Paper 89343, presented at the SPE/DOE Symposium on Improved Oil Recovery Symposium, April 17-21, Tulsa, Oklahoma.

Kumar, A. 2004. A Simulation Study of Carbon Sequestration in Deep Saline Aquifers', MS thesis, University of Texas at Austin.

Kumar, N. 2008. CO_2 Sequestration: Understanding the Plume Dynamics and Estimating Risk. MS thesis, University of Texas at Austin, Austin, Texas.

Law, D. 1996. Injectivity Studies. *Aquifer Disposal of Carbon Dioxide: Hydrodynamic and Mineral Trapping—Proof of Concept*, B. Hitchon, editor Geoscience Publishing: Sherwood Park, Alberta, Canada, 59-92.

Leonenko, Y., Keith, D.W., Pooladi-Darvish, M., and Hassanzadeh, H. 2006. Accelerating the Dissolution of CO_2 in Aquifers. Paper presented at the 8th International Conference on Greenhouse Gas Control Technologies, Trondheim, Norway, 19−22 June.

Lindeberg, E. and Wessel-Berg, D. 1997. Vertical Convection in an Aquifer Column Under a Gas Cap of CO_2. *Energy Conversion and Management* **38**: S229-S234.

Matilla, C.A., Oruganti, Y., and Bryant, S.L. 2008. Real-Time Assessment of CO_2 Migration Direction During Geologic Storage. Paper presented at the 9th International Conference on Greenhouse Gas Control Technologies (GHGT-9), Washington, DC, 16-20 November.

Meckel, T.A., Hovorka, S.D., and Kalyanaraman, N. 2008. Continuous Pressure Monitoring for Large Volume CO_2 Injections. Paper presented at the 9th International Conference on Greenhouse Gas Control Technologies (GHGT-9), Washington, DC, 16-20 November.

Miles, N., Davis, K., and Wyngaard, J. 2005. Detecting Leaks from CO_2 Reservoirs Using Micrometeorological Methods, Carbon Dioxide Capture for Storage in Deep Geologic Formations. *Results from the CO_2 Capture Project, Volume 2: Geologic Storage of Carbon Dioxide with Monitoring and Verification,* S.M. Benson, editor. Elsevier Science: London. 1031-1044.

Mo, S., Zweigel, P., Lindeberg, E., and Akervoll, I. 2005. Effect of Geologic Parameters on CO_2 Storage in Deep Saline Aquifers. Paper SPE 93952 presented at the Europec Biennial Conference, Madrid, 13-16 June.

Newmark, R.L., Ramirez, A.L., and Daily, W.D. 2002. Monitoring Carbon Dioxide Sequestration Using Electrical Resistance Tomography (ERT): A Minimally Invasive Method. Paper presented a the Sixth International Conference on Greenhouse Gas Control Technologies (GHGT-6), Kyoto, Japan, 1-4 October.

Nghiem L., Sammon, P., Grabenstetter, J., and Okhuma, H. 2004. Modeling CO_2 Storage in Aquifers with a Fully-Coupled Geochemical EOS Compositional Simulator. Paper SPE 89474 presented at the SPE/DOE Symposium on Improved Oil Recovery, Tulsa, Oklahoma, 17-21 April.

Nghiem, L., Yang, C., Shrivatava, V., Kohse, B., Hassam, M., Chen, D., and Card, C. 2009. Optimization of Residual Gas and Solubility Trapping for CO_2 Sequestration in Saline Aquifers. Paper SPE 119080 presented at the SPE Reservoir Simulation Symposium, The Woodlands, Texas, 2-4 February.

Nicot, J.P. 2008. Evaluation of Large-Scale CO_2 Storage on Fresh-Water Sections of Aquifer: An Example from the Texas Gulf Coast Basin *Int. J. Greenhouse Gas Control* **2:** 582-593.

Nighswander, J.A., Kalogerakis, N., and Mehrotra, A.K. 1989. Solubilities of Carbon Dioxide in Water and 1 wt.% NaCl Solution at Pressures up to 10 MPa and Temperatures from 80 to 200 °C. *J. Chem. Eng. Data* **34:** 355-360.

Noh, M., Lake, L.W., Bryant, S.L., and Arague-Martinez, A. 2004. Implications of Coupling Fractional Flow and Geochemistry for CO_2 Injection in Aquifers. Paper SPE 89341 presented at the SPE/DOE Symposium on Improved Oil Recovery, Tulsa, Oklahoma, 17-21 April.

Nolte, K.G., 1979. Determination of Fracture Parameters from Fracturing Pressure Decline. Paper SPE 8341 presented at the SPE Annual Technical Conference and Exhibition, Las Vegas, Nevada, 23-26 September.

Obdam, A., van der Meer, L.G.H., May, F., Kervevan, C., Bech, N., and Wildenborg, A. 2003. Effective CO_2 Storage Capacity in Aquifers, Gas Fields, Oil Fields and Coal Fields. *Greenhouse Gas Control Technologies*, J. Gale and Y. Kaya, editors. Pergamon, Amsterdam **1:** 339- 352.

Oldenburg, C.M., Bryant, S.L., Nicot, J.-P., Kumar, N., and Yingqi, Z. 2008. Certification Framework Based on Effective Trapping for Geologic Carbon Sequestration. Proc. of the 7th Annual Conference on Carbon Capture and Sequestration: Addressing the Knowledge, Policy, Regulatory and Technology Gaps To Expedite CCS Deployment, Pittsburgh, Pennsylvania, Abstract #817.

Oldenburg, C.M., Lewicki, J.L., and Hepple, R.P. 2003. Near-Surface Monitoring Strategies for Carbon Dioxide Storage Verification. Lawrence Berkeley National Laboratory Report LBNL-54089.

Omerod, W. 1994. *Carbon Dioxide Disposal from Power Stations,* IEA Greenhouse Gas R and D Programme: Gloucestershire, United Kingdom.

Orr, F.M. 2004. Storage of Carbon Dioxide in Geologic Formations. *Journal of Petroleum Technology* **56** (9): 90-97.

Oruganti, Y. and Bryant, S.L. 2008. Pressure Build-Up During CO_2 Storage in Partially Confined Aquifers. Paper presented at the 9th International Conference on Greenhouse Gas Control Technologies (GHGT-9), Washington, DC, 16-20 November.

Pearce, J.M., Chadwick, R.A., Bentham, M., Holloway, S., Kirby, and G.A. 2005. Monitoring Technologies for the Geological Storage of CO_2. UK Department of Trade and Industry Technology Status Review Report; No DTI/Pub URN 05/1033.

Peng, D.Y. and Robinson, D.B. 1976. A New Two-Constant Equation of State. *Ind. Eng. Chem. Fundamentals* **15** (1): 59-64.

Pruess, K., Xu, T., Apps, J., and García, J. 2003. Numerical Modeling of Aquifer Disposal of CO_2. *SPE Journal* **8** (1): 49-60.

Pruess, K. 2004. Numerical Simulation of CO_2 Leakage from a Geologic Disposal Reservoir, Including Transitions from Super-to-Subcritical Conditions, and Boiling of Liquid CO_2. *SPEJ* **9** (2): 237-248.

Riaz, A., Hesse, M., Thelepi, H.A., and Orr, F.M. Jr. 2006. Onset of Convection in a Gravitationally Unstable Diffusive Boundary Layer in Porous Media. *J. Fluid Mech.* **548:** 87 111

Riddiford, F.A., Tourqui, A., Bishop, C.D., Taylor, B. and Smith, M. 2003. A Cleaner Development: The In Salah Gas Project, Algeria. *Greenhouse Gas Control Technologies*, *Volume 1,* J. Gale and Y. Kaya, editors. Pergamon: Amsterdam, 595-600.

Rigg, A.J., Allinson, G., Bradshaw, J., Ennis-King, J., Gibson-Poole, C.M., Hillis, R.R., Lang, S.C., and Streit, J.E. 2001. The Search for Sites for Geological Sequestration of CO_2 in Australia: A Progress Report on GEODISC. *APPEA* **41** (1): 711—725.

Ruiz, J.H.J.L. 2005. An Advanced Vapor-Compression Desalination System. PhD dissertation, Texas A&M University, College Station, Texas.

Saripalli, K.P., Mahasenan, N.M., and Cook, E.M. 2002. Risk and Hazard Assessment for Projects Involving the Geological Sequestration of CO_2. Proc. of the Sixth International Conference on Greenhouse Gas Control Technologies (GHGT-6), Kyoto, Japan.

Saul, A. and Wagner, W. 1987. International Equations for the Saturated Properties of Ordinary Water Substance. *J. Phys. Chem. Ref. Data*, **16** (4): 893-901.

Schembre-McCabe, J.M., Kamath, J., and Gurton, R. 2007. Mechanistic Studies of CO_2 Sequestration. Paper IPTC 11391 presented at the International Petroleum Technology Conference, Dubai, 4-6 December.

Sengul, M. 2006. CO_2 Sequestration—A Safe Transition Technology. Paper SPE 98617 presented at the SPE International Health, Safety & Environment Conference, Abu Dhabi, 2-4 April.

Spiteri, E.J., Juanes, R., Blunt, M.J., Orr, F.M Jr. 2005. Relative Permeability Hysteresis: Trapping Models and Application to Geological CO_2 Sequestration. Paper SPE 96448 presented at the SPE Annual Technical Conference and Exhibition, Dallas, 9-12 October.

Stern, N. 2006. *Stern Review on the Economics of Climate Change*. Cambridge University Press: Cambridge, UK.

Strazisar, B.R., Klusman, R.W., and Wells, A.W. 2003. Surface Monitoring of Leakage from Geologic CO_2 Sequestration. Paper presented at the American Geophysical Union Fall Meeting, San Francisco, 8-12 December.

van der Meer, L.G.H. and van Wees, J.D. 2006. Limitations to Storage Pressure in Finite Saline Aquifers, and the Effect of CO_2 Solubility on Storage Pressure. Paper SPE 103342 presented at the SPE Annual Technical Conference and Exhibition, San Antonio, Texas, USA, 24-27 September.

van Engelenburg, B.C.W. and Blok, K. 1993. Disposal of Carbon Dioxide in Permeable Underground Layers: A Feasible Option?" *Climatic Change* **23:** 55-68.

Watson, M.N., Boreham, C.J., and Tingate, P.R. 2004. Carbon Dioxide and Carbonate Cements in the Otway Basin: Implications for Geological Storage of Carbon Dioxide. *APPEA J* **44**(1): 703-20.

Wigley, T.M.L., Richels, R., and Edmonds, J.A. 1996. Economic and Environmental Choices in the Stabilization of Atmospheric CO_2 Concentrations. *Nature* **379** (6562): 240-243.

Wilson, M. and Monea, M. 2004. IEA GHG Weyburn CO_2 Monitoring and Storage Operation Summary Report 2000 - 2004. Petroleum Technology Research Centre, Regina.

Xu, T, Apps, J.A., and Pruess, K. 2004. Numerical Simulation of CO_2 Disposal by Mineral Trapping in Deep Aquifers. *Applied Geochemistry***, 19** (6): 917-936.

Zhou, Q., Birkholzer, J.T., Rutqvist, J., and Tsang, C.-F. 2007. Sensitivity Study of CO_2 Capacity in Brine Aquifers With Closed Boundaries: Dependence on Hydrogeologic Properties. Proc. of the 6th Annual DOE-NETL Conference on Carbon Capture and Sequestration, Pittsburgh, Pennsylvania, 7-10 May.

APPENDIX. EXAMPLE CMG SIMULATION INPUT FILE

```
RESULTS SIMULATOR GEM 200800


DIM MDIMPL 100
TITLE1 'Engineered Case'
MAXERROR 20
RANGECHECK OFF
INUNIT FIELD
WSRF WELL 1
WSRF GRID TIME
WRST 1,0000
*OUTSRF *GRID *SW *SG *PRES *DENW *DENG *TEMP *SGRHYS SGHYS
SGDTHY STRMLN DPORMNR RFO POROS PERM
 *Z 'CO2' *W 'CO2' *Y 'H2O' *W 'H2O'VELOCRC VISG VISW RHOG

*OUTSRF *WELL *GHGGAS *GHGLIQ *GHGSCRIT *GHGSOL *GHGAQU
*GHGMNR *GHGTHY

OUTSRF RES ALL
WPRN GRID 0
OUTPRN GRID NONE
OUTPRN RES NONE

WRST 1,0000
*INVENTORY-CO2

RESULTS XOFFSET 0.0000
RESULTS YOFFSET 0.0000
RESULTS ROTATION 0.0000 **$ (DEGREES)
RESULTS AXES-DIRECTIONS 1.0 -1.0 1.0

GRID CART 50 50 50

KDIR DOWN

DI CON 500

DJ CON 500

DK CON 20
```

```
DEPTH TOP 20 20 1 6000

*Refine.txt
NULL CON 1.

*MOD

 1:50 1:50 1:50 = 0
 10:40 9:41 1:50 = 1


POR CON 0.25

PERMI CON 100
PERMJ EQUALSI
PERMK EQUALSI * 0.1


PINCHOUTARRAY CON 1

CPOR MATRIX 3E-6
PRPOR MATRIX 2,600
**$ Model and number of components
MODEL PR
NC 3 3
COMPNAME 'CO2' 'C1' 'H2O'
HCFLAG
0 0 0
VISCOR HZYT
MIXVC 1.0000000E+00
VISCOEFF    1.0230000E-01    2.3364000E-02    5.8533000E-02    -4.0758000E-02
9.3324000E-03
MW
4.401,0000E+01 1.6043000E+01 1.8015000E+01
AC
2.2500000E-01 8.0000000E-03 3.4400000E-01
PCRIT
7.2800000E+01 4.5400000E+01 2.1760000E+02
VCRIT
9.4000000E-02 9.9000000E-02 5.6000000E-02
TCRIT
3.04,200 00E+02 1.9060000E+02 6.4730000E+02
PCHOR
```

7.8000000E+01 7.7,000000E+01 5.2000000E+01
SG
8.1800000E-01 3.0000000E-01 1.0000000E+00
TB
-7.8450000E+01 -1.6145000E+02 1.0000000E+02
OMEGA
4.5723553E-01 4.5723553E-01 4.5723553E-01
OMEGB
7.7796074E-02 7.7796074E-02 7.7796074E-02
VSHIFT
0.0000000E+00 0.0000000E+00 0.0000000E+00
VISVC
9.4000000E-02 9.9000000E-02 5.6000000E-02
BIN
1.0300000E-01
2.0000000E-01 4.907,0000E-01

TRES 150
PHASEID GAS
CW 3.1e-6
REFPW 1900
SOLUBILITY HENRY
DERIVATIVEMETHOD NUMERALL
**DIFFUSION COEFFICIENT IN CM2/S
DIFFC-AQU
2.0E-05 0.0 0.0
*H2O_INCLUDED
*HENRY-CORR-CO2

*ENTHCOEF
4.7780500E+00 1.1443300E-01 1.0113200E-04 -2.6494000E-08
3.4706000E-12 -1.3140000E-16
-5.5811400E+00 5.6483400E-01 -2.8297300E-04 4.1739900E-07
-1.5255760E-10 1.9588570E-14
-2.4634,200 E+00 4.5739200E-01 -5.2512000E-05 6.4549000E-08
-2.0275900E-11 2.3631,000E-15

*TRACE-COMP 2

*SATWCUTOFF 0.0
*SWR-H2OVAP 0.0

*OGW_FLASH *ON

```
*METHOD-OGW 1

*NC-AQUEOUS 1
*COMPNAME-AQUEOUS 'NaCl'

*AQFILL *OFF
*PSAT -1

*SALINITY *MOLAL 1.89
*SALINITY-CALC *OFF

*AQUEOUS-DENSITY *ROWE-CHOU
*AQUEOUS-VISCOSITY *KESTIN

ROCKFLUID
RPT 1
*SGT
 0.0006000 0.0 1.00000 0.0
 0.0500000 0.0001 0.8800000 0.0
 0.0889000 0.001,0000 0.7023000 0.0
 0.1778000 0.01,00000 0.4705000 0.0
 0.2667,000 0.0300000 0.2963000 0.001,0000
 0.3556000 0.0500000 0.1715000 0.01,00000
 0.4444000 0.1,000000 0.0878000 0.0300000
 0.5333000 0.2000000 0.037,0000 0.8000000
 0.6222000 0.3500000 0.011,0000 3.0000000
 0.6500000 0.3900000 0.0 4.00000
 0.7111,000 0.5600000 0.0 8.00000
 0.8000000 1.00000 0.0 30.00000
*SWT
 0.2000000 0.0 1.00000 45.00000
 0.2899000 0.0022000 0.6769000 19.03000
 0.3778000 0.0180000 0.4153000 10.07,000
 0.4667,000 0.0607,000 0.2178000 4.90000
 0.5556000 0.1438000 0.0835000 1.80000
 0.6444000 0.2809000 0.0123000 0.5000000
 0.7,000000 0.4089000 0.0 0.0500000
 0.7333000 0.4855000 0.0 0.01,00000
 0.8222000 0.7709000 0.0 0.0
 0.9111,000 1.00 0.0 0.0
 1.00000 1.00000 0.0 0.0

*HYSKRG 0.3
```

```
INITIAL
VERTICAL *DEPTH_AVE *WATER_GAS
ZGAS
.001 .999 0

REFPRES
 2,600


REFDEPTH
 6000

DWGC
 4000.0

SWOC
 0.995
GASZONE NOOIL


NUMERICAL
PRECC 1.E-07
NORTH 80
ITERMAX 200
DTMIN 1.E-06
NORM PRESS 1,000
NORM SATUR 0.05
NORM GMOLAR 0.05
NORM AQUEOUS 0.05
MAXCHANGE SATUR 0.8
CONVERGE PRESS 1e-005
CONVERGE HC 0.001
CONVERGE WATER 0.001
CONVERGE MAXRES NORMAL
MAXCHANGE GMOLAR 0.8
DTMAX 75



RUN
DATE 2000 1 1
DTWELL 0.1
** WELL 1 'Well_Inj'
WELL 'Well_Inj'
```

```
INJECTOR 'Well_Inj'
INCOMP SOLVENT 1. 0.
OPERATE MAX STG 156e+006 CONT REPEAT
OPERATE MAX BHP 4,200 . CONT REPEAT
**$ rad geofac wfrac skin
GEOMETRY J 0.5 0.35 1. 0.
PERF GEO 'Well_Inj'
**$ UBA ff Status Connection
 25 21 48 1. OPEN
 25 22 48 1. OPEN
 25 23 48 1. OPEN
 25 24 48 1. OPEN
 25 25 48 1. OPEN
 25 26 48 1. OPEN
 25 27 48 1. OPEN
 25 28 48 1. OPEN
 25 29 48 1. OPEN



OPEN 'Well_Inj'


TIME 10

*DTMAX 30.

TIME        30
TIME        50
TIME        80
TIME        100
TIME        150
TIME        200
TIME        250
TIME        300
TIME        350
TIME        400
TIME        450
TIME        500
TIME        550
TIME        600
TIME        650
```

```
TIME      700
TIME      750
TIME      850
TIME      950
TIME      1,000
TIME      1050
TIME      1300
TIME      1400
TIME      1500
TIME      1600
TIME      1700
TIME      1800
TIME      1900
TIME      2000
TIME      2190
TIME      2555
TIME      2920
TIME      3285
TIME      3650
TIME      4015
TIME      4380
TIME      4745
TIME      5110
TIME      5475
TIME      5840
TIME      6205
TIME      6570
TIME      6935
TIME      7300
TIME      7665
TIME      8030
TIME      8395
TIME      8760
TIME      9125
TIME      9490
TIME      9855
TIME      10220
TIME      10585
TIME      10950

SHUTIN 'Well_Inj'

WPRN ITER NEWTON
DTWELL 0.01
```

```
WRST TNEXT

TIME    11315
TIME    11680
TIME    12045
TIME    12410
TIME    12775
TIME    13140
TIME    13505
TIME    13870
TIME    14235
TIME    14600

DTMAX 75

TIME    14965
TIME    15330
TIME    15695
TIME    16060
TIME    16425
TIME    16790
TIME    17155
TIME    17520
TIME    17885
TIME    18250
TIME    20075
TIME    21900
TIME    23725
TIME    25550
TIME    27375
TIME    29200
TIME    31025
TIME    32850
TIME    34675
TIME    36500

DTMAX 100

TIME    38325
TIME    40150
TIME    41975
TIME    43800
TIME    45625
TIME    47450
```

TIME	49275
TIME	51100
TIME	52925
TIME	54750
TIME	56575
TIME	58400
TIME	60225
TIME	62050
TIME	63875
TIME	65700
TIME	67525
TIME	69350
TIME	71175
TIME	73000
TIME	76650
TIME	80300
TIME	83950
TIME	87600
TIME	91250
TIME	94900
TIME	98550
TIME	102200
TIME	105850
TIME	109500
TIME	113150
TIME	116800
TIME	120450
TIME	124100
TIME	127750
TIME	131400
TIME	135050
TIME	138700
TIME	142350
TIME	146000
TIME	149650
TIME	153300
TIME	156950
TIME	160600
TIME	164250
TIME	167900
TIME	171550
TIME	175200
TIME	178850
TIME	182500

```
DTMAX 365
TIME        189800
TIME        195275
TIME        200750
TIME        206225
TIME        211700
TIME        217175
TIME        222650
TIME        228125
TIME        233600
TIME        239075
TIME        244550
TIME        250025
TIME        255500
TIME        260975
TIME        266450
TIME        271925
TIME        277400
TIME        282875
TIME        288350
TIME        293825
TIME        299300
TIME        304775
TIME        310250
TIME        315725
TIME        321200
TIME        326675
TIME        332150
TIME        337625
TIME        343100
TIME        348575
TIME        354050
TIME        359525
TIME        365000

STOP

**********TERMINATE
SIMULATION**********
```

VITA

Abhishek Anchliya graduated with a B.S. in petroleum engineering from Indian School of Mines (ISM), India in 2006. He is the recipient of the 2009 SPE Young Member Outstanding Service Award for his excellent contributions to Society of Petroleum Engineers (SPE). He has also won several scholarships from SPE and EAGE. Anchliya has accepted a Reservoir Engineering position with Chevron Energy Technology Company to work in the Houston office beginning in October 2009.

Mailing address:

Abhishek Anchilaya
c/o Dr. Christine Ehlig-Economides
Department of Petroleum Engineering
Texas A&M University 3116 TAMU
College Station, TX 77843-3116